Illinois U Library

IN TWO SECTIONS—SECTION ONE

Transactions

of the

ASME

High-Temperature Disk-Forging Developments for Aircraft Gas Turbines . *L. B. Fonda* 1

Heat Transfer by Free Convection From Heated Vertical Surfaces to Liquids . . . . . *Y. S. Touloukian, G. A. Hawkins, and M. Jakob* 13

Review of Data on Dynamic Viscosity of Water and Superheated Steam . . . . . *G. A. Hawkins, W. L. Sibbitt, and H. L. Solberg* 19

Temperature Distribution in Some Simple Bodies Developing or Absorbing Heat at a Linear Function of Temperature . . . . . *Max Jakob* 25

Research Work on Rail Sections . . . . . *Walter Leaf* 31

Recent Developments Concerning the Properties of Cast Steels . . . . *C. W. Briggs* 37

Temporary Installation of Shasta Turbines at Grand Coulee . . . . . *H. H. Sloane* 49

Applications of Mechanical Cascade Control Systems . . . . . *J. N. Swarr* 57

JANUARY, 1948

VOL. 70, NO. 1

Transactions

of The American Society of Mechanical Engineers

Published on the tenth of every month, except March, June, September, and December

---

OFFICERS OF THE SOCIETY:

E. G. Bailey, *President*

K. W. Jappe, *Treasurer* C. E. Davies, *Secretary*

COMMITTEE ON PUBLICATIONS:

H. L. Dryden *Chairman*

J. M. Juran John Haydock

Ronald B. Smith C. B. Campbell

George A. Stetson, *Editor* K. W. Clendinning, *Managing Editor*

ADVISORY MEMBER OF THE COMMITTEE ON PUBLICATIONS:

Hunter R. Hughes, Jr., Atlanta, Ga.

JUNIOR MEMBERS

Louis Feld, Harrison, N. J. John H. Prentiss, New York, N. Y.

Published monthly by The American Society of Mechanical Engineers. Publication office at 20th and Northampton Streets, Easton, Pa. The editorial department is located at the headquarters of the Society, 29 West Thirty-Ninth Street, New York 18, N. Y. Cable address, "Dynamic," New York. Price $1.50 a copy, $12.00 a year; to members and affiliates, $1.00 a copy, $6.00 a year. Changes of address must be received at Society headquarters three weeks before they are to be effective on the mailing list. Please send old as well as new address. . . . By-Law: The Society shall not be responsible for statements or opinions advanced in papers or . . . printed in its publications (B13, Par. 4). . . . Entered as second-class matter March 2, 1928, at the Post Office at Easton, Pa., under the Act of August 24, 1912. . . .

Copyrighted, 1948, by The American Society of Mechanical Engineers. Reprints from this publication may be made on condition that full credit be given the Transactions of the ASME and the author, and that date of publication be stated.

Illinois U Library

High-Temperature Disk-Forging Developments for Aircraft Gas Turbines

By L. B. Fonda,[1] West Lynn, Mass.

This paper is concerned chiefly with the Type I-40 turbine wheel which, with its buckets, comprises the high-temperature rotating part of the jet engine powering the P-80 airplane. Of interest are the conclusions drawn from bursting tests carried out on (179) turbine-wheel blanks and (6) bucketed turbine wheels. A brief discussion is presented of the circumstances which led to the launching of this gigantic investigation, the type of equipment used, the various alloys and forging practices investigated, and comparison of the actual results obtained. The most important consideration was found to be ductility; the best method of obtaining it—proper control of grain flow. The source of previous difficulty was found to be unsound forgings; the best method of prevention—extreme care in producing sound ingots and billets. Inspection methods developed for detection of any harmful defect—a combination of zyglo and supersonic testing.

Introduction

Four serious I-40 turbine-wheel failures—the last in flight—occurred early in 1945. Fortunately, there were no fatalities. As a result, the author's company undertook an organized program of bursting and sectioning wheel forgings from various sources, made from various materials, and representing various forging practices, heat-treatments, and methods of handling. In all, 185 wheels were burst, including 6 bucketed wheels. Sixteen additional forgings were sectioned for a complete survey of hardness and physical testing, and a large number of forgings, rejected on supersonic inspection, were sectioned to check the accuracy of the results obtained by this inspection method. The average weight was close to 400 lb for each forging.

Because of the large number of wheels tested it was possible to make direct comparisons, based upon bursting speed, which led to evaluation of numerous old and new forging methods, heat-treatments, processing methods, and alloy compositions. The results extensively affected the manufacturing processes in use by the various suppliers, as many new methods were devised by these manufacturers, and general improvement was realized.

The extensive scope of the program also permitted vast strides to be taken toward calibration and improvement of inspection methods as applied to the detection of defects in this type of austenitic forging. It was an excellent opportunity to prove the desirability and accuracy of supersonic inspection as applied to internal forging defects, as well as to develop more suitable technique. It proved also that gamma-ray and x-ray inspection methods were considerably limited when used for this application.

Above all, the composite nature of the program allowed for a clearer understanding of fundamental considerations underlying the good or bad performance of the bucket wheels in operation. Knowing these principles, it was possible more successfully to plan improved methods of manufacturing and to determine the reasons for some of our previous troubles.

Virtually complete histories were obtained from the manufacturers on each wheel tested, which enabled us to compare methods and to attempt correlation of various factors with bursting speed. Statistics were assembled in many ways to determine what relationships existed.

The specific problems involved at the beginning of this investigation were as follows:

1 To determine a method for separating good forgings from bad forgings: in the first stage of the program, by a destructive test; and in the second stage of the program, by a suitable sampling control chart based on the results of previous destructive tests.

2 To establish a rigorous inspection routine for detecting flaws in turbine-wheel forgings, especially of an internal nature.

3 To scrutinize the methods of the forging vendors, principally for the purpose of finding means of improving center ductility, soundness, and uniformity of forgings.

4 To investigate all the stress-producing factors in the design, manufacture, and operation of the Type I-40 wheel; especially, to develop a satisfactory means for determining the axial and radial temperature gradients in the wheel under actual conditions of operation.

5 To improve the basic contour of the turbine wheel so that the forging process could be improved, or so that the internal stresses could be relieved partially or entirely.

6 To investigate the high-temperature and high-speed properties of new alloys which promise to be useful on a long-range basis.

7 To accumulate fundamental data on the production alloy (Timken 16-25-6) and to investigate new methods of processing this material.

This paper will be confined principally to a metallurgical discussion of the latter two problems. Metallurgical considerations are important because we are dealing with unusually large forgings made from materials designed for high hardness and high strength at elevated temperatures, a combination of factors definitely not conducive to easy forgeability.

Chemical Composition

Because the operating temperature, at least at the rim of the wheel, is in the order of 1200 F, it is not possible to use the ordinary ferritic type of alloy which is capable of being heat-treated to the desired balance of strength and ductility. This type of alloy depends for its strength upon quenching and tempering treatments. Operational temperatures are higher than the tempering temperatures and, consequently, tempering would continue during operation of the engine, thereby reducing the strength and causing the material to become very weak.

The material used for gas-turbine bucket wheels must also be resistant to oxidation at temperature and to corrosion by combusted gases and, when ethyl gasoline is used as fuel, it must also be resistant to corrosion by lead compounds. Therefore the selection of wheel material is limited to the austenitic type of stainless alloys.

[1] Metallurgical Engineer, General Electric Company (River Works).

Contributed by the Aviation Division and presented at the Semi-Annual Meeting, Chicago, Ill., June 16–19, 1947, of The American Society of Mechanical Engineers.

Note: Statements and opinions advanced in papers are to be understood as individual expressions of their authors and not those of the Society.

As an austenitic alloy has no phase change within the ordinary range of heat-treating temperatures, it is not capable of being hardened by quenching. Heating to high temperatures merely results in grain growth and solution of carbides and intermetallic compounds. Quenching from this temperature retains this metallographic condition. Hardening is accomplished by working the metal below its recrystallization temperature. In the I-40 wheel, yield strength in the center area must be sufficiently high to minimize stretch during overspeed. Strain-relief-annealing is generally done at approximately the operating temperature and eliminates those peak strains which would be relieved in service.

Some of the austenitic alloys for high-temperature application have been designed so as to include elements which cause age-hardening. After quenching from a temperature high enough to cause solution of carbides and intermetallic compounds (segregated due to forging or rolling of the metal), the part is reheated to a lower temperature which causes them to precipitate from this supersaturated solution in a fairly homogeneous pattern. The amount of precipitation is dependent both upon the temperature and the length of time at which the metal is heated or "aged" at this temperature. Although higher strengths are obtainable by cold-working most of these age-hardenable bucket-wheel alloys, it is generally more desirable to eliminate cold work, as this is hard on forging equipment, increases machining difficulties, reduces the ductility, and does not produce as consistent results as solution treatment followed by age-hardening.

Compositions of the various alloys investigated in the bursting tests are given in Table 1.

The alloys mentioned in Table 1 were designed for cold work except modified inconel which is an age-hardening alloy. Experiments on age-hardening of Timken alloy carried out during the wheel-bursting investigation met with at least a fair degree of success. EME alloy produced excellent center ductility, considering its cold-worked condition. Both 19-9-DL and CSA produced very high bursting speeds in comparison to Timken alloy, processed in the same manner. Bursting data on all alloys other than Timken 16-25-6 are scanty but indicate that even better results might have been produced if various processing combinations had been investigated on the scale to which Timken alloy was subjected.

Timken alloy 16-25-6 has long been the standard-production bucket-wheel material because of its acceptable combination of forgeability, machinability, weldability, yield strength, and 1200 F rupture strength. Many other alloys have been found which excel Timken 16-25-6 in one or more of these characteristics, but, as yet, none has been proved to be superior in all five. We have had an almost unlimited amount of manufacturing experience with Timken alloy, but not with any of the other alloys investigated during the bursting program. To prove acceptable for production use, the material must be capable of being processed without difficulty as well as having acceptable mechanical properties.

Modified Inconel is capable of producing higher physical and rupture properties than Timken alloy and has acceptable forgeability. We formerly experienced machining difficulties with this material. This difficulty has now been somewhat overcome, although the machinability still does not compare favorably with Timken alloy. However, it has not yet been proved that the weldability is equivalent to Timken alloy, and as the alloy content is greater, the cost is correspondingly more.

EME alloy has been reported to be more easily forgeable than Timken alloy (also developing better center ductility). No difficulty has been experienced in machining. We have had no experience with welding. Yield strength can perhaps be developed equivalent to Timken alloy, but to date it has not been proved that the 1200 F rupture strength is equivalent to Timken alloy. Because of its lower alloy content, presumably, it can be made less expensively.

19-9-DL alloy is more easily forgeable, and, on the basis of our limited experience, is perhaps comparable in weldability and machinability to Timken alloy. Yield strengths and 1200 F rupture strengths have been produced equivalent to, and in some cases higher than, Timken alloy. However, the composition is a delicate balance of several different phases, and we believe that the resulting properties are much more sensitive to slight changes in composition than Timken alloy. Hence it might be considerably more difficult to produce consistent lots on a large scale. Due to the lower alloy content it can be produced at a lower cost. Our processing experience is limited.

CSA, on the basis of very limited experience, seems to be comparable to Timken alloy in forgeability and machinability. We have had practically no welding experience with this material. Our limited test data show the material to be superior to Timken alloy in both yield strength and 1200 F rupture strength. Alloy content is lower. However, our experience with this material is so extremely limited that present comparison as a production material would not be soundly based.

Actual data on performance in an I-40 jet engine is not available on any of these alloys except Timken 16-25-6.

Equipment and Method of Testing

The wheel blank employed for bursting tests incorporated the general dimensions of a bucketed I-40 wheel, except for the omissions of cooling vanes, buckets, and bucket slots. Principal dimensions are shown in Fig. 1. The stress distribution for this design is shown on the curve in Fig. 2, while that for the bucketed I-40 wheel (as used in the engine) is shown in Fig. 3.

In comparing the average tangential rim stress of a wheel blank of this design to similar stresses in a smaller turbosupercharger-wheel blank of the same standard material (Timken 16-25-6 alloy), it was possible to set up a ratio of bursting speeds. Thus

TABLE 1 COMPOSITIONS OF VARIOUS ALLOYS

Name of alloy	C	Mn	P	S	Si	Cr	Ni	Mo	N_2	W	Cb	Ti	Al	Fe
Timken 16-25-6	0.12 max	2.00 max	0.030 max	0.030 max	1.00 max	15.0 to 17.5	24 to 27	5.5 to 7.0	0.10 to 0.20	...	..	..	..	Bal
EME	0.12 to 0.17	0.40 to 0.60	0.030 max	0.030 max	0.40 to 0.60	18.75 to 19.75	11.50 to 12.50	...	0.10 to 0.20	3.0 to 3.5	0.85 to 1.25	..	..	Bal
19-9-DL	0.28 to 0.35	0.75 to 1.50	0.040 max	0.040 max	0.30 to 0.80	18 to 20	8 to 10	1.0 to 1.5	..	1.0 to 1.5	0.20 to 0.55	0.20 to 0.50	..	Bal
Modified inconel	0.10 max	0.40 to 0.80	0.010 max	0.010 max	0.40 to 0.70	14 to 16	72 to 76	...	..	...	...	2.00 to 2.75	0.40 to 0.90	5.5 to 7.5
CSA	0.20 to 0.30	4.0 to 5.5	0.030 max	0.030 max	0.30 to 0.80	18 to 20	5.0 to 6.0	1.0 to 1.5	..	1.0 to 1.5	0.20 to 0.55	..	..	Bal

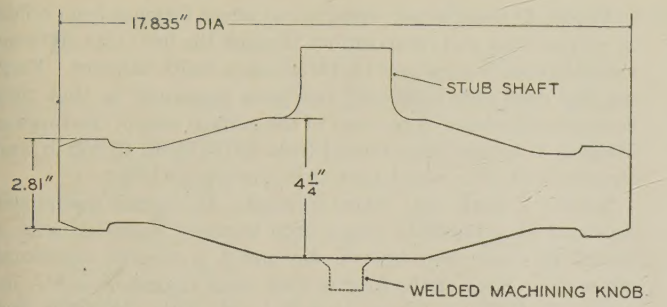

Fig. 1 Major Dimensions of Type I-40 Wheel Blank, Machined for Bursting Test

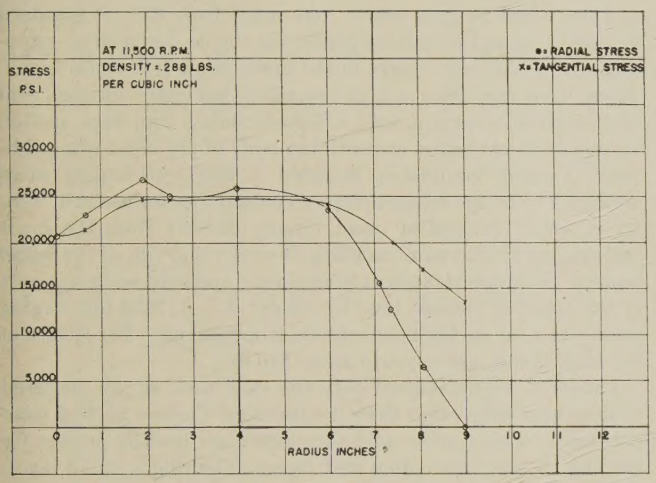

Fig. 2 Stresses in Type I-40 Wheel; Without Buckets

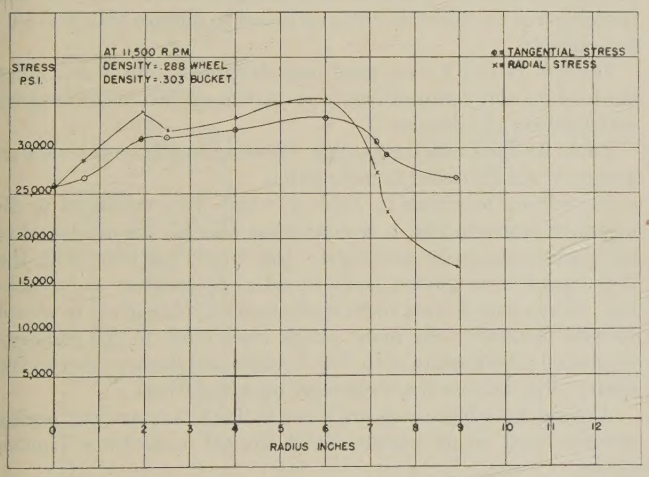

Fig. 3 Stresses in Type I-40 Wheel; With Buckets

it was calculated that the normal bursting speed of the blank shown in Fig. 1 should be 25,000 rpm, whereas the average bursting speed of the smaller wheel blank (on which a vast amount of data were available) had been 49,000 rpm. When it was found that very few of the I-40 wheels reached or exceeded the calculated bursting speed, it was realized that the center rather than the rim was the critical area, and that the quality of this center area was much more difficult to control in a large forging than in a small one. (Comparative sizes of the jet and the supercharger wheels with buckets are shown in Fig. 4.)

Each wheel blank had three holes drilled and tapped in the stub shaft to which an adapter and spindle were attached. The

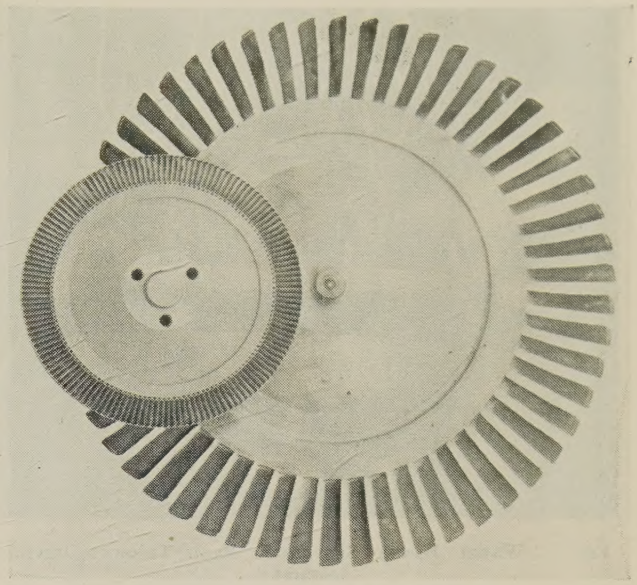

Fig. 4 Comparative Sizes of Small Type B Supercharger Wheel and Large Type I-40 Jet-Engine Wheel

spindle was suspended from a Type B turbosupercharger wheel and shaft installed in a standard bearing and pump casing, as shown in Figs. 5 and 6. Flexible steam lines conducted steam through nozzles attached indirectly to the bearing and pump casing, and in this manner the Type B turbine wheel supplied motive power to the I-40 wheel blanks. The lubrication system and tachometer assembly were installed in the same manner as those of a standard supercharger.

Each I-40 wheel blank was suspended in a large armor-plate ring for the safety of the test personnel; the ring was lined with approximately 6 in. of laminated boiler plate to absorb the bursting impact. Wheels tested without a similar boiler-plate lining were practically pulverized against the armor plate.

The entire test assembly was located in a pit with adequate protection, in the form of steel cover plates, for test personnel and observers. All instrumentation and control apparatus extended from the pit to a central control panel.

For the purpose of obtaining significant information regarding diametric stretch versus speed, tests were conducted in a series of 1-min steps beginning at 13,000 rpm and extending to bursting speed in 3000-rpm speed increments. After each run the wheels were decelerated to standstill for measurements of the outside diameter in three marked locations, in addition to wheel-temperature measurements, which were employed in calculating the temperature-corrected diametric expansion.

Summary of Tests Made

In discussing the data obtained from bursting the numerous wheel forgings included in this investigation, it has been deemed advisable to refer to the actual vendors of the forgings as A, B, C, etc.

Vendor A manufactured both the steel used as raw material and the wheel forgings which were made from it. Its standard process consisted of casting 16-in-diam round tapered ingots from a 12-ton electric-arc furnace. Its forging equipment consisted of a 1650-ton hydraulic forging press for billets, and a 20,000-lb open-frame steam hammer used in conjunction with segmental dies (about 4 in. in width), which were flat except for the contour of the hub section and the stub shaft. The standard forging slug used was a 440-lb section of $10^1/_4$ in. round billet stock whose surface was machined to eliminate surface defects.

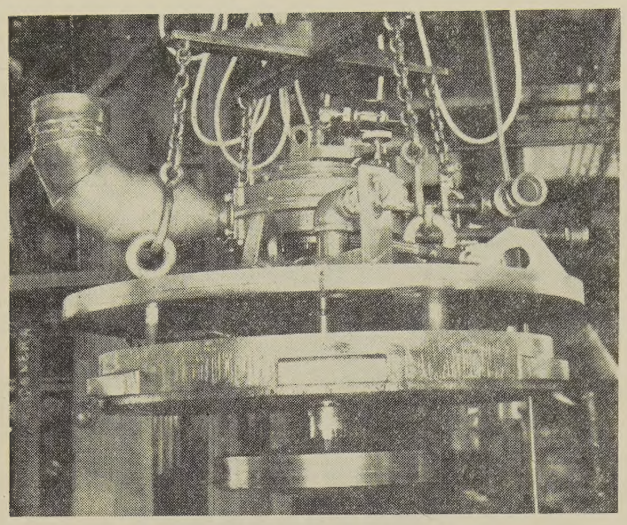

Fig. 5 Wheel Blank Suspended From Turbine-Driving Assembly
(Ready to lower into bursting pit.)

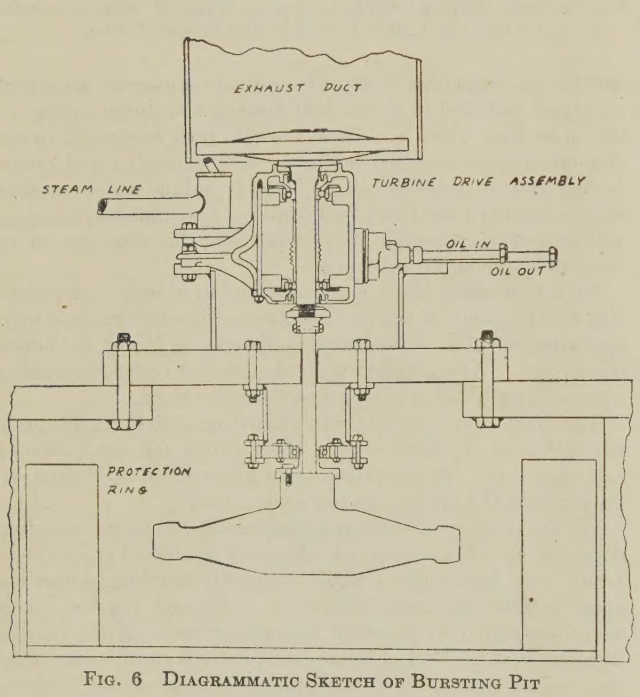

Fig. 6 Diagrammatic Sketch of Bursting Pit

Vendor B manufactured only the steel used as raw material. Its standard process consisted of casting 19-in-diam fluted round ingots from a 25-ton electric-arc furnace. Its forging equipment consisted of a 1500-ton mechanically operated forging press, which was used to cog these ingots into billets whose standard size was $8^1/_2$ in. square. Billet quality was controlled by etch-test inspection on the ends and zyglo inspection on the surface of the billets.

Vendor C manufactured only the wheel forgings (made in most cases from billets supplied by vendor B). Its forging equipment used in connection with this work consisted of a 25,000-lb and a 35,000-lb steam drop hammer equipped with completely contoured, closed, drop-forging dies, and utilizing a suitable trimming press between hot and cold forging operations. The standard forging slug used was a 330-lb section of the $8^1/_2$-in-sq billet stock manufactured by vendor B.

Vendor D made a few experimental wheel forgings from billets of various sizes and compositions through the use of its 2000-ton steam-hydraulic press and 12,000-lb steam smith hammer. Forging dies used were contoured but were segmental in that they covered only about 75 per cent of the surface area of the forging. Weights of forging slugs ranged from 550 lb down to 350 lb, and sizes from $10^1/_2$ in. round down to $6^1/_2$ in. square billet.

Vendor E made only wheel forgings. Its forging equipment consisted of a 12,000-lb steam drop hammer, equipped with a completely contoured bottom die and a contoured segmental upper die. Sizes of the forging slugs used ranged from $6^3/_4$ in. square down to 6 in. square, weighed approximately 330 lb and were made by forging down larger billets obtained from vendor B.

Vendor F manufactured both the steel used as raw material and the wheel forgings which were made from it. Its standard process consisted of casting preformed ingots designed to represent one of the early stages in the upset of an I-40 wheel blank. These were cast from a high-frequency induction furnace, and each individual casting had a 7-in-diam hot top, kept molten by means of an electric arc until the body of the ingot was solidified. Forging equipment included a 2500-ton forging press equipped with nine separate sets of contour dies for use in a "center reversal" process of upset forging directly from the ingot (amounting to alternate kneading of center and rim of the wheel blank). Solution treatment between hot and cold work was part of the standard process used by vendor F. A 7500-ton forging press was used during final cold-work operations. The weight of the forging slug was approximately 510 lb.

Vendor G manufactured only the steel used as raw material (this was an alloy other than the standard Timken 16-25-6 composition). This vendor used the electric-arc heating process for keeping the hot top molten and thereby assuring a sound ingot. The standard billet-forging process included special equipment for removing surface defects, and octagon billets made by this process were machined to $10^1/_2$-in. round to remove scale and surface defects.

Vendors H and J were steel manufacturers from which billet stock of special compositions was purchased for wheel forgings manufactured by vendor C.

Table 2 shows relative average bursting speeds of the various groups of wheels tested to destruction.

In addition to wheels in Table 2, which were machined to dimensions shown in Fig. 1, several other wheels were machined to more advanced stages and burst. One wheel was burst with the (54) bucket slots gashed (smooth sides) preparatory to broaching. Seven wheels were burst with these slots broached (serrated to hold buckets). Six more wheels were burst in the vacuum-overspeed pit complete with (54) buckets and flash-welded to the shaft. Fig. 4 shows the completely bucketed wheel.

Average bursting speeds are given in Table 3 (standard forging practice used on all wheels, which are all made from Timken alloy).

Because of the severe wind resistance encountered in running the gashed and broached wheels to the necessarily high speeds in the bursting pit, it was impossible to reach the bursting speed until helium gas had been admitted to the pit to lower the density of the atmosphere.

Bursting speeds of the (179) wheel blanks ranged from 14,300 to 26,400 rpm. The six bucketed wheels tested burst over a range of 16,000 to 21,900 rpm.

In addition to the (185) wheels which were burst, 16 additional wheels were sectioned for complete metallurgical survey, including physical testing. These wheels were selected as representing individual alloys, forging practices, heat-treatments, etc. The results obtained were considered to be an important adjunct to the bursting data, as physical properties obtained from the burst

TABLE 2 RELATIVE AVERAGE BURSTING SPEEDS OF WHEELS

Item	Material and process	Vendor of mat'l	Vendor of forging	No. of wheels burst	Avg burst'g speed, rpm	Consistency of burst'g speed[a]
1	Timken alloy—center reversal forging from preformed ingot, solution treated, cold-worked at 1200 F, strain-relief annealed 10 hr at 1200 F	F	F	8	25328	E
2	CSA material—solution-treated cold-worked at 1200 F, strain-relief-annealed	H	C	1	25000	...
3	Modified Inconel material — solution-treated and aged	G	D	6	24215	E
4	19-9-DL material—solution-treated and cold-worked at 1250 F, strain-relief-annealed	J	C	2	24138	G
5	Timken alloy, cold-worked at 1500 F, no solution treatment, strain-relief-annealed 4 hr at 1200 F, 6-in-sq billet stock used	B	E	1	23513	...
6	EME material—no solution treatment, cold-worked at 1250 F, strain-relief-annealed	A	A	5	22941	E
7	Timken alloy, cold-worked on press with full-contour dies	A	A	1	22800	...
8	Timken alloy, cold-worked at 1500 F, no solution treatment, strain-relief-annealed 4 hr at 1200 F, 6 1/2-in-sq billet stock used	B	E	2	22400	VG
9	Timken alloy, cold-worked at 1500 F, no solution treatment, strain-relief-annealed 4 hr at 1200 F, 6 3/4-in-sq billet stock used	B	E	1	22400	...
10	Timken alloy, center reversal process on first six forging operations by vendor F, finished according to standard hammer-forging process of vendor C; no solution treatment	F	C	1	22400	...
11	Timken alloy, cold-worked on rim only	A	A	2	22218	VG
12	19-9-DL material—solution-treated, cold-worked at 1650 F, strain-relief-annealed	J	C	1	22000	...
13	Timken alloy, solution-treated and aged	B	C	4	21906	VG
14	Timken Alloy, stub-shaft machined into billet before forging wheel blank, cold-worked, no solution treatment	A	A	3	21833	VG
15	19-9-DL material, cold-worked at 1650 F, no solution treatment	J	C	1	21300	...
16	Timken alloy, solution-treated and aged	A	A	5	21270	VG
17	Timken alloy, cold-worked at 1350 F, no solution treatment, shot-blasted after machining	B	C	3	21113	G
18	Timken alloy, solution-treated, cold-worked at 1250 F, strain-relief-annealed 8 hr at 1200 F	B	C	4	21063	F
19	Timken alloy, cold-worked at 1250 F, no solution treatment, strain-relief-annealed 4 hr at 1200 F, 3-in-hole bored through center	A	A	1	20850	...
20	Timken alloy, solution-treated, cold-worked at 1250 F, strain-relief-annealed 4 hr at 1200 F	A	A	6	20592	G
21	Timken alloy, cold-worked at 1200 F, strain-relief-annealed 50 hr at 1200 F	B	C	2	20522	VG
22	Timken alloy, cold-worked at 1200 F, strain-relief-annealed 4 hr at 1450 F	B	C	2	20514	G
23	Timken alloy, hot work only, finished stub shaft, no allowance for cooling vanes, 3-in-diam hole bored through center	B	D	3	20513	VG
24	Timken alloy, cold-worked at 1200 F, no solution treatment, strain-relief-annealed 10 hr at 1200 F, before welding on machining knob	A	A	2	20450	F
25	Timken alloy, cold-worked at 1200 F, strain-relief-annealed 4 hr at 1450-F	A	A	4	20422	G
26	Timken alloy, cold-worked at 1250 F, no solution treatment, strain-relief-annealed 8 hr at 1200 F; no machining knob welded on	B	C	5	20388	F
27	Timken alloy, solution-treated, prestressed by cold-spinning, no strain-relief-anneal	A	A	2	20350	VG
28	Timken alloy, solution-treated only (no subsequent treatment)	B	C	5	20288	VG
29	Timken alloy, solution-treated, prestressed by cold-spinning, no strain-relief-anneal	B	C	5	20258	G
30	Timken alloy, (billet stock made from 20-in-diam ingots), cold-worked at 1200 F, strain-relief-annealed 4 hr at 1200-F	A	A	3	20231	G
31	Timken alloy, cold-worked at 1350 F, no solution treatment, strain-relief-annealed 8 hr at 1200 F, machining knob welded on	B	C	10	20055	VP
32	Timken alloy, hot-worked only, finished at 1700 F, strain-relief-annealed 4 hr at 1200 F	B	C	4	19800	VG
33	Timken alloy, cold-worked at 1250 F, no solution treatment, strain-relief-annealed 4 hr at 1200 F; no machining knob welded on	A	A	20	19775	VP
34	Timken alloy, cold-worked at 1250 F, no solution treatment, strain-relief-annealed 50 hr at 1200 F	A	A	6	19701	F
35	Timken alloy, cold-worked at 1200 F, no solution treatment, strain-relief-annealed 4 hr at 1200 F; machining knob welded on	A	A	26	19282	VP
36	Timken alloy, solution-treated, strain-relief-annealed 4 hr at 1200 F; no cold work	A	A	2	19125	VG
37	Timken alloy, hot-worked only, finished at 1800 F, strain-relief-annealed 4 hr at 1200 F	A	A	3	18730	VG
38	Timken alloy, hot-worked only, finished at 1800 F, strain-relief-annealed 4 hr at 1200 F, 3-in. hole bored through center	A	A	1	18125	...
39	Timken alloy, cold-worked at 1200 F, no solution treatment, strain-relief-annealed 10 hr at 1200 F, machining knob welded on, subsequently strain-relief-annealed 10 hr at 1000-F	A	A	3	17993	P
40	Timken alloy, cold-worked at 1350 F, no solution treatment, strain-relief-annealed 4 hr at 1200 F, 3-in. hole bored through center	B	C	1	17100	...
41	Timken alloy, cold-worked at 1350 F, no solution treatment, strain-relief-annealed 8 hr at 1200 F, 1 1/2-in. hole bored through center	B	C	1	16865	...

TABLE 3 AVERAGE BURSTING SPEEDS OF WHEELS

Item	Machined condition	Vendor of material	Vendor of forging	No. of wheels burst	Avg burst'g speed, rpm	Consistency of bursting speed
A	Gashed slots	A	A	1	24800	..
B	Broached slots	A	A	7	22444	F
C	Bucketed	A	A	6	18357	F

fragments of wheels after testing were proved to be practically valueless because of the cold work which takes place in stretching during test and in striking the pit lining after bursting. Minute cracks in the burst fragments, when present, also cause deviation from true physical values.

Physical testing done on wheels sectioned rather than burst showed that forgings from the same group as item 1 of Table 2 had by far the highest center ductility in spite of the fact that both yield and tensile strengths were equal to or higher than all of the other Timken alloy wheels sectioned (see Fig. 7). The high center ductility resulted from completely radial-flow lines brought about by elimination of the billet stage during manufacture. The high strength is evidently the result of the center-reversal method of forging. These properties corresponded to the consistently high bursting speed of item 1.

A sectioned forging representing those in the same group as item 3 exhibited slightly lower yield and tensile strengths but higher ductility than item 1. Item 3 (modified inconel material) is an alloy especially designed to develop its physical properties through age-hardening rather than through cold-working. High ductility is obtained by solution-treating, and evidently is not seriously lowered through the precipitation which takes place during the aging treatment, although this aging increases both hardness and strength. Corresponding bursting speeds were somewhat lower than item 1, although much more closely grouped together. The total range of bursting speeds in item 3 was less than 450 rpm for the entire 6 wheels tested.

While these two items showed the outstanding physical properties of those wheels which were sectioned, other groups having high bursting speeds showed, in general, fairly good center ductility, and good yield and tensile strengths. Wheels in groups showing low bursting speeds, in almost every case exhibited at least one or two center physical tests with from "nil" to 2 or 3 per cent elongation (in 2 in. on a standard 0.505-in-diam tensile bar).

During the first stage of the testing program, many wheels were burst which obviously contained mechanical defects. This occurred primarily because they formed the larger part of the wheels on hand or readily available. Such forgings are responsible for a large percentage of the low bursting speeds recorded. Later, when more forgings were available, all defective wheels were rejected and only those proved mechanically sound by our inspection procedure were subjected to the bursting test. Bursting of these defective wheels served several worth-while purposes:

1 It made possible a high degree of development in our inspection procedures by allowing us to make a direct correlation of the indications found with the bursting speed, and also by inspection of the burst fragments.

2 It allowed us to discover that a relation existed between center ductility and the extent of internal defects.

3 It furnished a definite standard for measuring the improvements brought about by newer forging practices which were introduced during the latter part of the program.

Standard inspection procedure included the following: (1) Etching of the entire surface area before machining to uncover serious surface defects, this being done by immersion in a tank of aqua regia; (2) x ray through the center section for detection of large internal defects, this being done on a 1,000,000-v machine, utilizing a lead collar around the stub shaft to prevent diffusion; (3) preliminary zyglo test to show surface defects on wheels in the rough-machined condition, this being done by immersion in a fluorescent penetrant followed by examination under ultraviolet light; (4) supersonic examination of the interior for detection of all internal flaws, this being done by scanning the wheel in both axial and radial directions, and photographing the resulting wave pattern for use as a permanent record; (5) a final zyglo examination of the wheel surface in the finish-machined condition immediately prior to burst-testing. This served not only to show whether surface defects noted in preliminary zyglo examination had been removed by machining, but in the case of increasing intensity, as compared to the original indications, it pointed out a very serious axial type of defect (see Figs. 8 and 9), which combined with low center ductility was certain to cause low bursting speed. These defects were perpendicular to the operational stresses at the center of the wheel. Presumably welding the machining knob over this area (see dotted line in Fig. 1) aggravated this condition.

Conclusions and Recommendations

Ductility. The outstanding conclusion to be drawn from this bursting investigation is that the most important factor contributing to high and consistent bursting speed is ductility. With good center ductility the harmful effect of minor discontinuities or mechanical defects is minimized. When ductility is low, these defects tend to act as stress raisers, and this accounts for low bursting speeds. When ductility is high, these ordinarily localized stresses are redistributed, and the minor defects are not so highly stressed. Therefore in such a case the bursting speed more nearly approaches that of a sound forging. However, when ductility becomes exceedingly high (such as in the case of the purely solution-treated wheel of items 28 and 36), yield strength is correspondingly low, and an excessive amount of stretch is obtained before bursting. This would cause obvious difficulties in the case of a bucketed wheel operating in a unit.

In our bursting tests, wheels in the solution-treated condition burst at rather surprisingly high speeds (see item 28) considering their initial low hardness. Hardness surveys of burst fragments from these wheels showed a marked increase in Brinell hardness over original values. This indicated that the material was considerably cold-worked by excessive stretch during test, and accounted for the comparatively good bursting speeds, because of the increased yield strength during overspeeding. Then too, the high ductility involved was sufficient to overcome sudden failure due to possible defects of a minor nature. However, stretch of a magnitude sufficient to increase materially the yield strength could not be tolerated if it occurred during actual operation, because it would cause loosening of the buckets and probable rubbing of the bucket tips against the shroud ring. Therefore wheels in the purely solution-treated condition cannot be used in I-40 units.

The principle just outlined was the basis used to devise the procedure for prestressing of wheel blanks immediately prior to finish-machining. This method involved controlled overspeeding of an oversized wheel blank for the purpose of inducing cold work in those areas where it was most urgently needed. After prestressing, the distorted wheel blank was machined to the dimensions shown in Fig. 1. The remachined blank was then burst in the regular manner.

Prestressing was not commercially practical for Timken alloy I-40 wheel blanks, because it was found that the critical portion of the cold work took place at a speed just below the bursting speed. Due to the variations in bursting speed from wheel to

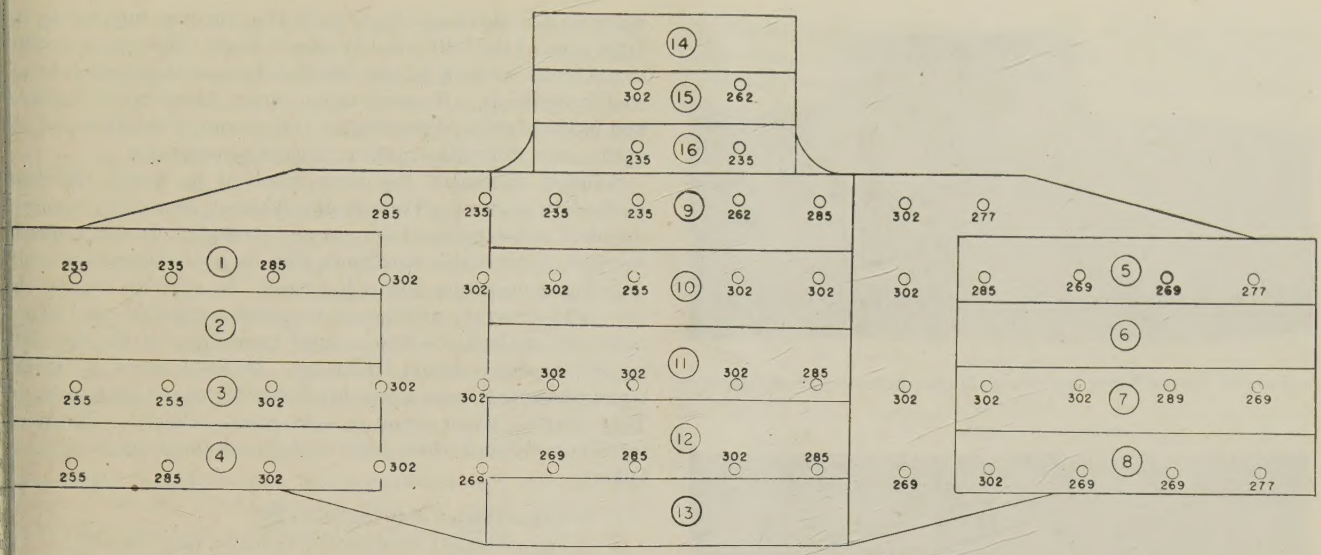

0.505 BARS PULLED AT ROOM TEMPERATURE

Bar No.	Y.S. (0.0002-in. per in.)	T.S.	El.	R.A.
1	93750 psi	131500 psi	24 per cent	43.97 per cent
2	89250	129000	21.5	46.02
3	90375	130000	20.5	46.89
4	96000	133500	20.5	44.55
5	76125	120000	31	49.46
6	73875	119000	24	44.85
7	79500	121500	29	48.29
8	83250	126500	23.5	49.18
9	75000	117000	28.5	50.29
10	97500	140500	22	40.96
11	106125	148000	17.5	35.35
12	106500	141500	6.5	14.47
13	93375	135000	14	25.79

0.250 BARS PULLED AT ROOM TEMPERATURE

Bar No.	Y.S. (0.0002-in. per in.)	T.S.	El.	R.A.
14	95500	134600	24	46.32
15	74904	120500	29	48.77
16	65562	110400	36	46.93

NOTE: Forging Procedure-Upset directly from ingot into special contour dies to hot-forged blank at temperature 1950 F; Forged under 2500-ton steam ress; solution-treated by quenching in water from 2200 F; cold-worked on 7500-ton press after heating to 1200 F; strain-relief annealed 1200 F for 10 hr; ir cooled.

endor's Analysis:

C	Mn	P	S	Si	Ni	Cr	Mo	N_2
0.09	1.40	0.022	0.018	0.96	25.50	16.86	6.30	0.15

FIG. 7 SURVEY OF BRINELL HARDNESS AND PHYSICAL TESTING OF WHEEL FROM SAME GROUP AS ITEM 1

heel, it was impossible to regulate the prestressing speed closely nough to secure the necessary amount of cold work without racking or bursting the wheel blank during the prestressing peration. (Items 27 and 29 show no advantage over item 28 hich was not prestressed. The probable reason is that the heels were not prestressed at a sufficiently high speed before machining.)

Grain Flow and Grain Refinement. The primary factor to be onsidered in obtaining the desired ductility throughout the heel blank was shown to be proper control of grain flow within e forging. Thus, other factors being equal, the more cometely radial that the flow lines within the wheel blank become, e higher the bursting speed should be. The use of billet stock smaller cross section insured a higher upset ratio and therefore ore complete reversal of the direction of the flow lines. This sulted in somewhat higher bursting speeds (see items 5, 8, and . Use of preformed ingots employed by vendor F entirely nitted the billet stage during forging and insured completely dial flow lines. This contributed greatly toward the fact that heels supplied by this vendor burst at the highest speeds of y tested (see item 1). However, no wheels processed to item were tested in a unit. Possible manufacturing difficulties, such machining and flash welding have been reported from other urces. Gyroscopic tests to determine the effect of radial-flow es at the stub junction have not been carried out.

In securing the proper grain flow, it seemed evident that precautions should at the same time be taken to insure sufficient grain refinement through enough hot-working to break up the dendritic structure. (Complete proof of this point is lacking, as no cast I-40 wheel was tested. However, cast wheels of other types made in the past have appeared to be inferior to forged wheels both in soundness and physical properties.) Thus in wheels upset from billet stock, the ratio of hot-working reduction from ingot to billet should be as great as is commercially practical. Maximum reduction ratio plus maximum upset ratio would produce maximum grain refinement and therefore should give the best type of forging which could be made from billet stock (see items 5, 8, and 9). Wheels in items 26 and 31 showed a notably dendritic structure in the center, indicating insufficient grain refinement. Consequently, bursting speed was below average and consistency of bursting speed was not particularly good. In this instance, dendritic structure as well as axial-flow lines at the center of the wheel just below the exit surface were due, at least in part, to prolonged contact with the comparatively cold lower hammer die which chilled the hot metal at this section and prevented proper flow under the hammer blows.

When the billet stage is eliminated by using the preformed ingot, allowance must be made for an additional amount of hot-working during actual die-forging of the wheel blank, to make up for the grain refinement which would ordinarily be obtained by

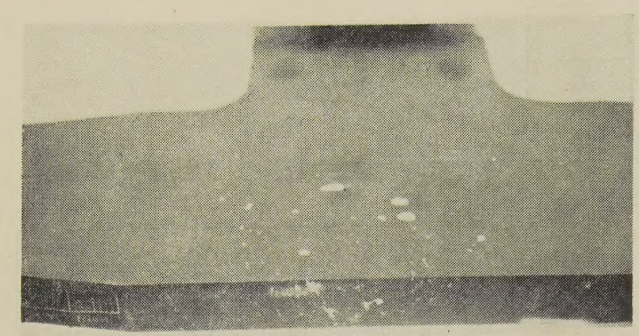

Fig. 8 Zyglo View of Axial Defects Showing Surface Indications

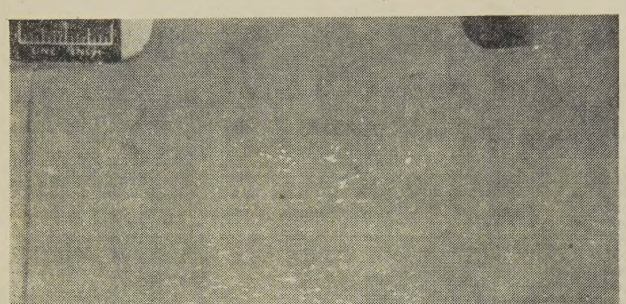

Fig. 9 Zyglo View Showing Defects Following Pattern of Grain Flow Within Forging

the conventional process of cogging the ingot down to a billet. This was ingeniously accomplished in the "center-reversal" process by means of press-forging with several sets of contour dies, molding the ingot into a wheel blank by alternate kneading of the center and rim of the forging. Chilling due to prolonged die contact was avoided because only one press blow was delivered after each time the blank was heated in the forging furnace. The advantages of this operation are that the total amount of grain refinement is at least comparable to that obtained by the conventional forging process, while at the same time the kneading forms the flow lines into the positions most advantageous for operating conditions. Item 10 tends to indicate that the substitution of conventional die-forging on this same type of wheel blank for the center-reversal process has seriously lessened the degree of grain refinement obtained and thereby decreased the bursting speed. Also, this wheel was not solution-treated, while all wheels forged by vendor F were given a solution treatment between hot and cold work.

Solution Treatment. Solution treatment consists of heating the metal to a temperature sufficiently high to dissolve the carbides and intermetallic compounds in an austenitic solid solution. Temperatures used for this purpose ranged from 2100 F to 2250 F for Timken alloy, and forgings were held at this temperature for at least 1 hr to allow sufficient time for solution to take place. In most cases the forgings were water-quenched from the solution temperature to cool the metal quickly through the precipitation range (approximately 1200 F to 1500 F). Precipitation (or aging as it is also called) is a fairly slow process, but due to th large mass of the I-40 wheel forging, it might occur on air-coolin in the center where it is least desirable because this portion woul cool most slowly. If precipitation occurs, these brittle carbid and intermetallic compounds are thrown out of solution and a apt to cause difficulties in the cold-working operation.

Solution treatment has been involved in several differe methods of processing Timken alloy wheels. In itself, it increa ductility and decreases hardness and strength. It also tends t equalize the variable conditions due to poor control over th finishing temperature during hot work. In order to recover th lost yield strength, subsequent treatments must be used whi cause the material to lose a large percentage of the ductili gained through solution treatment. In most cases the subs quent treatments cause a certain amount of precipitation to occu They involve either aging or cold work. Practices involvi solution treatment which were used during the program were a follows:

1 Solution-treated only (see item 28).
2 Solution-treated, strain-relief-annealed (see item 36).
3 Solution-treated, aged (see items 3, 13, and 16).
4 Solution-treated, hammer cold-worked, strain-relief-an nealed (see items 1, 2, 4, 12, 18, and 20).
5 Solution-treated, cold-worked by prestressing (see item 27 and 29).

For reasons concerning excessive stretch and low strength, a previously noted, the first two practices could never be used fo wheels actually operating in units. The third practice (solutio treatment plus aging) produces wheels with good ductility, te sile strength, and hardness almost equivalent to that obtaine in cold-worked wheels, but with yield strength intermedia between a purely solution-treated wheel and a cold-worked whe This practice resulted in consistent bursting speeds for the Ty I-40 wheel, but might not be adaptable to some other type o wheel which requires higher yield strength. It depends upon th precipitation-hardening principle. Modified Inconel alloy best adapted to this practice as its chemical composition includ certain elements which combine to cause a hard precipitate whi quickly raises the strength, while at the same time retaining very high ductility. Certain problems in welding this materi however, are still to be solved.

The fourth practice produces wheels with the highest yi strength, although the ductility depends upon a number of oth factors in the processing, notably the temperature at which th cold-working is performed. Practically all of those wheels whi were cold-worked were worked within the precipitation ran (1200 F to 1500 F). The higher temperatures were favored b the manufacturers because of less damage to forging equipme Precipitation is promoted by cold work, and metallograph study of wheels made in this manner showed dense precipitat especially in the grain boundaries which considerably lowere the ductility. It is possible that wheels cold-worked below th precipitation-temperature range after solution treatment woul have much better ductility. Actually, this is what has bee done in the fifth practice (prestressing) where the temperatu of cold work (only slightly above room temperature) is far belo the precipitation range. As has been previously noted, ou limited experiments in prestressing I-40 wheels were not to successful.

Most of the outstanding groups of wheels tested (both from th point of view of bursting speed and consistency of burstin speed) embraced solution treatment as part of the manufacturin process. The fact that solution treatment is also included in th processes which showed lower bursting speeds indicates that whe solution treatment is used in conjunction with certain benefici

actors of good processing, the bursting speeds are consistently igh, but that presence of these other factors is necessary for ood bursting speed, not solution treatment alone.

Foundry and Forge-Shop Practice. It has become fully evident om all of the historical data and test results accumulated during e bursting program that, in order to make good wheels, we must art with sound ingots. Vendors F and G used an electric arc keep ingot hot tops molten until the body of the ingot had lidified, thereby improving the soundness of their metal. None f the wheels made from this metal showed center defects. All of e vendors were careful about removing surface defects from the gots, by grinding, machining, or chipping methods.

Billet inspection included both zyglo for surface defects, and ched cross sections for the discovery of poor center conditions. upersonic inspection of billets was recommended, and some exerimentation was done, but this was not used as a production spection tool for this program. Vendor F, in eliminating the illet stage of manufacture, thereby eliminated a very serious urce of defects. Those vendors who used round billets took eavy machining cuts to remove the surface defects.

Vendors A and C developed special intermediate dies for preminary upset of the billets, which not only prevented twisting t also helped pack the metal at the ends of the billets, thereby oviding better grain refinement. In delivering only one press ow per forging heat, vendor F kept the metal hot and successlly avoided forging defects.

Vendor A used gamma-ray inspection and later installed a 000,000-v x-ray machine, thereby providing a means of detectg some types of serious internal defects.

Fig. 10 shows a disk type of defect which is undetectable by ray examination but is very readily located by supersonic inection.

Recapitulation. Summing up the conclusions presented, the ost important consideration is that sound wheels should be oduced from sound ingots (and sound billets, if forged by the nventional procedure). Good ductility is the best insurance at minor defects will not affect materially the bursting speed the wheel, other factors being equal. Good control over ain flow within the forging is the greatest step in the direction obtaining high over-all ductility in the plane of maximum ess. The proper use of solution treatment may be an addinal step in this direction. Conscientious use of the proper mbination of inspection procedures (zyglo and supersonic) ould prevent the use of any defective forgings. With this owledge available, future designers of this type of apparatus may perhaps be spared the tragedy of serious accidents.

It is hoped that a study of the information developed by this investigation may prove useful in the manufacture of other highly stressed rotating parts.

Acknowledgment

The author acknowledges the active participation of members of the Thomson Laboratory and Aircraft Gas Turbine Engineering Division (General Electric Company, River Works) during the execution of this investigation, as well as the excellent cooperation obtained from the vendors of forgings and alloy billet stock involved in the tests.

Special thanks are due to C. B. Haughton and B. A. Robbins of the Aircraft Gas Turbine Engineering Division, for their part in direction of the engineering aspects of this program, and to W. L. Badger and R. B. Johnson of the Thomson Laboratory, for their valuable advice on the metallurgical problems discussed in this paper.

Discussion

R. W. Andrews, Jr.[2] The benefits to be gained by press-forging in accomplishing more uniform cross-sectional working should tend to produce more uniform properties in the critically stressed hub area, provided the dies are heated to minimize loss of heat by conduction, and the entire forging cycle is performed at an adequate speed. To gain this advantage, a forging press is necessary of sufficient capacity to permit the use of closed dies. This action should be contrasted with that of a large forging hammer which delivers a large amount of energy at the surface of the work, tending to produce nonuniform cross-sectional working. In addition, the forging efficiency of the hammer must be considered since it depends upon the mass of the anvil, sow block, and attendant subbase. The number of blows required and the loss of heat during hammer-forging will influence materially the properties of the resultant forging.

The stress conditions represented in Figs. 2 and 3 of the paper are evidently those resulting from centrifugal forces only at room temperature. To these must be added the stresses which result from the temperature differential between the rim and the hub in normal operation so that the operating values would be approximately twice those shown on the curves. This further empha-

[2] Aluminum Company of America, Pittsburgh, Pa. Mem. ASME.

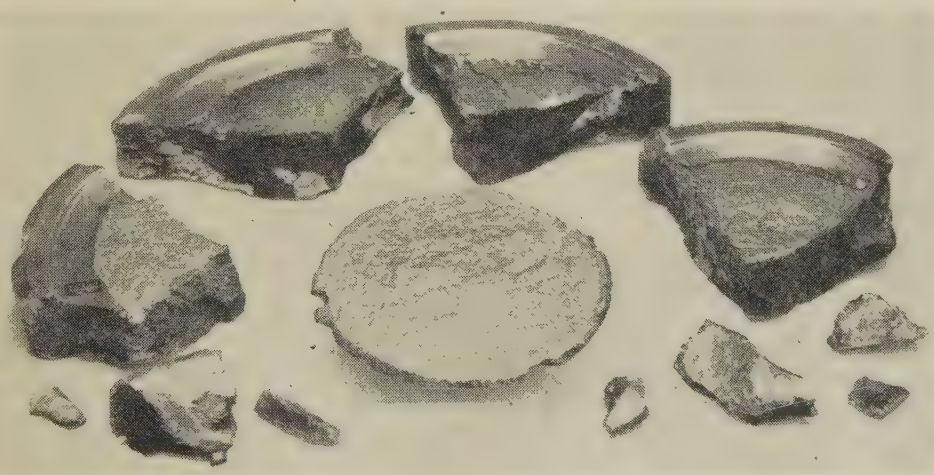

Fig. 10 Burst Fragments of I-40 Wheel Showing Disk Type of Crack

sizes the author's conclusion that ductility is of prime importance in the critical area of the hub.

The employment of nondestructive examination of the billets and forgings is a distinct advance. Further information on the interpretation and correlation of supersonic observations would be of interest, and it would be of value to know which of the five or more commercial types of supersonic devices was employed.

Supersonic examination can reveal defects which are so small as to be obscured by diffusion of x ray or gamma rays but, since it involves measurement of energy of so low an order of magnitude, its interpretation assumes great importance. Each alloy will behave in a different manner in this type of examination, and the sensitivity will vary with the frequency of the pulse. Except in the case of one fluid-immersed double-crystal device, only areas between essentially parallel surfaces can be explored successfully and, in the usual case of thin materials of 1 in. or less, the reflected pulse on the oscilloscope screen is obscured by the pattern of the initial pulse. To make a thorough examination, a number of observations must be made since each observation represents only the conditions in the path of the pulse, representing an area roughly the equivalent of the contact area between the oil, the object, and the searching crystal.

However, defects can be quite definitely located by triangulation and can often be identified in scope and character by this means.

C. A. Crawford.[3] It seems interesting that all four of the materials, CSA, modified inconel, 19-9-DL, and EME, showed a bursting strength higher than the majority of the forgings tested, but it is unfortunate that additional data have not been assembled on these other alloys as they obviously show much promise as wheel material.

It is particularly interesting that the materials, items 1, 3, and 6 in Table 2 of the paper, were graded as excellent with reference to consistency of bursting speed, which, obviously, is a requirement of prime importance.

The only part of this test work with which the writer has previously been familiar is the testing of the wheels in item 3. All concerned were favorably impressed with the remarkably close agreement in bursting speeds of the six wheels, all of which fell within 450 rpm, as stated in the text. This uniformity has been observed in the measurement of other physical properties of the age-hardenable material.

Quite a number of wheels of other designs have been forged from the same alloy as item 3 and its later modification, and many tensile-test specimens, both radial and tangential, have shown a high degree of uniformity among wheels from a number of different heats forged by two different forging firms.

In our opinion, the age-hardenable type of material is distinctly superior for rotor wheels subjected to high stresses.

The work reported by the author, obviously, represents a great expenditure of time and money and is a valuable contribution to the stock of information available to many engineers who are now interested in gas-turbine design.

Martin Fleischmann.[4] Reviewing the conclusions and recommendations made in this paper the following comments are offered under the same headings as used by the author:

Ductility. We agree with the author that a certain amount of center ductility in bucket wheels is desirable in order to distribute operating stresses and prevent stress concentrations due to minor mechanical and metallurgical irregularities. The value for cente ductility required in any particular application, however, seem open to discussion. As only very small stretch is allowed durin the operation of the wheel, high ductility could never be utilize fully in the sense that considerable plastic flow would be pe missible. The bursting speed of a bucket wheel may be influ enced by the ductility or plasticity of the material but depend mainly upon the effective yield strength. Unfortunately, it ha not been possible actually to correlate the yield-strength valu of the material with the bursting speed of bucket wheels, becaus quite often the internal residual stresses, introduced by the so-called "cold-working" of the forgings, are added to the stresse arising from rotation and yielding will occur sooner in regions o residual tensile stress. For this reason it may be well to examine the effect of the cold-working operation.

The mechanical properties and with them the bursting speed o the 16-25-6 wheels are largely controlled by the cold-working operation. It is of utmost importance that the shape of the forging prior to cold-working shall be of such dimensions that the cold work will produce a uniform flow of material from the center of the piece toward the rim. The amount of deformation should be uniform for each unit of the cross section. Cold-working between 5 and 15 per cent should be sufficient to assure high yield strength without too much sacrifice in ductility.

Grain Flow and Grain Refinement. We think that proper emphasis has been placed upon grain flow and grain refinement in relation to the quality of a wheel forging. The use of the smallest possible billet size and, if desired, the drawing out of the stub shaft prior to upset-forging will help materially in arriving at the proper grain flow, insuring best physical properties in the radial sections of the wheel. Additional steps in the hot-forging of the wheels may have to be incorporated to arrive at the best method of manufacture.

Solution Treatment. Although solution treatment will put the 16-25-6 alloy into its most ductile condition, the drastic water-quenching of such large sections is liable to create undesirably high stresses in the body of the forging. Since the heating and cold working in the usual temperature range of 1200 F to 1300 F will also cause more abundant precipitation in the grain boundaries when the alloy has been previously solution-quenched serious loss of malleability may develop while the cold working is in progress. In these circumstances, excessive amounts of cold working often result in cracking of the pieces.

These difficulties may be avoided simply by reheating the hot-worked forgings to 2000 F to 2150 F and allowing them to cool in air. Such an equalizing treatment has the added benefit of eliminating the incidental cold-working effects which occur during hot-forging, owing to chill on surfaces in contact with the dies and to variable low finishing temperatures.

J. Y. Riedel.[5] From the point of view of the manufacturer of forgings, the data presented are of great value because they enable a comparison of the relative value of so many different manufacturing techniques.

Our experience confirms the conclusion that the manufacture of sound forgings requires the production of sound ingots, particularly when the size of the forging is as large as the I-40 wheel or larger. This is undoubtedly due to the inherent character of the so-called superalloys, i.e., their high strength at high temperatures prevent the penetration of mechanical hot work so that the healing of voids is not as readily accomplished as with the lower strength ferritic alloys. We have observed that mechanical hot work is less effective, due to lack of penetration, when the work is done on a hammer than when it is done on a press.

[3] Development and Research Division, The International Nickel Company, New York, N. Y. Mem. ASME.

[4] Metallurgical Engineer, Steel and Tube Division, The Timken Roller Bearing Company, Canton, Ohio.

[5] Tool Steel Engineer, Bethlehem Steel Company, Bethlehem, Pa.

We are also in complete accordance with the conclusion that radial flow lines are desirable in the I-40 wheel. This goes back to one of the basic fundamentals of forgings, namely, that the flow lines should be in the direction of maximum stress.

In the author's second conclusion a comment is made as to the possible effect of radial flow lines in the stub shaft of wheels made by the "center-reversal" process. We would like to point out that there actually are no flow lines at all in the stub shaft. This is due to the fact that in this process the stub is cast on the ingot, and grain refinement is obtained by expanding and compressing the metal alternately in the stub, both radially and longitudinally. Thus the net effect is that the metal has received grain refinement by virtue of the hot-working without imparting directional flow lines. The stub is in exactly the same location in both the ingot and the finished forging.

With respect to the center-reversal process, as described under "Summary of Tests Made," it should be mentioned that the cold work was done on a 7500-ton forging press. This fact is recorded in Fig. 7 of the paper but not in the first description. This is important since it is impossible to cold-work an I-40 wheel on a 2500-ton press using full-contour dies.

The cold-work operation was the source of much trouble in the manufacture of I-40 wheels. The reason for this situation is readily understandable when the author tells us that prestressing of wheels by spinning in order to cold work them is impractical because ".....it was found that the critical portion of the cold work took place at a speed just below the bursting speed." The accurate development of this phase of manufacture was found equally difficult when working a 500-lb forging on a heavy press designed to forge ingots as large as 500,000 lb. The foregoing discussion merely points to the fact that the development of alloys or treatments which avoid the necessity of cold work would greatly facilitate the production of this type of forging.

A. O. Schaefer.[6] The results of the testing program described in this paper, yielded information quickly during an emergency period when it was badly needed. This information guided manufacturers in the improvement of their products and aided in the establishment of a system of nondestructive testing more adequate than had been used formerly.

Little issue can be taken with the author's conclusions. Sound ingots, sound billets, good ductility, and proper grain flow are desirable factors in all forgings. The difficulty in the present instance was occasioned by the relative unfamiliarity of the forging industry with working materials as refractory as these required for their high-temperature properties.

The author has rightly pointed out that the test procedure described evaluated forgings solely on the basis of their ability to withstand bursting stresses imposed by high-speed rotation. Other conditions must be met in service including temperature gradient, and the altered stress pattern resulting from the load on the blades, the mass of the blades themselves, and the welded-on shaft. The welding on of the shaft and the centering button also complicated matters.

The matter of solution treatment before cold-working was the basis of a discussion which has not yet been finally answered. The author has listed the various combinations of solution treatment, strain-relief-annealing, aging, cold-working, prestressing, and so on, which were tried. It is noted that cold-working was usually carried out at a temperature of 1200 F, which may be expected to result in minimum ductility. It would have been interesting to note the results of solution-quenching, followed by cold-working at either a lower temperature (1100 F, for example), or a higher temperature (1300–1400 F). Higher ductility might be expected in either case.

With regard to EME alloy, the author mentions the lack of data on rupture strength at 1200 F. Typical values of this, obtained after cold-working to a Brinell hardness comparable to that required for Type I-40 rotors, are as follows:

Stress to produce rupture at 1200 F	At 100 hr 49,800 to 59,500 psi	At 1000 hr 39,000–43,000 psi

It is interesting to note that no EME rotor forgings were made or tested which had been solution-quenched between hot and cold working.

The author and his company are to be congratulated for releasing information which furnishes us so much food for thought.

A. G. Holms.[7] The author has presented overwhelming evidence to show that forging practice is a major factor in determining disk strength, and that it is desirable to have the direction of forging deformation coincide with the direction of the important stresses. It is generally recognized that forming processes improve the mechanical properties of a material in the direction of forming, but the author states in his conclusions: "The outstanding conclusion to be drawn from this bursting investigation is that the most important factor contributing to high and consistent bursting speed is ductility." This statement is not a logical consequence of the author's published data. In his summary of tests made, the author says, "..... forgings from the same group as item 1 of Table 2 had by far the highest center ductility in spite of the fact that both yield and tensile strengths were equal to or higher than all of the other Timken alloy wheels sectioned." From this it appears that the higher tensile strength could be responsible for the better performance of item 1. In the next paragraph he says, "A sectioned forging representing those in the same group as item 3 exhibited slightly lower yield and tensile strengths but higher ductility than item 1." Here a material with greater ductility than item 1 burst at a lower speed. The explanation is apparently that the disks of item 3 had lower tensile strength than item 1. From the author's data it appears that a logical conclusion would be that the tensile strength was the controlling factor.

Author's Closure

Press-forging such as mentioned by Mr. Andrews was very successfully used by vendor F in the manufacture of the forgings tested in item 1. Uniformity in working was accomplished by use of several sets of carefully designed dies used in the proper sequence. Loss of heat was minimized by location of a specially designed forging furnace so close to the press that a manipulator could reach between the jaws of the press, lift out a forging slug, and deposit it immediately on the dies. Only one press blow was delivered per forging heat. A direct comparison can be made with hammer-forging by considering item 10, which was started in this manner and finished on a 35,000-lb steam drop hammer. Item 10 was definitely inferior.

We are aware that the stress conditions, represented in Figs. 2 and 3 of the paper, would be altered by additional stresses resulting from the temperature differential between the rim and the hub in normal operation. However, rather than becoming twice the values shown on the curves, we feel that the radial stresses would be increased more nearly 50 per cent during operation while the tangential stresses would actually decrease. Ductility in the critical area of the hub, as Mr. Andrews states, is of prime importance. The operating temperature at the center is not

[6] Executive Metallurgical Engineer, The Midvale Company, Nicetown, Pa.

[7] Engineer, Flight Propulsion Research Laboratory of the National Advisory Committee for Aeronautics, Cleveland, Ohio. Jun. ASME.

sufficiently high materially to alter the room-temperature ductility values.

The supersonic device used in this investigation was not a commercial machine but rather a laboratory model. It was an ultrasonic tester of the reflectoscope type, built by the Thomson Laboratory (General Electric Company, River Works) under special Sperry license for our own use only. It employed two Rochelle-salt crystals at a frequency of $^3/_4$ megacycle. A good description of supersonic inspection, as applied to the I-40 wheel forgings covered in this paper, has been written by the late R. S. Davidson of the Thomson Laboratory.[8] Further information on interpretation and correlation would be too lengthy to include here.

It is quite true that the actual interpretation of supersonic indications is of very great importance. We feel that the carrying out of the I-40 wheel-bursting program was a most excellent opportunity to further the accuracy of interpretation. We have found that while higher frequencies increase the sensitivity on this application, less divergence of the beam is encountered. Inspection of our I-40 wheels included a number of observations involving among others, scanning in different directions, i.e., axially through the hub from both opposite faces, axially through the rim at several locations, and radially through the entire diameter of the wheel blank.

Mr. Crawford's comments are in agreement with our conclusions. We also consider it unfortunate that additional data were not obtained on all of the alloys. The program was brought to a halt at the end of the war with the completion of perhaps less than half of the testing originally planned. Wheels not tested included several more variations in forging practice for Timken alloy, additional wheels made from CSA and 19-9-DL, as well as other alloys not mentioned in this paper, including low carbon N-155, Turbelloy No. 4, BSA, and low carbon 17-W.

Mr. Fleischmann comments that high ductility could never be fully utilized during operation because more than a small amount of plastic flow would not be permissible. However, it would seem that in cases of emergency, much less damage would be caused to a plane or its occupants by a distorted rotor which would act as a warning signal, than by sudden failure of a defective wheel. Considerable stretch could take place in an I-40 engine, being shown by roughness of operation, before actual failure of wheel or buckets would occur.

Mr. Fleischmann feels that the troubles caused by solution treatment outweigh the benefits it imparts. Our experience has shown the opposite to be true. During the past year, approximately 1500 supercharger wheels have been forged at the author's plant from 16-25-6 alloy using a full solution treatment between hot and cold work. These wheels have shown a consistently marked increase in center ductility over those previously made without using solution treatment as part of the forging practice. We have never found that solution treatment causes cracking to occur during subsequent cold-working, but rather that this has been sharply reduced by the use of solution treatment. The small size of the supercharger-wheel forging (60 to 65 lb) permits the use of air-cooling rather than water-quenching from the solution temperature. However, water-quenching was used in the manufacture of many I-40 forgings tested during the bursting program. Vendor F used it on all wheels made by that company without experiencing trouble. Vendor C, however, reported cracks due to water-quenching after solution treatment.

Mr. Riedel's comments on press-forging supplement those expressed by Mr. Andrews. Mention has been made in the text of the use of a 7500-ton forging press for cold work. His comments on grain refinement in the stub shaft are very enlightening.

Mr. Schaefer's comments are appreciated by the author. In regard to the rupture strength he has given for EME alloy, we have not been able to reproduce his figures. The highest 100-hr strength at 1200 F, which we could obtain from a wheel forging, was slightly in excess of 46,000 psi, as contrasted to an average of 48,000 psi, for similar tests on 16-25-6 alloy. Could it be that Mr. Schaefer's rupture-test specimens were taken from bar stock rather than from a forging? This often results in higher rupture strength.

Mr. Holms disagrees with the outstanding conclusion of the entire investigation, "that the most important factor contributing to high and consistent bursting speed is ductility." Like Mr. Fleischmann, he points out that the bursting speed depends mainly upon the strength of the material. As proof, he calls attention to the fact that the wheels in item 1 (of Table 2) burst at higher speeds than those in item 3, which had higher ductility but slightly lower yield and tensile strength. While these statements are quite true, the author feels that consideration should also be given to other factors (in addition to physical properties) in arriving at over-all conclusions. As an example, let us consider item 34 which had an average bursting speed of 19,701 rpm for six wheels which were tested. Physical tests made on another forging from this group showed both yield and tensile strengths to be higher than item 3 (which had an average bursting speed of 24,215 rpm), but center ductility to be very much lower (2.5 per cent average elongation for item 34, as compared to 22.5 per cent average elongation for item 3). Consistency of bursting speed was also much poorer for item 34, as it was in every other case of low ductility encountered throughout the investigation, e.g., following table:

RPM BURSTING SPEED

Item 3	Item 34
24035	17550
24035	19000
24130	19000
24275	19660
24400	21000
24415	22000

Nondestructive inspection of wheels in item 34 indicated defects not shown in item 3. Because ductility was low, these defects had a marked effect on lowering the bursting speed.

Numerous other examples could be cited but space does not permit. However, a confidential report to the Air Corps on this investigation considers each item in greater detail. In view of the fact that center ductility was the one property which showed any semblance of correlation with bursting speed, it was emphasized in this report as the outstanding factor contributing to high and consistent bursting speed.

[8] "Supersonic Flaw Detection Is Non-Destructive," by R. S. Davidson, *Industry and Power*, April, 1947, p. 79.

Heat Transfer by Free Convection From Heated Vertical Surfaces to Liquids[1]

By Y. S. TOULOUKIAN,[2] G. A. HAWKINS,[3] and M. JAKOB[4]

The present investigation deals with the study of heat transfer by natural convection from vertical cylindrical surfaces to water and ethylene glycol. The results are correlated within the laminar range for ($N_{Gr} \cdot N_{Pr}$) from $2(10^8)$ to $4(10^{10})$ according to the expression

$$N_{Nu} = 0.726(N_{Gr} \cdot N_{Pr})^{1/4}$$

and within the turbulent range for ($N_{Gr} \cdot N_{Pr}$) from $4(10^{10})$ to $9(10^{11})$ the correlation is best represented by the expression

$$N_{Nu} = 0.0674\,[N_{Gr}(N_{Pr})^{1.29}]^{1/3}$$

The foregoing correlations represent the experimental data with a mean deviation of 5.6 per cent and 3.5 per cent for the laminar and turbulent ranges, respectively. The ranges of some of the important variables involved in the tests are given in Table 1 of the text.

Nomenclature

The following nomenclature is used in the paper:

a = subscript stands for air
A_s = active surface area of test section, sq ft
$c = \left[\dfrac{g(t_s - t_m)}{4\nu^2 t_m}\right]^{1/4} \sim \dfrac{1}{\sqrt{\nu}}$, $ft^{-3/4}$
c_p = specific heat at constant pressure, Btu $lb_m^{-1}F^{-1}$
C = a dimensionless constant
f = a functional relationship
g = standard gravitational acceleration, ft hr^{-2}
G = subscript stands for ethylene glycol
h_c = mean heat-transfer coefficient of free convection, Btu $hr^{-1}ft^{-2}F^{-1}$
k = thermal conductivity, Btu $hr^{-1}ft^{-1}F^{-1}$
L = active height of test section, ft
n = exponent of dimensionless groups of numbers
N_{Gr} = Grashof number: $\left[\dfrac{L^3\rho^2 g\beta(t_s - t_m)}{\mu^2}\right]_f$
N_{Nu} = Nusselt number: $\left[\dfrac{h_c L}{k}\right]_f$
N_{Pr} = Prandtl number: $\left[\dfrac{c_p \mu}{k}\right]_f$
q_c = rate of heat transfer by convection, Btu hr^{-1}
q_l = parts of heat input not given up from active surface area of test section by free convection, Btu hr^{-1}
q_t = rate of total heat input, Btu hr^{-1}
t_s, t_m = temperature; test surface, fluid bulk, deg F
t_f = surface fluid-film temperature: $t_f = \dfrac{t_s + t_m}{2}$, deg F
v = velocity in vertical direction, ft hr^{-1}
W = subscript stands for water
x = vertical distance from lower edge of plane, ft
y = horizontal distance from plane surface, ft
φ, ξ = mathematical functions
ν = kinematic viscosity, ft^2hr^{-1}
β = thermal coefficient of cubical expansion, deg F^{-1}
ρ = density, $lb_m ft^{-3}$
μ = dynamic viscosity, $lb_m hr^{-1}ft^{-1}$

TABLE 1 RANGE OF EXPERIMENTS ON WATER AND ETHYLENE GLYCOL

Item	Symbol	Units	Maximum	Minimum
Surface height	L	ft	3.02	0.50
Surface temperature	t_s	deg F	239.0	90.5
Temperature difference	$(t_s - t_m)$	F	83.5	3.5
Total heat input	q_t	Btu hr^{-1}	4229.5	245.9
Total heat losses in per cent of input	$\frac{q_l}{q_t} \times 100\%$	—	8.5	3.1
Heat transferred by convection	$\frac{q_c}{A_s}$	Btu $hr^{-1}ft^{-2}$	1880	625
Coefficient of heat transfer by convection	h_c	Btu $hr^{-1}ft^{-2}F^{-1}$	151.0	17.6
Nusselt number	N_{Nu}	—	903.0	89.2
Grashof number	N_{Gr}	—	$326(10^9)$	$2.25(10^8)$
Prandtl number	N_{Pr}	—	117.77	2.43
Grashof number times Prandtl number	$(N_{Gr} \cdot N_{Pr})$	—	$904(10^9)$	$2.80(10^8)$

Introduction

The heat transfer by free convection from vertical plane surfaces, cylinders, and wires has been rather extensively studied in connection with gases but not for liquids. In fact, data on free heat transfer from vertical surfaces submerged in liquids are almost nonexistent, while only a scant amount of work exists on horizontal surfaces in liquids.

The present experimental investigation was undertaken to secure and correlate free-convection data in liquids. Its results not only should yield some practical information in this field, but also should be of a more general scientific interest.

Basic Considerations in the Design of Experimental Apparatus

Some of the factors of primary importance which had to be considered in the present investigation were the following:

1 The use of cylindrical surfaces against plane surfaces for test sections.

2 The minimum size of the liquid container in which the test section is placed.

3 The various heights of heated sections to be used in the experiments.

Although the use of a plane surface would have been preferable from the standpoint of general interest, thorough consideration led to the decision to use a cylindrical surface because of its over-

[1] Based on a doctorial thesis, Purdue University, Lafayette, Indiana, 1946, by one of the authors.[2]

[2] Assistant Professor, School of Mechanical Engineering, Purdue University, Lafayette, Ind.

[3] Westinghouse Research Professor of Heat Transfer, Purdue University. Mem. ASME.

[4] Nonresident Research Professor of Heat Transfer, Purdue University; Research Professor of Mechanical Engineering, Illinois Institute of Technology, and Consultant in Heat Research, Armour Research Foundation, Chicago, Ill. Mem. ASME.

Contributed by the Heat Transfer Division and presented at the Semi-Annual Meeting, Chicago, Ill., June 16–19, 1947, of The American Society of Mechanical Engineers.

Note: Statements and opinions advanced in papers are to be understood as individual expressions of their authors and not those of the Society.

whelming practical advantages over the plane surface. The most important advantages are as follows:

(*a*) A cylindrical test section can readily be prepared of standard pipe sections of any desired diameter.

(*b*) A cylindrical test section has edge losses on its two ends only and these can be considered as constant for any height of the test section. For a plane rectangular section, heat losses on all four edges have to be considered and the losses on the vertical edges increase with the height of the section.

(*c*) Uniform heating of a cylindrical section is easier to provide.

(*d*) A cylindrical section would require a smaller size of liquid bath. It also presents symmetry in any horizontal cross section.

Whereas the development of the boundary layer and its effect on heat transfer will not be necessarily the same for cylindrical and plane surfaces, the difference will be significant only if the radius of the surface curvature is relatively small. In a recent paper on forced convection from horizontal cylindrical surfaces, Jakob and Dow (1)[5] present a detailed discussion of this problem and arrive at some interesting conclusions. J. B. Carne (2) in an experimental study of the influence of diameter on heat transfer by free convection in air, develops a limited correlation according to which the difference in the coefficient of heat transfer for diameters of 2 in. and 3 in., is of the order of 0.5 per cent.

On the basis of all available evidence it can be stated that the results obtained in the present investigation on cylinders of 2.75 in. diam can be applied with reasonable certainty to plane surfaces of equal heights.

As this investigation is concerned with heated surfaces submerged in an unrestricted medium, it is necessary to ascertain the size of container such that the fluid thickness will be large enough to simulate this condition. This thickness should be larger than the sum of the thicknesses of the boundary layers developed on the test surface and the wall of the container. Estimates of this boundary-layer thickness for air are not too difficult to make; however, such is not the case for water and ethylene glycol. An attempt is made in the following manner to estimate whether the boundary layer on a vertical surface would be thicker or thinner for a liquid than for air. According to Schmidt and Beckmann (3) there exists a universal function

$$\varphi = \frac{v_x}{4\nu c^2 x^{1/2}} = f\left(\frac{cy}{x^{1/4}}\right) = f(\xi)$$

They show by experimental evidence that for values of the function $\xi \geqslant 4$ the velocity function becomes virtually negligible. Hence from the foregoing relationship

$$y = \frac{4x^{1/4}}{c}$$

is that thickness of the boundary layer beyond which the fluid velocity may be neglected, compared to the mean velocity of the boundary layer.

Assuming that $\nu_a \approx 9\nu_w$, then $y_a/y_w \approx 3$. Because $c^2\nu$ is nearly constant, hence φ and v_x are the same for air and water at any fixed height x. This would mean that for the same height x and the same temperature difference between the surface and the fluid, the boundary layer in water would be about one third that in air. However, it may well be that owing to the larger heat capacity of liquids, the flow of heat and the fluid velocity beyond $\xi = 4$ may still be appreciable in the case of liquids. Schmidt and Beckmann do not make any definite statements as to the influence of the Prandtl number in the solution of their differential equations. These equations have been numerically solved by Pohlhausen for $N_{Pr} = 0.73$ only, and Schmidt and Beckmann state that they should first be evaluated for larger Prandtl numbers before any definite conclusions can be drawn. Furthermore, the experimental results of Schmidt and Beckmann are not valid for surfaces higher than 2 ft. Hence the foregoing reasoning may be open to question.

As to the selection of the different heights of heated surfaces for the test sections, it was intended that both laminar- and turbulent-flow regions be covered in the tests. Taking the evidence presented by Griffiths and Davis (4) as a guide, it was felt that experiments with heights of 6 in. to 36 in. should cover the turbulent as well as the laminar-flow regions to be encountered in natural convection in liquids.

Description of Experimental Apparatus

Tests were conducted on vertical brass cylinders 2.75 in. OD and of three different heights, namely, 6 in., 18 in., and 36.25 in. These brass cylinders were supported between two other composite sections and mounted in an assembly frame where they were held in place under the pressure of a compression plate, Fig. 1. This assembly was placed at the center of a container 12 in. ID, thus leaving a radial distance of 4.625 in. between the surface of the test section and the inner wall of the shell. Each of the auxiliary composite sections, mentioned as supporting the active test section, consists of three parts, namely, an end cap, a lava section, and a brass section.

The end caps were made of transite board. Five thermocouples were placed symmetrically at three levels 0.5 in. apart, the first level being at the interface between the end-cap and the test section. The location of these thermocouples across the diameter of the end cap was so chosen that each would represent approximately equal concentric areas of the cross section of the end-cap

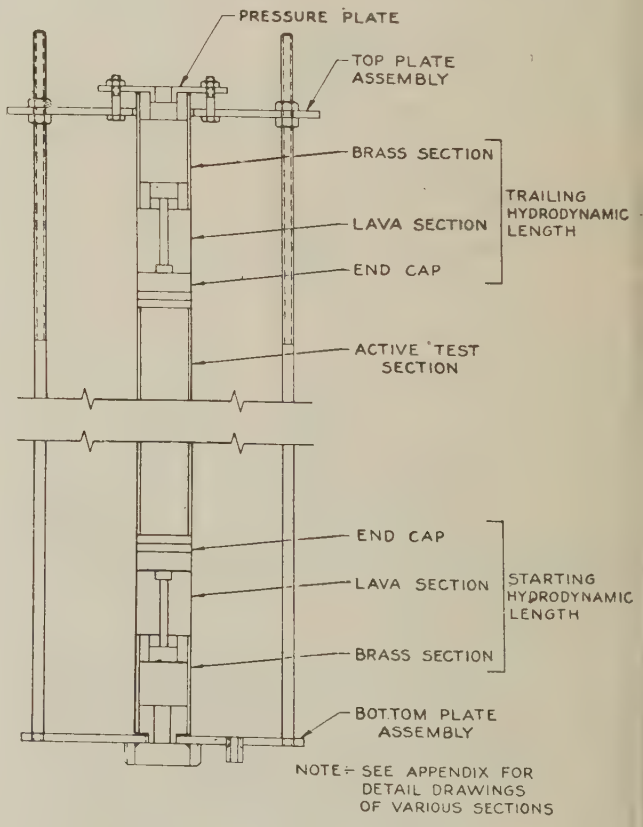

Fig. 1 Test-Section Assembly

[5] Numbers in parentheses refer to the Bibliography at the end of the paper.

With the 15 thermocouples thus located in each end cap, it was possible to make a thorough study of the temperature gradients in these sections in both the radial and axial directions. This information was used to compute the heat loss by conduction across the top and bottom end caps.

The lava and brass sections, while they provided a means for mounting the test section proper, also constituted the major part of the unheated hydrodynamic starting and trailing lengths (see Fig. 1). The function of these unheated lengths was to insure that the free convection currents enter and leave the test section parallel to the surface and not at an angle to it. These hydrodynamic lengths were kept constant with all three test sections.

The test sections were heated by means of electric heater elements, constructed of chromel-A resistance ribbon. Since it was necessary to maintain the surface temperature of the test sections uniform over their entire length, it was apparent that the heat input would have to be varied along the test sections. This was achieved, within practicable limits, by winding the 6-in., 18-in., and 36-in. heaters in one, two, and three independent sections, respectively. The power input to the various sections was controlled by separate variable-voltage transformers.

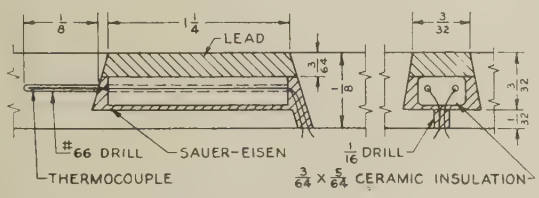

Fig. 2 Surface-Thermocouple Installation

Thermocouples used for the measurement of the surface temperatures were placed inside the wall of the brass pipe in order to avoid disturbances on the surface of the heated test sections. Slots were cut into the wall of the brass pipe and a hole was drilled at one end of this slot almost parallel to the surface of the pipe (see Fig. 2 for details). The thermocouples were then inserted into these holes and the wires brought out in an isothermal plane along the length of the slots for a distance of 1.25 in. before being taken out radially on the inside of the brass pipe. The thermocouple wires in the slots were protected by a ceramic insulator and held in place by Sauer-eisen. A strip of lead was pounded into the remaining recess in the slots, and the surface was made perfectly smooth. Three, five, and nine couples were used on the 6-in., 18-in., and 36-in. sections, respectively.

The axial and radial temperature distributions within the fluid bulk were measured by eight, twelve, and sixteen couples in the 6-in., 18-in., and 36-in-section tests, respectively. From the point of the junction the thermocouple wires parted vertically in opposite directions; they were held in place by special clamping devices once they were out of the fluid bath. By this method the thermocouple wires themselves served as their own means of support, thus making unnecessary any outside supports which would have interfered with the convection currents.

Test Procedure

The range of test-section surface temperatures covered was from 90 to 190 F in the water tests and 100 to 240 F in the ethylene-glycol tests. For each fluid the respective temperature range was covered in five, approximately equal, increments thus making five tests per fluid, per test section; or a total of 30 tests. Ample time was allowed in each test to reach steady-state conditions; this time varied from 6 to 24 hr, depending upon the height of the section, surface temperature, and the fluid under test. During this time the power input, surface temperatures, and some of the fluid bulk temperatures were observed at frequent intervals. When no change was found in the observations it was assumed that equilibrium was reached and six complete sets of readings were taken.

Computation Methods

The steady-state heat transfer by convection is given by the equation

$$q_c = A_s h_c (t_s - t_m)$$

In this equation all the terms are known through direct measurements, except h_c. The term q_c can be found by deducting from the measured value of the power input to the heater all heat dissipated in any form other than by free convection by the active test section. Heat losses occurred as follows:

(*a*) By conduction across top and bottom end caps.
(*b*) By conduction through electrical leads.
(*c*) By conduction through thermocouple wires passing through the top and bottom end caps.

Items (*a*) and (*b*) were taken into consideration only, while item (*c*) was ignored as it proved to be negligible.

The heat loss through the ends of the active test section was evaluated by a graphical method. The method depends upon the fact that the heat-flow lines must cross the isotherms at right angles (5). By an appropriate plotting of the isotherms for the end caps, the heat-flow lines were constructed in such a manner as to form curvilinear squares together with the isotherms. By this well-known technique the heat flow crossing the interface between the end of the test section and the face of the end cap was determined.

The heat loss by conduction through the electrical leads to the heater was calculated by the simple equation of conduction with the aid of data secured on the temperature gradients along the lead wires. Special auxiliary tests were conducted to secure these data.

In the correlation of the test results, the physical properties of water and ethylene glycol were taken at t_f. The thermal coefficient of cubical expansion β was evaluated on the basis of t_f and t_m.

Discussion of Results

The data on water and ethylene glycol are correlated according to Nusselt's equation

$$N_{Nu} = C(N_{Gr} \cdot N_{Pr})^n \qquad [1]$$

for $(N_{Gr} \cdot N_{Pr})$ within the range of $2(10^8)$ and $4(10^{10})$. This correlation leads to the values of $C = 0.726$ and $n = 1/4$ for the laminar boundary-layer case. The mean deviation within this range is 5.6 per cent and the maximum deviation 11.2 per cent, Fig. 3.

In the range of $(N_{Gr} \cdot N_{Pr})$ from $4(10^{10})$ to $9(10^{11})$, the data cannot be satisfactorily correlated by a single expression of Nusselt's type; however, separate correlations of the data on water and ethylene glycol give constants $C_W = 0.0778$ and $C_G = 0.0939$, respectively, with $n = 1/3$ in both cases, Fig. 4. Nusselt (6) in his theoretical paper indicates that in cases where the effect of viscosity can be neglected, data on various fluids can be satisfactorily represented by Boussinesq's correlation

$$N_{Nu} = C[N_{Gr}(N_{Pr})^2]^n \qquad [2]$$

If the fluid acceleration can be neglected (in free convection), then data on various fluids can be satisfactorily represented by Nusselt's correlation given by Equation [1]. Using Equation [2],

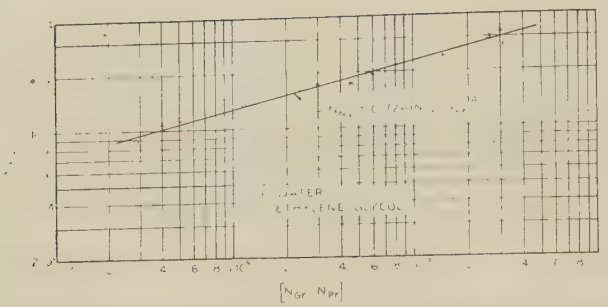

Fig. 3 Free-Convection Correlation for the Laminar Region

Fig. 4 Nusselt's Type Correlation for Free Convection for Turbulent Region

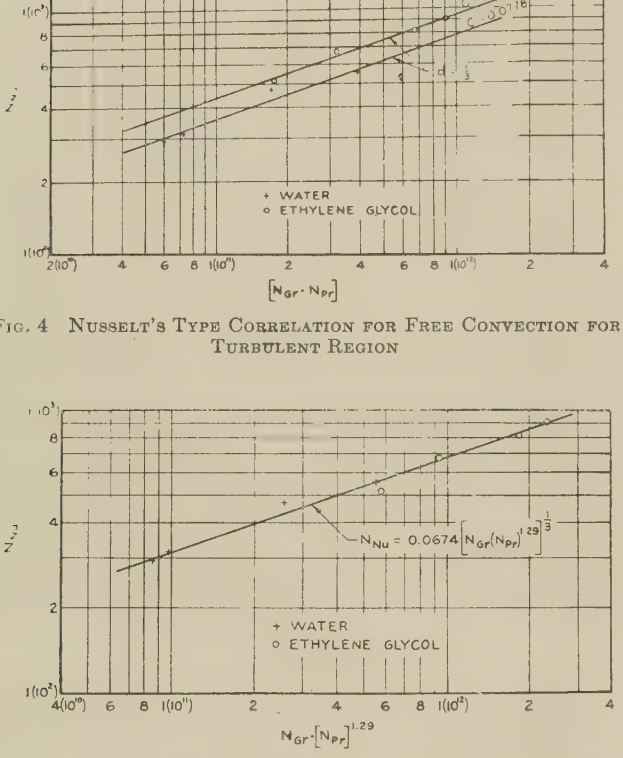

Fig. 5 Free-Convection Correlation for Turbulent Region

Beckmann (7) was able to obtain a single correlation for hydrogen, carbon dioxide, and air, while he obtained three separate correlations for these three gases using Equation [1]. Neither Equation [1] nor [2] led to a unique correlation of the data on water and ethylene glycol. Hence it was presumed that in the present experiments neither the fluid acceleration nor the viscosity can be entirely neglected and that N_{Pr} should have an exponent between 1 and 2. A plot of N_{Gr} versus N_{Pr} was made at constant N_{Nu}, on logarithmic paper, and the slope of the line was found to be 1.29. By using a correlation of the form

$$N_{Nu} = C[N_{Gr}(N_{Pr})^{1.29}]^n \quad [3]$$

it is possible to obtain a satisfactory correlation of the water and ethylene-glycol data in the turbulent boundary-layer range. This correlation leads to the values of $C = 0.0674$ and $n = 1/3$. The mean deviation within this range is 3.5 per cent, and the maximum deviation 9.5 per cent, Fig. 5.

The correlations presented in this work represent the data on water and ethylene glycol in a satisfactory manner. The mean deviations of 5.6 per cent and 3.5 per cent in the laminar and turbulent ranges, respectively, are of the same order of magnitude as the estimated probable experimental accuracy of 2 to 3 per cent, with a possible maximum of 5 per cent in a few extreme instances.

The authors do not know of any other data on free convection in liquids over vertical heated surfaces. However, King (8) presents a correlation of data on wires, horizontal and vertical cylinders, plates and bodies of other geometrical shape in gases and liquids, covering a range of $(N_{Gr} \cdot N_{Pr})$ from (10^{-4}) to (10^{12}). The portion of King's correlation corresponding to the range of the present investigation is reproduced in Fig. 6, together with the data of the various investigators on which King's correlation is based. King represents the data over the wide range indicated by a single curve; however, he observes: "It is probable that if more accurate data were available several curves could be plotted . . . . . and the curves for streamline and turbulent flow might be distinguished."

The data obtained in the present investigation are also shown in Fig. 6, together with Lorenz' (9) simple theoretical equation for laminar free convection. It is seen that for $(N_{Gr} \cdot N_{Pr})$ within the range of $2(10^8)$ and $4(10^{10})$ the results of the present investigation are in good agreement with the other experimental data shown in Fig. 6. Within this range the present data are correlated by Equation [1], with $n = 1/4$ and $C = 0.726$, while King's recommended curve is close to a straight line with $n = 1/3$. The constant $C = 0.726$ is appreciably higher than those predicted by existing theories which, however, have not been checked accurately by previous experiments on liquids. The fact that the present experiments lead to a higher value of C than the theory may be due to an unforeseen influence of the Prandtl number or to

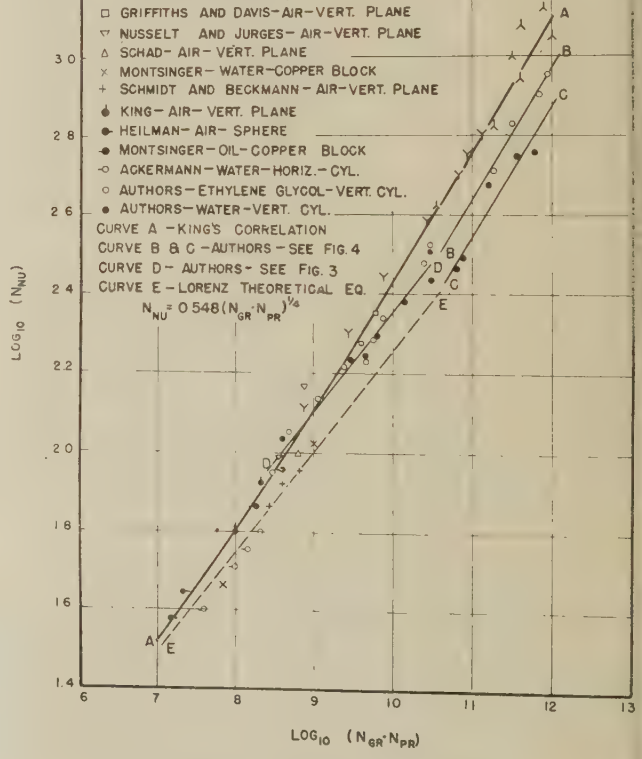

Fig. 6 Free Convection in Gases and Liquids

an additional effect upon convection of the large starting and trailing lengths used in the present experiments.

For $(N_{Gr} \cdot N_{Pr})$ above $4(10^{10})$, it is clearly seen from both Figs. 4 and 6 that two separate curves can be drawn through the results for water ($N_{Pr} \approx 3$ as an average) and ethylene glycol ($N_{Pr} \approx 40$ as an average). As previously explained, the correlation by a single curve is given in Fig. 5 (Equation [3]). Within this region King's curve is partly based upon data of Colburn which, according to King, were obtained for water flowing at low velocities (about 1 ips or less) in a long vertical 3-in. pipe. This condition can hardly be described as free convection. The nature of heat transfer with forced convection inside tubes, even at low velocities, is quite different from that on the outside of tubes by free convection. By free convection it is understood that the movement of the fluid is caused by virtue of the difference in density, hence by buoyant force only. On this basis the use of Colburn's data for the purpose of correlating free convection data is questionable. The points of Griffiths and Davis (4) for air over vertical cylinders which King has included in his correlation are also somewhat higher than the authors' for liquids. This may be due to the effect of the end caps of their cylinders as mentioned already by King.

Also there are some data available, obtained under boiling conditions, which may be compared with the present results. Jakob and Linke (10) conducted such experiments with water and carbon tetrachloride (CCl_4) and studied the heat transfer on a vertical heated plate 6 in. high × 1.38 in. wide. For moderate rates of boiling they found $C = 0.61$ and $n = 1/4$ for the laminar range. This value is 16 per cent lower than the present correlation corresponding to about the same range of $(N_{Gr} \cdot N_{Pr})$. It can be assumed that in their experiments a short range of turbulent convection existed between the state of moderate boiling and violent stirring action due to the vapor bubbles. Assuming $n = 1/3$ for turbulent convection, an estimate led to the values of $C = 0.10$ and 0.08 for water and carbon tetrachloride, respectively. These values, as those in the laminar region, are of the same order of magnitude as the constants C_W and C_G found for water and ethylene glycol in the present investigations.

Acknowledgment

The authors are indebted to the Purdue Research Foundation for making funds available for carrying out this work.

BIBLIOGRAPHY

1 "Heat Transfer From a Cylindrical Surface to Air in Parallel Flow With and Without Unheated Starting Sections," by M. Jakob and W. M. Dow, Trans. ASME, vol. 68, 1946, pp. 123–134.

2 "Heat Loss by Natural Convection From Vertical Cylinders," by J. B. Carne, *Philosophical Magazine and Journal of Science*, London, Edinburg, Dublin, vol. 24, series 7, 1937, pp. 634–653.

3 "Das Temperatur und Geschwindigkeitsfeld vor einer Wärme abgebenden senkrechten Platte bei naturerlicher Konvektion," by E. Schmidt and W. Beckmann, *Tech. Mech. Thermodynam.*, vol. 1, 1930, pp. 341–349 and 391–406.

4 "The Transmission of Heat by Radiation and Convection," by E. Griffiths and A. H. Davis, Department of Science and Industrial Research, Special Report No. 9, revised edition, H. M. Stationery Office, London, England, 1931.

5 "Heat Transmission," by W. H. McAdams, second edition, McGraw-Hill Book Company, Inc., New York, N. Y., 1942, pp. 16–18.

6 "Das Grundgesetz des Wärmeueberganges," by W. Nusselt, *Gesundheits Ingenieur*, vol. 38, 1915, pp. 477–490.

7 "Die Wärmeuebertragung in zylindrischen Gasschichten bei natuerlicher Konvektion," by W. Beckmann, *Forschung*, vol. 2, 1931, pp. 165–179.

8 "The Basic Laws and Data of Heat Transmission," by W. J. King, Trans. ASME, vol. 54, 1932, pp. 347–353.

9 "Über das Leitungsvermoegen der Metalle für Wärme und Electricitae," by L. Lorenz, *Annalen der Physik und Chemie* (Neue Folge), vol. 13, 1881, pp. 422–477 and 582–606.

10 "Der Wärmeuebergang beim Verdampfen von Fluessigkeiten an senkrechten und waagerechten Flaechen," by M. Jakob and W. Linke, *Physikalische Zeitschrift*, vol. 36, 1935, pp. 267–280.

11 "Introduction to Heat Transfer," by A. I. Brown and S. Marco, first edition, McGraw-Hill Company, New York, N. Y., and London, England, 1942, p. 111.

12 "The Analogy Between Fluid Friction and Heat Transfer," by Th. von Kármán, Trans. ASME, vol. 61, 1939, p. 705.

Discussion

R. C. Martinelli.[6] From a simple balance of buoyant and viscous drag (or acceleration) forces, it can be demonstrated that the Grashof modulus is directly related to the Reynolds modulus; in effect the Grashof modulus is a Reynolds modulus in which the velocity of flow is replaced by the variables which establish the flow velocity.

It has been shown by many authors that the best empirical correlation of turbulent forced-convection heat-transfer data is attained by means of a plot of N_{Nu}/N_{Pr}^n versus N_{Re} rather than a plot of N_{Nu} versus $N_{Re} \cdot N_{Pr}$. Therefore it is recommended that turbulent free-convection data be plotted as N_{Nu}/N_{Pr}^n versus N_{Gr} rather than the present system of plotting N_{Nu} versus $N_{Gr} \cdot N_{Pr}$.

Extrapolating from turbulent forced-convection data, the exponent n should lie in the neighborhood of 0.4. The authors indicate an exponent of $1.29 \times 0.333 = 0.43$ which appears quite reasonable.

Myron Tribus.[7] It would be of interest to know the *local* heat-transfer conductances as well as the averaged values. Since the authors indicate several sections were heated separately, perhaps they can compare their data with the following observation.

In turbulent flow, since the exponent of $1/3$ on Grashof's number causes the dimension L to drop out of the equations, no variation in heating intensity from top to bottom should occur.

In laminar flow, since by definition the *average* conductance is given by

$$h_a = \frac{\int_0^l h_x dx}{\int_0^l dx}$$

it should follow that the *local* conductance is given by

$$\mathrm{Nu}_x = \frac{3}{4}\,\mathrm{Nu}_{av} = 0.545\,(\mathrm{Gr} \times \mathrm{Pr})^{1/4}$$

Do the author's data confirm this?

Authors' Closure

May we express our thanks to Dr. Martinelli and Professor Tribus for their valuable comments. Dr. Martinelli's observation about the relationship between the Grashof and Reynolds numbers is well known to the authors, and has been discussed by A. I. Brown and S. M. Marco (11).

The authors have chosen to present their results in the form given in the present paper because in their opinion the results are more easily understood from a physical viewpoint if N_{Nu} is employed as ordinate, since it may be interpreted as a generalized coefficient of heat transfer or an apparent conductivity (12).

The interest shown by Professor Tribus in the local heat-

[6] General Engineering and Consulting Laboratory, General Electric Company, Schenectady, N. Y. Jun. ASME.

[7] Resident Engineer, University of California, Los Angeles, Calif.

transfer conductances is very well justified. However, to secure such data requires much more elaborate design of the experimental apparatus. In the present investigation the 6-in. test section had a single heater, the 18-in. test section had two 9-in. heaters, and the 36-in. test section had three 12-in. heaters. Hence in the opinion of the authors it would not be readily feasible to estimate the local coefficient with any degree of confidence. The fact that, as indicated in the paper, it was not possible to maintain a truly constant surface temperature even with the present multisectional heater arrangement will add to the difficulty of obtaining reliable predictions. It is the intent of the authors to continue the present studies and it is hoped that it may be feasible to redesign the present test apparatus so that data relating to point values for conductances may be obtained.

Review of Data on Dynamic Viscosity of Water and Superheated Steam

By G. A. HAWKINS,[1] W. L. SIBBITT,[2] and H. L. SOLBERG[3]

The authors have compiled the experimental data obtained by numerous investigators relative to the viscosity of water and water vapor. These data and the experimental methods have been evaluated and are discussed.

Introduction

THE viscosity values for water and steam are necessary to the solution of many fluid-flow and heat-transfer relations used by engineers. In heat-transfer work, for example, the viscosity factor appears in the Prandtl and Reynolds numbers.

A survey of the literature reveals a lack of agreement between various investigators in so far as values for the viscosity of steam are concerned. In order to summarize the data so that the engineer may select those which he feels are most reliable, this review has been prepared. The subject matter will be divided into three general sections, as follows: (*a*) The viscosity of the saturated liquid; (*b*) the viscosity of the subcooled or compressed liquid; and (*c*) the viscosity of the vapor.

The lack of agreement between independent investigators is not surprising, when one considers the enormously difficult experimental problems which confront experimenters pursuing research work dealing with the determination of the viscosity of saturated liquids and superheated vapors.

Viscosity of the Saturated Liquid

All of the existing data which are known to the authors have been plotted in Fig. 1. All of the data are in agreement up to 620 F. Beyond 620 F and up to the critical, serious disagreement exists. For most engineering purposes the following relation may be used for computing the viscosity of the saturated liquid between 212 F and 620 F

$$\mu = \frac{-2.185}{1 - 0.04012t - 0.0000051547t^2}$$

when t is in deg F, and μ in centipoise units.

For temperatures between 0 F and 212 F, and at atmospheric pressure, values may be obtained from Table 1, which was compiled by Dorsey (12).[4]

Viscosity of the Subcooled or Compressed Liquid

Sigwart (9), Hawkins, Solberg, and Potter (7), and Timroth (26) conducted experiments to determine the viscosity of subcooled or compressed water. The Purdue University investigators found that pressures up to 3500 psia had little influence at four different temperatures. Sigwart found that pressure influenced the viscosity. At a temperature of 212 F and pressure of 4408.8 psia the viscosity was approximately 21 per cent higher than that at the saturation condition. At 572 F and 4408 psia the increase in viscosity over that at the saturation pressure was about 7.22 per cent. For the same high pressure the increase was approximately 16.7 per cent at a temperature of 662 F. Timroth (26) found that the pressure influenced the viscosity less than that found by Sigwart. The results obtained by Sigwart and Timroth are compared in Fig. 2. Bridgman (13) found that

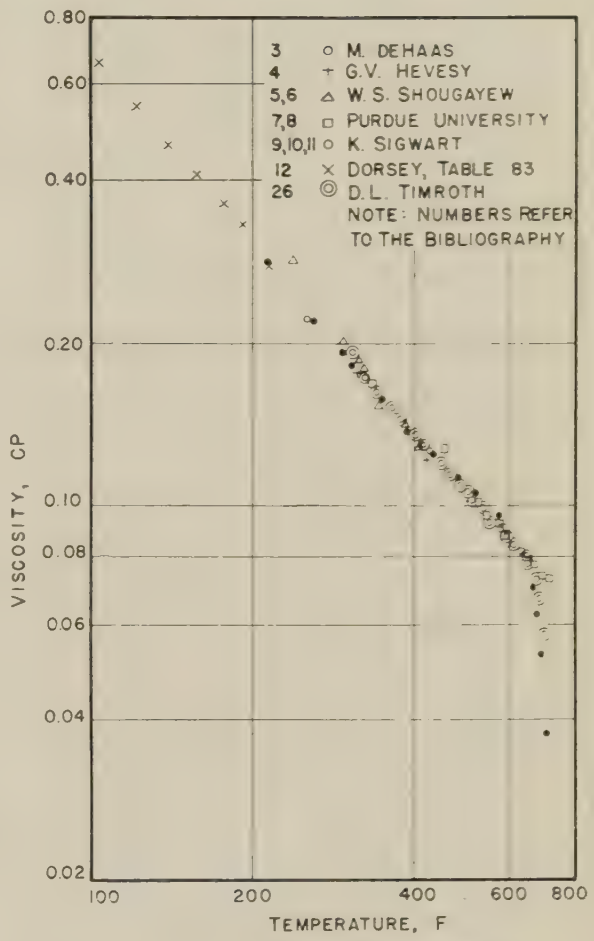

Fig. 1 Viscosity of Saturated Water

TABLE 1 VISCOSITY VALUES FOR WATER

Temperature, deg F	Viscosity, centipoises
32	1.794
50	1.310
68	1.009
86	0.800
104	0.653
122	0.549
140	0.470
158	0.407
176	0.357
194	0.317
212	0.284

[1] Westinghouse Research Professor of Heat Transfer, Purdue University, Lafayette, Ind. Mem. ASME.

[2] Senior Engineer, Clinton Laboratories, Oak Ridge, Tenn. On leave of absence from Purdue University. Jun. ASME.

[3] Head, School of Mechanical Engineering, Purdue University. Mem. ASME.

[4] Numbers in parentheses refer to the Bibliography at the end of the paper.

Contributed by the Heat Transfer Division and presented at the Semi-Annual Meeting, Chicago, Ill., June 16–19, 1947, of The American Society of Mechanical Engineers.

Note: Statements and opinions advanced in papers are to be understood as individual expressions of authors and not of the Society.

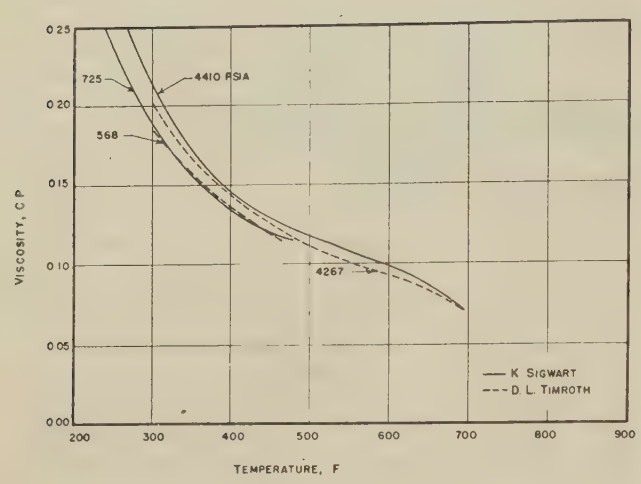

FIG. 2 COMPARISON OF DATA ON EFFECT OF PRESSURE ON VISCOSITY OF WATER

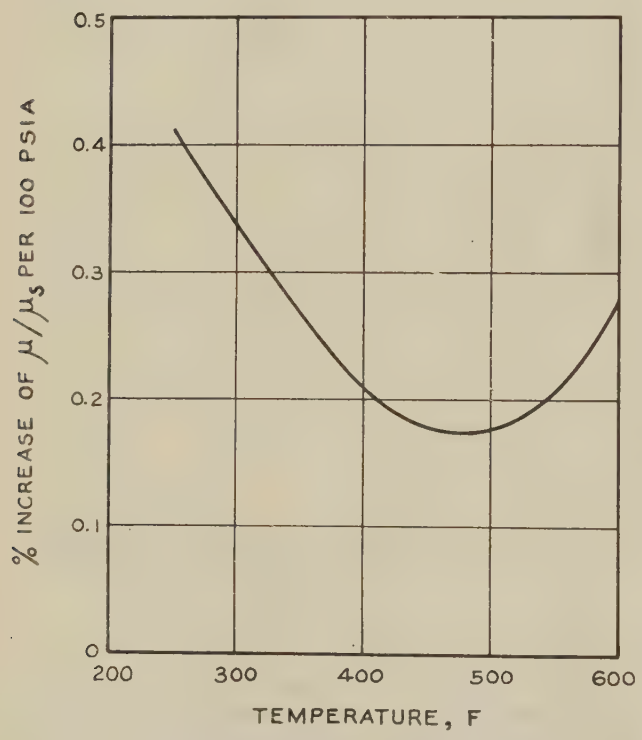

FIG. 3 RECOMMENDED RATIOS FOR VISCOSITY OF SUBCOOLED WATER

at 167 F the increase in viscosity between 0 and 1000 atm was less than 10 per cent, or less than 0.01 per cent per atm.

Until additional data are available, Fig. 3 may be used for computing the viscosity of a subcooled liquid between the temperatures of 250 F and 600 F. The data used for establishing the figure are those of Sigwart.

VISCOSITY OF WATER VAPOR

The following data are now available from seven different experimental investigations of the viscosity of water vapor:

1 Speyerer (14) in 1925.
2 Schougayew (16) in 1933.
3 Schiller (18) in 1934.
4 Hawkins and co-authors (7) in 1935.
5 Sigwart (9) in 1936.
6 Hawkins and co-authors (20) in 1940.
7 Timroth (26) in 1940.

The data are in good agreement for the viscosity at 1 atm pressure over a wide temperature range. However, large differences were reported for the pressure coefficient of viscosity by the various investigators.

In 1925, H. Speyerer (14), a student of Professor Nusselt, measured the viscosity of steam over the range 212 F to 662 F and pressures from 1 atm to 146.06 psia. Speyerer employed a brass capillary-tube viscosimeter, the tube of which was 2.4 meters long and had an internal diameter of 2 mm. The constant-pressure lines when plotted are straight and come closer together with decreasing pressure. Speyerer found that the Sutherland (15) equation expressed the experimental results in a satisfactory manner. Speyerer avoided the necessity of making correction for end effects by using the middle portion of the capillary to ascertain the pressure drop. The effect of this technique upon the flow conditions was not known. Inaccuracies in the pressure-drop readings may have occurred due to vapor condensation in the lines to the manometer legs.

Schougayew (16, 17) measured the viscosity of steam up to a pressure of 1367 psia and a temperature of 752 F by means of a capillary of the Rankine type. Schougayew found that the viscosity was independent of pressure (a function of temperature only), as reported in Table 2.

TABLE 2 VISCOSITY OF DRY SATURATED AND SUPERHEATED STEAM

Temperature, deg F	Viscosity, centipoise
212	0.0125
302	0.0145
392	0.0163
482	0.0183
572	0.0202
662	0.0222
752	0.0241

The Rankine method may introduce effects of unknown magnitude at high temperatures and pressures. The leaching action of the water vapor on the glass may have influenced the results. Constant temperature conditions were not maintained during an experiment.

Schiller (18) published data on the viscosity of steam for pressures up to 440 psia and temperatures up to 539.6 F. These measurements were made by use of a calibrated discharge nozzle. Schiller developed this interesting method in order to avoid the difficult experimental measurement of small pressure differentials at high pressures. He assumed that the viscosity of water was known. Then he evaluated the viscosity of steam in relation to that of water by determining the velocity at which the discharge coefficient of a nozzle shows an abrupt increase for water and for steam and then equating the two Reynolds numbers. This unique method is indirect and involves a number of factors which may produce unknown effects upon the experimental results.

Hawkins, Solberg, and Potter (7) (1935) used a Lawaczeck viscosimeter to determine the viscosity of steam at pressures up to 3500 psia. Essentially, they measured the time of fall of a cylindrical body in an accurately bored cylinder containing a fluid of known viscosity, and then measured the time of fall of the same body when the cylinder contained water or steam under test conditions. The measurements of pressure, temperature, and time were made with great care. However, it has been shown that viscosimeters of this general type are not suitable for use in the turbulent range with gases. If the unknown fluid has a viscosity-density isotherm differing greatly from that for the calibrating fluid, then large errors may be introduced, especially in the high-pressure range. An examination of the data reported indi-

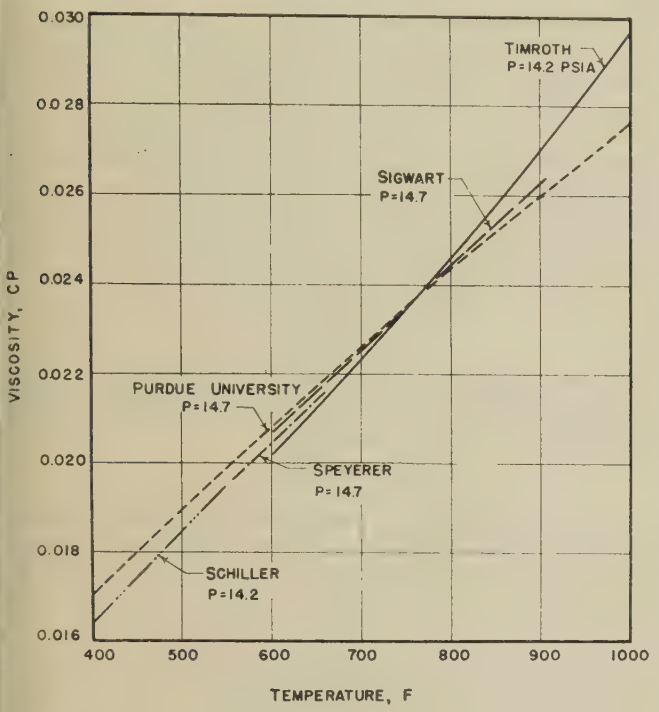

Fig. 4 Comparison of Data on Superheated Steam at 1 Atm

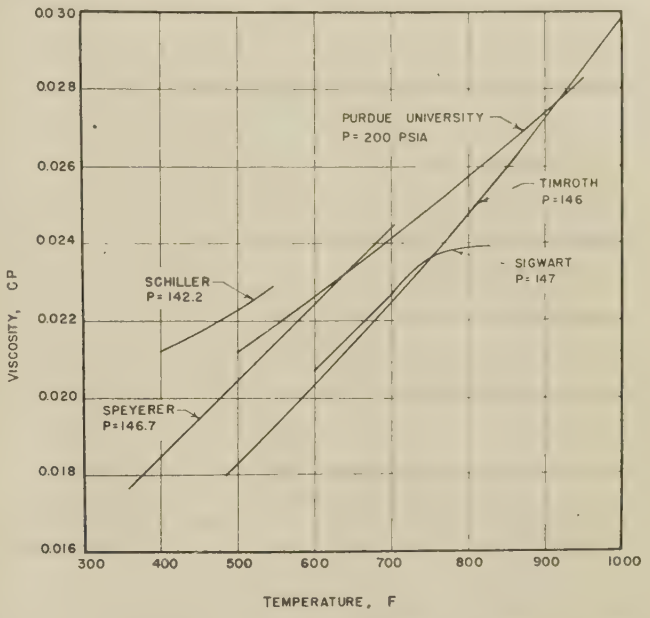

Fig. 5 Comparison of Data on Superheated Steam at Pressure of Approximately 150 Psia

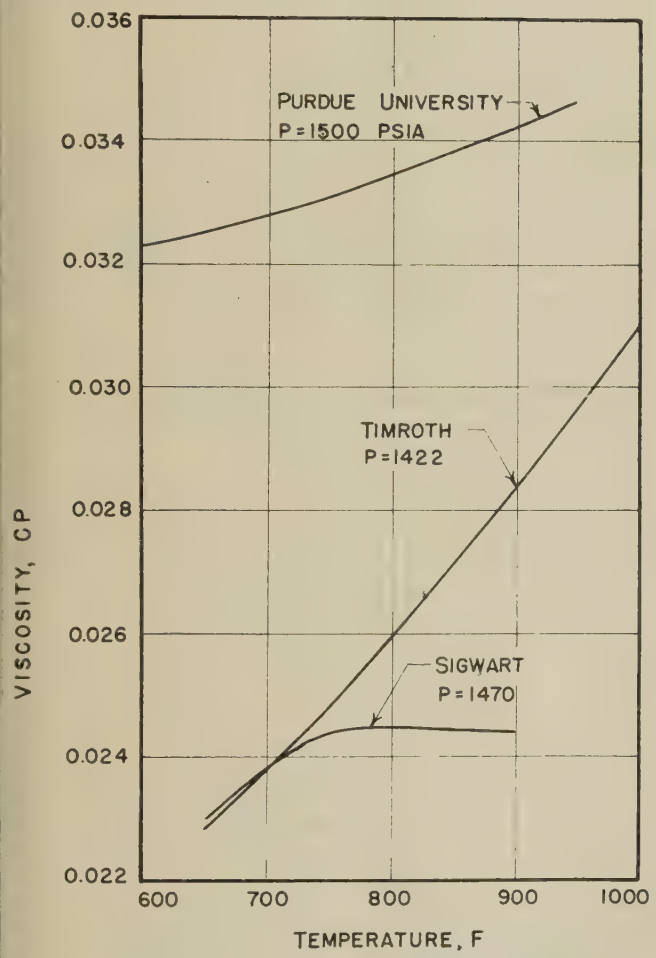

Fig. 6 Comparison of Data on Superheated Steam at Pressure of Approximately 1400 Psia

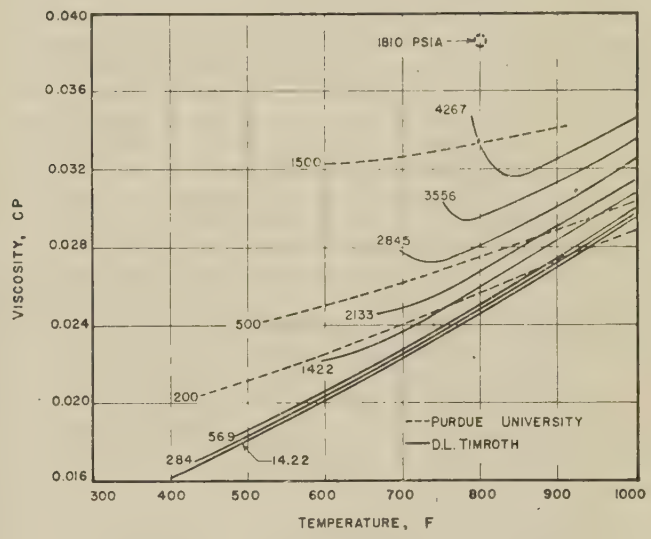

Fig. 7 Comparison of Data on Superheated Steam by D. L. Timroth and Purdue University

cates that, in general, viscosity values obtained by this experimental method are unduly high. If these reported viscosity values were high, then a considerable portion of the Reynolds numbers exceeded the critical value during these experiments. It would appear that the theory of the Lawaczeck viscosimeter has not been sufficiently developed to the point where it is acceptable for evaluating the viscosity of vapors and gases in the high-pressure regions, unless it has been calibrated with a fluid of viscosity-density isotherms nearly identical to that of the fluid which is to be evaluated.

Sigwart (9) reported measurements of the viscosity of water vapor reaching into the critical region. The viscosity was evaluated from the pressure loss, measured with a pressure balance, for the fluid in laminar flow through a straight capillary. Sigwart used the entire length of the capillary (approximately 14 in.) to obtain a pressure drop which was measured on a ring

balance. Consequently, it was necessary to correct for the pressure-drop effects at the ends. The data reported indicate that the pressure drops measured were in the range of 0.184 to 0.247 in. Hg, and the possible accuracy was to 0.00197 in. Hg. These tests by Sigwart were carried out with the greatest care; however, it is not evident that the variable physical states of the fluid in the manometer legs did not affect the pressure-drop readings. If these conditions did produce errors, it is probable that they would not be systematic errors. If the pressure-drop measurements were as accurate as reported, then no satisfactory explanation of the surprisingly low pressure coefficient of viscosity can now be made.

As a consequence of the disagreements in the determination of the viscosity, Hawkins, Solberg, and Potter (20) chose a different experimental method to check the results of their earlier investigation (7). They used the steady-flow capillary method as exploited by Speyerer. A thick-walled nickel capillary 103.2 ft was used; consequently, the corrections for end effects were negligible. The differential mercury manometer was connected to the capillary in such a way as to avoid the variable physical state of the fluid in the vertical manometer legs. The rather large pressure drops were measured by making a radiograph of the high-pressure differential mercury manometer. The constants in the viscosity equation were obtained from calibration tests with nitrogen and water; consequently, the final values for the viscosity of steam were independent of the numerical values of the physical dimensions of the capillary, if these dimensions did not change during the experiments. Deformation of the cross-sectional area of the capillary due to bending was found to be negligible. The effect of curvature of the coil was established by calibration tests. Partial corrections were made for the effect of high temperatures upon the physical dimensions of the capillary. However, corrections for the effect of high pressures upon the deformation of the cross-sectional area may have been necessary in spite of the heavy capillary wall (0.25 in. OD $\times$ 0.09294 in. ID.)

Timroth and Vargaftik (19) published a critical analysis of the available data for the viscosity of steam. It was shown that the extrapolation of Sigwart's data might have been erroneous. Values of the viscosity of steam were calculated for temperatures up to 1022 F and pressures up to 250 atm on the basis of theoretical works of viscosity.

Timroth (26) published extensive data relative to the viscosity of steam in 1940. In the experiments Timroth used a short capillary tube and measured the pressure drop by means of a special ring balance.

The agreement at atmospheric pressure and disagreement at higher pressures of the various data are shown in Figs. 4, 5, 6, and 7. Discussions of the various investigators have been presented in the literature (10, 21, 22, 23, and 27).

Conclusions

The data accumulated by numerous investigators on the viscosity of saturated water are in excellent agreement except in the vicinity of the critical region (620 F up to the critical point). It is obvious that the experimental problems are vastly multiplied as the critical point is approached; consequently, high precision may be difficult to obtain in this region.

All experimental data on the viscosity of compressed liquid water indicate that the increase with pressure is small for the range of industrial pressures. The experimental data agree only as to the order of magnitude of the pressure coefficient of the viscosity, thus more work is needed to obtain accurate data in this region. The actual errors in these experimental values are small; consequently, they are satisfactory for most design work.

Serious disagreement exists in the data for the viscosity of water vapor, as determined by the various investigators. The vapor region needs to be investigated further. This field of research remains as a challenge to investigators. The research workers at Purdue University are now undertaking a new investigation which will cover the determination of the viscosity of superheated steam and other vapors.

Until such time as order can be brought out of chaos, the extensive values of the viscosity of steam as published by Leib (25) (based upon the data of Hawkins and co-authors) and those of Timroth are available for those who wish to use them.

Acknowledgment

The authors wish to express their appreciation to Mr. G. H. Van Hengel and to Dr. Max Jakob for their suggestions during the preparation of this paper.

BIBLIOGRAPHY

1 "Standard Substances for the Calibration of Viscometers," by E. C. Bingham and R. F. Jackson, Bulletin, Bureau of Standards, vol. 14, 1918–1919, pp. 59–86.

2 "Steam Research in Europe and America," by M. Jakob, *Engineering*, London, England, vol. 132, December 11, 1931, pp. 744–746.

3 Communication From the Laboratory of Physics at the University of Leiden, by M. de Haas, no. 12, 1894.

4 "Die Beweglichkeit der Ionen, die dem Lösungsmittel eigen sind," by G. von Hevesy, *Zeitschrift für Elektrochemie*, vol. 27, 1921, pp. 21–24.

5 "Experimental Data and the Interpolation Formula for the Viscosity of Water," by W. S. Schougayew, Izvestiva, VTI, No. 7, 1934, pp. 47–49.

6 "Viscosity of Water at Temperatures Above 100 Deg," by W. S. Schougayew, *Journ. Exp. i. Theor. Phys.* (U.S.S.R.), vol. 4, 1934, pp. 760–765.

7 "The Viscosity of Water and Superheated Steam," by G. A. Hawkins, H. L. Solberg, and A. A. Potter, Trans. ASME, vol. 57, 1935, pp. 395–400.

8 Discussion of reference (7), Trans. ASME, vol. 58, 1936 pp. 258–262.

9 "Messungen der Zähigkeit von Wasser und Wasserdampf bis ins kritische Gebiet," by K. Sigwart, *Forschung auf dem Gebiete des Ingenieurwesens*, vol. 7, 1936, pp. 125–140.

10 "Zähigkeit von Wasser und überhitztem Dampf," by K. Sigwart, *Forschung auf dem Gebiete des Ingenieurwesens*, vol. 7, 1936, pp. 310–311.

11 Discussion of reference (23), by K. Sigwart, *Forschung auf dem Gebiete des Ingenieurwesens*, vol. 10, 1939, pp. 101–102.

12 "Properties of Ordinary Water-Substances," by N. E. Dorsey, Reinhold Publishing Company, New York, N. Y., 1940.

13 "The Physics of High Pressure," by P. W. Bridgman, The Macmillan Company, New York, N. Y., 1931.

14 "Die Bestimmung der Zähigkeit des Wasserdampfes," by H. Speyerer, *Forschungsarbeiten auf dem Gebiete des Ingenieurwesens*, No. 273, 1925.

15 "The Viscosity of Gases and Molecular Force," by W. Sutherland, *Philosophical Magazine*, vol. 36, 1893, pp. 507–531.

16 "Zähigkeit des Wasserdampfes bei Hohen Drucken," by W. S. Schougayew, *Physikalische Zeitschrift der Sowjetunion*, vol. 5, 1934, pp. 658–665.

17 "The Viscosity of Steam at High Pressures," by W. S. Schougayew, *Journ. Exp. i. Theor. Phys.* (U.S.S.R.), vol. 3, 1933, p. 247.

18 "Bestimmung der Zähigkeit von Wasserdampf," by W. Schiller, *Forschung auf dem Gebiete des Ingenieurwesens*, vol. 5, 1934, pp. 71–74.

19 "On the Viscosity and Heat Conduction of Steam at High Temperatures and Pressures," by D. L. Timroth and H. B. Vargaftik, *Journal of Technical Physics* (U.S.S.R.), vol. 9, 1939, pp. 461–469 (in Russian).

20 "The Viscosity of Superheated Steam," by G. A. Hawkins, H. L. Solberg, and A. A. Potter, Trans. ASME., vol. 62, 1940, pp. 677–688.

21 "Zähigkeit von Wasserdampf," by W. Fritz, *Zeit. V.D.I.*, vol. 79, 1935, pp. 792–793.

22 "Zähigkeit des Wasserdampfes," by G. Ruppel, *Forschung auf dem Gebiete des Ingenieurwesens*, vol. 6, 1935, pp. 155–156.

23 "Zähigkeit von Wasserdampf," by H. Speyerer, *Forschung auf dem Gebiete des Ingenieurwesens*, vol. 10, 1939, pp. 100–102.

24 "The Viscosity of Gases at High Pressures," by E. W. Comings, B. J. Mayland, and R. S. Egly, University of Illinois, Engineering Experimental Station, Bulletin No. 354, 1944.

25 "The Viscosity of Steam," by E. F. Leib, *Combustion*, vol. 12, December, 1940, p. 45.

26 "Determination of Viscosity of Steam and Water at High Temperatures and Pressures," by D. L. Timroth, *Journal of Physics* (U.S.S.R.), vol. 2, 1940, pp. 419–435.

27 "The Engineers' Digest," by D. W. Rudorff, American edition, vol. 3, 1946, pp. 367–370.

Discussion

E. W. Comings.[5] The authors have pointed out the experimental difficulties encountered in the determination of the viscosity of steam, especially in the vicinity of the critical region. These difficulties are in large measure due to the relatively high critical temperature of steam and its effect on the precision of the experimental measurements. This situation, together with the large disagreement between the results of different investigators, indicate the need for additional criteria for judging the accuracy of experimental data. An infallible criterion is probably not available but several useful ones are worth mentioning. These are as follows:

1 The existence of turbulence as predicted by Reynolds number is an indication of questionable results. Conditions selected to insure laminar flow at low pressures and also near the critical pressure frequently result in turbulent flow at intermediate pressures.

2 The ratio of the viscosity of steam at an elevated pressure to its viscosity at 1 atm and at the same temperature should be expected to increase with pressure to an extent somewhat comparable with other gases and vapors. This ratio for all other vapors increases rather slowly with pressures for temperatures below the critical up to 1.3 to 1.5 until the pressure approaches the critical pressure. The ratio then increases rapidly with pressure (for temperatures just above the critical) to 3 to 4 and higher (24). Results which differ widely from this general behavior should be questioned.

3 The foregoing indicates that a graph of a viscosity isotherm is useful in evaluating experimental data. Such a graph should extrapolate smoothly from high pressure to the viscosity values at 1 atm.

4 It need not be mentioned here that careful consideration should be given the precision of the measurements. The determination of small pressure differentials, flow rates, and apparatus constants are likely to be troublesome and should be corrected for both pressure and temperature effects when necessary. It is particularly noteworthy that the viscosity is related to the fourth power of the radius of the flow tube, and minor changes in this dimension are greatly magnified in the results.

Separate examples of published data on the high-pressure viscosity of other gases as well as steam can be cited where each of the foregoing points has been overlooked.

[5] Professor of Chemical Engineering, Chemical Engineering Division, University of Illinois, Urbana, Ill.

G. H. Van Hengel.[6] In this excellent survey on the viscosity of steam and water, we may conclude that two series of data are now available for superheated steam, viz., those by Purdue University and those by Timroth. The first series were based upon test data on a very long capillary tube; the second series on a very short one. These data on superheated steam agree very well for steam at atmospheric pressure, but at 1500 psi, the Purdue University values are 25 per cent higher than the Timroth values. Some new experiments seem to be necessary to get a better agreement, but as long as no agreement exists one or the other set of data has to be chosen.

In some private correspondence with Prof. G. A. Hawkins, the writer found in the original paper two complete tables on the viscosity of superheated steam, which would be very useful to all engineers for flow and heat-transfer problems. The writer would like to see these tables published, especially the one of Timroth's data, as they are not easy to obtain and were recalculated from the metric into the English system.

Author's Closure

The authors thank Professor Comings for his excellent discussion dealing with viscosity determinations. Mr. Van Hengel's interest and co-operation in the preparation of this paper are deeply appreciated. The tables of Timroth's data in mimeograph form may be obtained from the authors upon request. Procedures regarding the length of manuscripts prevented inclusion of these tables in this paper.

[6] Engineer, Production-Mechanical, The Detroit Edison Company, Detroit, Mich. Mem. ASME.

Temperature Distribution in Some Simple Bodies Developing or Absorbing Heat at a Linear Function of Temperature

By MAX JAKOB,[1] CHICAGO, ILL.

In a previous paper the temperature distribution in electrical coils of simple shape has been studied under the assumption of constant current, uniform and constant surface temperature, and linear increase of the electric resistance with temperature. It covered also the case of exothermic chemical reactions in similar configurations and under analogous conditions. The present investigation deals with bodies of the same form, but producing Joulean heat or heat of reaction at a rate decreasing linearly with rising temperature, or absorbing heat by endothermic reaction with a constant positive or negative temperature coefficient. The equations of temperature distribution derived in the paper are closely related to the previous ones in their form as well as in the occurring functions.

Nomenclature

The following nomenclature is used in the paper:

f = a function
g = a function
$i = \sqrt{-1}$
k; k_s = thermal conductivity of material at temperature t or t_s, respectively
M = constant of integration
$m = q_s'''/k_s$
N = constant of integration
$n = m\epsilon$
$p = -n$
q''', q_s''' = time rate of heat developed in unit volume at temperature t or t_s, respectively.
r = distance of any point in cylinder or sphere from center line or center, respectively
s = half-thickness of plate, radius of cylinder or sphere
t; t_0; t_s = temperature at any point, center, or surface, respectively
x = distance of any point in plate from median plane
$y = r\sqrt{-n}$
$z = \theta\sqrt{r}$
ϵ = temperature coefficient
θ; θ_0 = $t - t_s$; $t_0 - t_s$, respectively
$\xi = x/s$ or r/s
$\sigma = s\sqrt{n}$

Introduction

The author has previously[2] studied the temperature distribution in electric coils of simple cross-sectional shape for the case of uniform and constant surface temperature, constant electric current, and linear increase of the electric resistance with temperature.[3] The present paper is devoted to the related case of linear decrease of the electric resistance with increasing temperature t, which occurs in electrolytes, melted and solid salts, semiconductors as silicon carbide used in rod form for electrical heaters, Nernst and Auer lamp materials, and particularly in all sorts of carbon, as arc-lamp carbons, graphite electrodes, and the product known as Kryptol, composed of graphite, carborundum, and clay and used for electric-resistance furnaces.

Again, as in the previous paper,[2] equations of the temperature distribution θ/θ_0 in plane plates, cylinders, and spheres will be derived where $\theta = t - t_s$ is the excess of the temperature t, of any point of the body above surface temperature t_s and $\theta_0 = t_0 - t_s$ is that excess in the center of the body. These equations will hold also for exothermic chemical reactions with a constant negative temperature coefficient of heat development in the same way as the equations of the previous paper can be used for exothermic reactions with constant positive temperature coefficient. The temperature coefficient ϵ is defined by the equation

$$q'''/k = (q_s'''/k_s)(1 + \epsilon\theta) \qquad [1]$$

where the subscript s refers to the temperature t_s. Quasi-stationary conditions are supposed to prevail in the reactions. For instance, a reacting substance may be moved through a tube so slowly that the influence of movement is negligible, and constant heat development or absorption can be assumed at any point of the reacting body.

In endothermic reactions, where the heat absorption increases linearly with the temperature, the temperature distribution θ/θ_0 is the same as that in exothermic reactions with negative temperature coefficient; however, θ and θ_0 have negative values. In endothermic reactions with negative temperature coefficient, on the other hand, θ/θ_0 is the same as in electric coils or exothermic reactions with positive temperature coefficients, and again θ and θ_0 are both negative.

A surprising result of the previous paper[2] was that infinitely high temperature was approached at relatively small currents when $s\sqrt{\epsilon q_s'''/k_s}$ approached certain finite values, s being the half-thickness of the plate or the radius of cylinder or sphere. This had to be considered as a theoretical upper limit, never reached in practice since the coil would burn through and the linear relationship between electric resistance and temperature would change long before that limit had been attained. In a

---

[1] Research Professor of Mechanical Engineering, Illinois Institute of Technology; Consultant in Heat Research, Armour Research Foundation; nonresident Research Professor of Heat Transfer, Purdue University. Mem. ASME.

Contributed by the Heat Transfer Division and presented at the Semi-Annual Meeting, Chicago, Ill., June 16–19, 1947, of The American Society of Mechanical Engineers.

Note: Statements and opinions advanced in papers are to be understood as individual expressions of their authors and not those of the Society.

[2] "Influence of Nonuniform Development of Heat Upon the Temperature Distribution in Electrical Coils and Similar Heat Sources of Simple Form," by M. Jakob, Trans. ASME, vol. 65, 1943, pp. 593–605.

[3] More exactly, for linear increase of q'''/k with the temperature where q''' is the time rate of heat developed in unit volume and k is the equivalent (apparent) thermal conductivity of the coil material.

similar way when temperature excesses theoretically would approach infinitely large negative values the endothermic reaction or the decrease of electric resistance will stop before the temperature in the center has reached the absolute-zero point.

As in the previous paper[2] the calculations are based on the equation

$$\frac{q'''}{k} = m + n\theta = m\left(1 + \frac{n}{m}\theta\right) = m(1 + \epsilon\theta) \ldots\ldots [2]$$

where m and n are constants. However, m, n, and ϵ, formerly considered as positive, may have positive or negative values. Comparison with Equation [1] shows that

$$m = q_s'''/k_s$$

and

$$n = \frac{q''' - q_s'''}{k\theta}$$

The Plane Plate

For heat development with $\epsilon < 0$ the same differential equation is valid as previously[2] used for $\epsilon > 0$, namely

$$\frac{d^2\theta}{dx^2} = \frac{q'''}{k} \ldots\ldots\ldots\ldots\ldots\ldots [3]$$

where x is the perpendicular distance of a point of the plate from the median plane and

$$q''' \gtreqless 0; \quad m \gtreqless 0; \quad n \lesseqgtr 0; \quad \epsilon = \frac{n}{m} \lesseqgtr 0 \ldots\ldots [4]$$

Using Equation [2], the general solution of Equation [3] becomes

$$\theta = \frac{m}{p} + Me^{-x\sqrt{-n}} + Ne^{x\sqrt{-n}} \ldots\ldots\ldots\ldots [5]$$

where M and N are arbitrary constants.

The boundary conditions are

$$x = 0 \quad d\theta/dx = 0 \ldots\ldots\ldots\ldots\ldots\ldots [6]$$

$$x = s \quad \theta = 0 \ldots\ldots\ldots\ldots\ldots\ldots [7]$$

Herewith Equation [5] converts to

$$\theta = \frac{m}{n}\left[\frac{\cosh\,(x\sqrt{-n})}{\cosh\,(s\sqrt{-n})} - 1\right] \ldots\ldots\ldots\ldots [8]$$

Introducing as previously

$$\xi = x/s \quad \text{and} \quad \sigma = s\sqrt{n}$$

$$\theta = \frac{1}{\epsilon}\left[\frac{\cosh\,(i\xi\sigma)}{\cosh\,(i\sigma)} - 1\right] \ldots\ldots\ldots\ldots\ldots [9]$$

$$\theta_0 = \frac{1}{\epsilon}\left[\frac{1}{\cosh\,(i\sigma)} - 1\right] \ldots\ldots\ldots\ldots\ldots [10]$$

$$\frac{\theta}{\theta_0} = \frac{\cosh\,(i\xi\sigma) - \cosh\,(i\sigma)}{1 - \cosh\,(i\sigma)} \ldots\ldots\ldots\ldots [11]$$

which differ from the equations of the previous paper for positive ϵ only in so far as the cosines are replaced by hyperbolic cosines, and their arguments are multiplied by $i = \sqrt{-1}$.

Table 1 and Fig. 1 show the temperature distribution for different values of $i\sigma$. The column for $i\sigma = 0$ gives the parabolic distribution which holds for all cases of the former and of the present paper. The lowest curve in Fig. 1, represents the limit

TABLE 1 TEMPERATURE DISTRIBUTION IN PLANE PLATES

$i\sigma =$ / ξ	0 θ/θ_0	2 θ/θ_0	5 θ/θ_0	10 θ/θ_0	∞ θ/θ_0
0	1.000	1.000	1.000	1.000	1.000
0.1	0.990	0.993	0.998	1.000	1.000
0.2	0.960	0.971	0.993	1.000	1.000
0.3	0.910	0.933	0.982	0.999	1.000
0.4	0.840	0.879	0.963	0.998	1.000
0.5	0.750	0.803	0.930	0.993	1.000
0.6	0.640	0.707	0.876	0.982	1.000
0.7	0.510	0.583	0.787	0.950	1.000
0.8	0.360	0.429	0.642	0.865	1.000
0.9	0.190	0.237	0.400	0.632	1.000
1.0	0.000	0.000	0.000	0.000	...

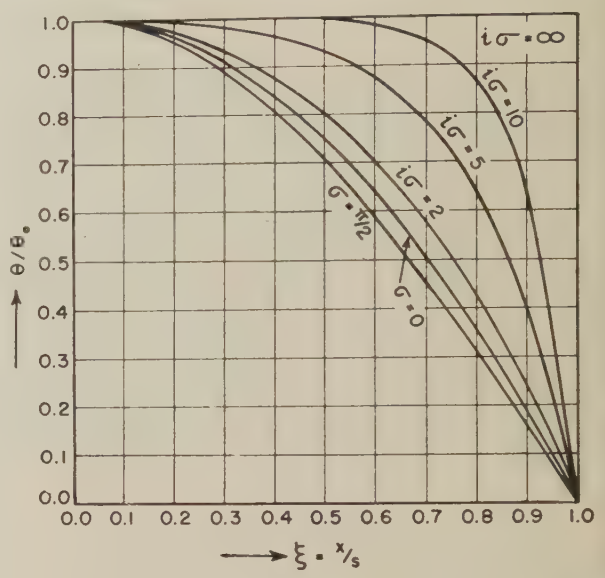

Fig. 1 Temperature Distribution in Infinitely Wide Plates

$\theta \to \infty$ previously found for $\sigma \to \pi/2$ when $n > 0$ (case of positive ϵ).

When heat is absorbed in an endothermic reaction in the range where the simple relation of Equation [2] is valid and $\epsilon > 0$, i.e., more heat is absorbed at higher temperature

$$q''' \gtreqless 0; \; m \lesseqgtr 0; \; n \lesseqgtr 0; \; \epsilon = \frac{n}{m} \gtreqless 0 \ldots\ldots [12]$$

Hence

$$\frac{d^2\theta}{dx^2} + n\theta = -m \ldots\ldots\ldots\ldots\ldots\ldots [13]$$

The general solution of this differential equation is

$$\theta = -\frac{m}{n} + Me^{-x\sqrt{-n}} + Ne^{x\sqrt{-n}} \ldots\ldots [14]$$

Equations [6] to [11] and Fig. 1, remain valid. However since $\epsilon > 0$, and the terms in square brackets are negative, the temperature excesses θ and θ_0 are found to be negative, as it must be with an endothermic reaction.

The Cylinder

Again, for heat development with $\epsilon < 0$, the same differential equation is valid as previously used for $\epsilon > 0$, that is

$$\frac{d^2\theta}{dr^2} + \frac{1}{r}\frac{d\theta}{dr} = -\frac{q'''}{k} \ldots\ldots\ldots\ldots [15]$$

where r is the radial distance of a point of the cylinder from the center line. Equation [4] can also be used unchanged.

Employing Equation [2] and introducing $y = r\sqrt{-n}$, the solution of this equation becomes

$$\theta = -\frac{m}{n} + MJ_0(iy) + NY_0(iy) \quad [16]$$

where J_0 and Y_0 are the Bessel functions of zero order first and second kind, respectively, or

$$\theta = -\frac{m}{n} + MJ_0(ir\sqrt{-n}) + NY_0(ir\sqrt{-n}) \quad [17]$$

The boundary conditions are

$$r = 0 \qquad d\theta/dr = 0 \quad [18]$$

$$r = s \qquad \theta = 0 \quad [19]$$

Herewith Equation [17] becomes[4]

$$\theta = \frac{m}{n}\left[\frac{J_0(ir\sqrt{-n})}{J_0(is\sqrt{-n})} - 1\right] = \frac{m}{n}\left[\frac{I_0(r\sqrt{-n})}{I_0(s\sqrt{-n})} - 1\right] \quad [20]$$

where I_0 is the modified Bessel function of zero order and first kind.

Introducing $\xi = r/s$ and $\sigma = s\sqrt{n}$

$$\theta = \frac{1}{\epsilon}\left[\frac{I_0(i\xi\sigma)}{I(i\sigma)} - 1\right] \quad [21]$$

$$\theta_0 = \frac{1}{\epsilon}\left[\frac{1}{I_0(i\sigma)} - 1\right] \quad [22]$$

$$\frac{\theta}{\theta_0} = \frac{I_0(i\xi\sigma) - I_0(i\sigma)}{1 - I_0(i\sigma)} \quad [23]$$

which again differ from the previously derived equations for positive ϵ only[5] by the factor i and the use of the modified Bessel function I_0 instead of the ordinary Bessel function J_0.

Table 2 and Fig. 2 show the temperature distribution with $i\sigma$ as parameter. The lowest curve represents the limit $\theta \to \infty$ previously found for $\sigma \to 2.4048 \ldots$ (the first zero point of the function J_0) when $n > 0$.

Equations [20] to [23] are also valid for heat absorption by an endothermic reaction with $\epsilon < 0$ in the range where Equation [12] can be assumed. Again θ and θ_0 become negative in this case.

The Sphere

For heat development with $\epsilon < 0$, as previously for $\epsilon > 0$

$$\frac{d^2\theta}{dr^2} + \frac{2}{r}\frac{d\theta}{dr} = -\frac{q'''}{k} \quad [24]$$

where r is the radial distance of any point from the center of the sphere. Again Equation [4] will be assumed.

Using Equation [2] again and introducing $p = -n$

$$\frac{d^2\theta}{dr^2} + \frac{2}{r}\frac{d\theta}{dr} - p\theta = -m \quad [25]$$

Considering the reduced equation

$$\frac{d^2\theta}{dr^2} + \frac{2}{r}\frac{d\theta}{dr} - p\theta = 0 \quad [26]$$

[4] In the analogous derivation of the previous paper[2] the following typographical errors may be corrected: In Equation [34] the expression $\frac{1}{\sqrt{n}}\frac{d\theta}{dr}$ should stand instead of $\frac{d\theta}{dr}$ and $-M$ instead of M. In Equation [42] the numerator θ has been omitted.

[5] The symbol ξ is used here for the symbol ρ of the previous paper.

TABLE 2 TEMPERATURE DISTRIBUTION IN CYLINDERS

$i\sigma =$	0	2	5	10	∞
ξ	θ/θ_0	θ/θ_0	θ/θ_0	θ/θ_0	θ/θ_0
0	1.000	1.000	1.000	1.000	1.000
0.1	0.990	0.992	0.998	1.000	1.000
0.2	0.960	0.969	0.990	0.999	1.000
0.3	0.910	0.928	0.976	0.998	1.000
0.4	0.840	0.870	0.952	0.996	1.000
0.5	0.750	0.792	0.913	0.991	1.000
0.6	0.640	0.692	0.852	0.976	1.000
0.7	0.510	0.568	0.757	0.940	1.000
0.8	0.360	0.414	0.608	0.848	1.000
0.9	0.190	0.227	0.372	0.611	1.000
1.0	0.000	0.000	0.000	0.000	...

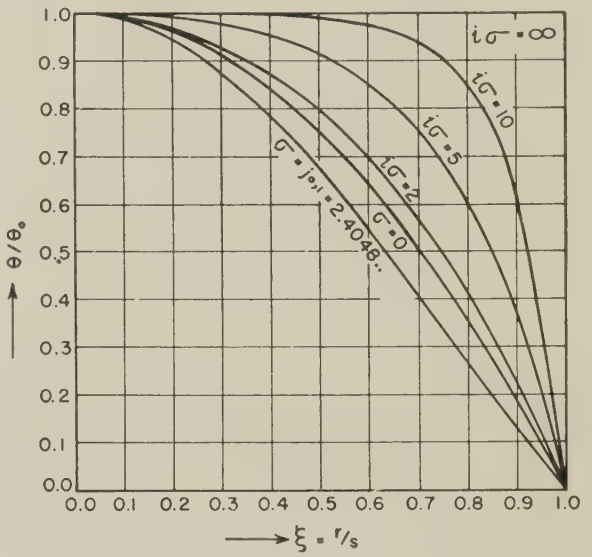

Fig. 2 Temperature Distribution in Infinitely Long Cylinders

and substituting $\theta = z/\sqrt{r}$

$$\frac{d^2z}{dr^2} + \frac{1}{r}\frac{dz}{dr} - \left(p + \frac{1}{4r^2}\right)z = 0 \quad [27]$$

Substituting[6] $r = y/\sqrt{p}$, the solution of Equation [26] becomes

$$z = MI_{1/2}(y) + NI_{-1/2}(y) \quad [28]$$

where $I_{1/2}$ and $I_{-1/2}$ are the modified Bessel functions of $^1/_2$ and $-^1/_2$ order and first kind.

But according to the theory of Bessel functions

$$I_{1/2}(y) = \sqrt{\frac{2}{\pi y}}\sinh(y) \quad [29]$$

and

$$I_{-1/2}(y) = \sqrt{\frac{2}{\pi y}}\cosh(y) \quad [30]$$

Herewith the solution of Equation [25] becomes

$$\theta = -\frac{m}{n} + \frac{M}{r\sqrt[4]{-n}}\sqrt{\frac{2}{\pi}}\sinh(r\sqrt{-n}) + \frac{N}{r\sqrt[4]{-n}}\sqrt{\frac{2}{\pi}}\cosh(r\sqrt{-n}) \quad [31]$$

[6] Two typographical errors in the corresponding equations of the former paper[2] may be corrected. On p. 598, column 1, line 6 from the bottom the first sign should be +, instead of =, and in the following line it should read $y/\sqrt{n}$ instead of $y\sqrt{n}$.

Using the boundary condition of Equation [18]:

$$\frac{d\theta}{dr} = 0 - N \cdot \infty = 0$$

which is possible only if $N = 0$

Using also the second boundary condition, Equation [19], Equation [36] turns into

$$\theta = \frac{m}{n}\left[\frac{\sinh(r\sqrt{-n})}{r\sqrt{-n}} \cdot \frac{s\sqrt{-n}}{\sinh(r\sqrt{-n})} - 1\right] \quad \ldots\ldots [32]$$

Introducing again ξ and σ

$$\theta = \frac{1}{\epsilon}\left[\frac{\sinh(i\xi\sigma)}{i\xi\sigma} \cdot \frac{i\sigma}{\sinh(i\sigma)} - 1\right] \quad \ldots\ldots\ldots [33]$$

$$\theta_0 = \frac{1}{\epsilon}\left[\frac{i\sigma}{\sinh(i\sigma)} - 1\right] \quad \ldots\ldots\ldots\ldots [34]$$

$$\frac{\theta}{\theta_0} = \frac{\dfrac{\sinh(i\xi\sigma)}{i\xi\sigma} - \dfrac{\sinh(i\sigma)}{i\sigma}}{1 - \dfrac{\sinh(i\sigma)}{i\sigma}} \quad \ldots\ldots\ldots\ldots [35]$$

which differ from the previously derived equations for positive ϵ only[5] by the factor i and hyperbolic sines replacing the sines.

Table 3 and Fig. 3 show the temperature distribution. The lowest curve represents the limit $\theta \rightarrow \infty$ previously found for $\sigma \rightarrow \pi$ when $n > 0$.

The same equations are valid for heat absorption by an endothermic reaction with negative ϵ in so far as Equation [12] can be assumed. Again θ and θ_0 take negative values.

TABLE 3 TEMPERATURE DISTRIBUTION IN SPHERES

$i\sigma =$ / ξ	0 θ/θ_0	2 θ/θ_0	5 θ/θ_0	10 θ/θ_0	∞ θ/θ_0
0	1.000	1.000	1.000	1.000	1.000
0.1	0.990	0.992	0.997	1.000	1.000
0.2	0.960	0.968	0.988	0.999	1.000
0.3	0.910	0.926	0.970	0.998	1.000
0.4	0.840	0.865	0.942	0.995	1.000
0.5	0.750	0.773	0.898	0.985	1.000
0.6	0.640	0.684	0.831	0.967	1.000
0.7	0.510	0.556	0.731	0.930	1.000
0.8	0.360	0.399	0.579	0.832	1.000
0.9	0.190	0.220	0.357	0.592	1.000
1.0	0.000	0.000	0.000	0.000	...

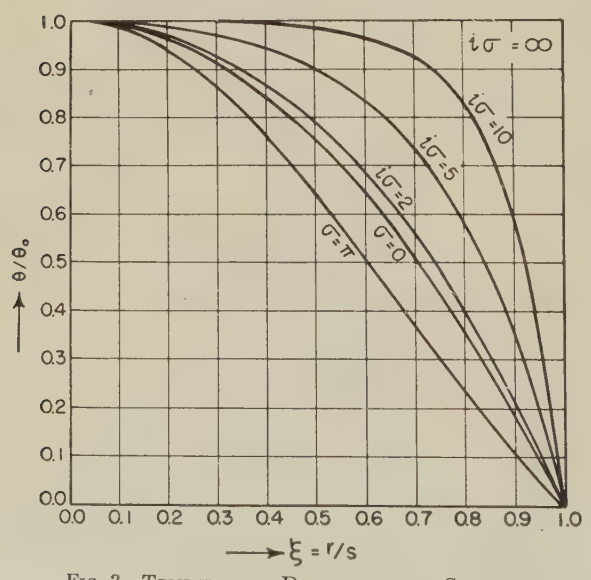

Fig. 3 Temperature Distribution in Spheres

Conclusions

If in each volume element of an infinitely wide plane plate, an infinitely long cylinder, or a sphere which are held at constant surface temperature, either Joulean heat or heat of reaction is developed at a steady rate, then the temperature distribution in a direction perpendicular to the surface can be represented by a parabola with the apex in the median plane, center line, or center, respectively. If the rate of heat development is steady, but increases linearly with the temperature, then the line of temperature distribution is less strongly curved than a parabola. Dimensionless equations for the temperature distribution in the three mentioned bodies have been derived in a previous paper[5] and can be brought to the common form

$$\frac{\theta}{\theta_0} = \frac{f(\xi\,\sigma) - f(\sigma)}{1 - f(\sigma)} \quad \ldots\ldots\ldots\ldots\ldots [36]$$

where the symbol f stands for the cosine-function, the Bessel function of zero order and first kind, and the function of sine divided by its argument, respectively, in the cases of plate, cylinder, and sphere. The other symbols used in the equation are defined in the present paper.

In this paper, it is shown that for a steady rate of heat development which decreases linearly with increasing temperature (as in graphite electrodes) and for endothermic heat absorption (endothermic reaction) at a rate which increases linearly with the temperature, the temperature lines are more strongly curved than a parabola and may be expressed by

$$\frac{\theta}{\theta_0} = \frac{g(i\xi\sigma) - g(i\sigma)}{1 - g(i\sigma)} \quad \ldots\ldots\ldots\ldots\ldots [37]$$

where $i = \sqrt{-1}$ and g stands for the hyperbolic cosine function, the modified Bessel function of zero order and first kind, or the function of hyperbolic sine divided by its argument, for the three forms of bodies, respectively.

However, the temperature excesses θ and θ_0 have both negative values in the case of the endothermic reaction, as they would in the case of endothermic reaction with negative temperature coefficient which is covered by Equation [36].

The parabola divides the curves represented by Equations [36] and [37] in two families, the first limited by a curve where the temperature would become infinitely large, the second limited by the line $\theta/\theta_0 = 1$.

Tables have been calculated and graphs drawn for the different cases with values of σ as parameter.

Discussion

G. M. Dusinberre.[7] The present paper is limited in the introduction to the case of constant electric current where this is the source of heat. It may also be noted that it is limited to constant thermal conductivity. A more general form of the differential equation for one-dimensional heat flow is

$$\frac{d}{dx} k \frac{dt}{dx} + q''' = 0 \quad \ldots\ldots\ldots\ldots\ldots [38]$$

and this takes the form of the author's Equation [3] only if k is constant.

A treatment under these two limitations may be adequate for a coil of insulated wire where (*a*) all elements of the electrical path are in series, and thus the current is everywhere the same, and (*b*) the effective thermal resistance in the direction of heat

[7] Professor of Mechanical Engineering, University of Delaware, Newark, Del. Mem. ASME.

flow depends mostly on the insulating material and very little on the properties of the electric conductor, and may be substantially constant with temperature.

However, a system such as a graphite electrode is homogeneous; the same material serves as the path for electrical flow and for heat flow. Here it seems that if the variation of electric resistance is going to be important, we should also take account of (*a*) the variation of thermal conductivity, which usually goes hand in hand with electrical conductivity, and (*b*) the variation of current density, since here the system is better represented by a number of electric paths in parallel. In this case $q''' = E^2\gamma$, where E is the electrical potential gradient, and γ the electrical conductivity.

For such a system, if we can assume $k = C_1 + C_2t$, $t = C_3 + C_4k$, $q''' = E^2\gamma = C_5 + C_6t = C_7 + C_8k$, Equation [38] of this discussion takes the form

$$\frac{d}{dx} k \frac{C_4 dk}{dx} + C_7 + C_8k = 0$$

or

$$\frac{d^2}{dx^2}(k^2) + \frac{2C_7}{C_4} + \frac{2C_8}{C_4} k = 0$$

This is the simplest form, but the writer cannot find a convenient solution. Then we might as well work directly in terms of t

$$\frac{d}{dx}(C_1 + C_2t)\frac{dt}{dx} + C_5 + C_6t = 0$$

$$C_1 \frac{d^2t}{dx^2} + C_2t\frac{d^2t}{dx^2} + C_2\left(\frac{dt}{dx}\right)^2 + C_5 + C_6t = 0$$

This can be solved by writing t as a power series in x. The constant term is the temperature at the origin. If here $dt/dx = 0$, coefficients of odd powers vanish. The writer has not investigated the convergence of this series, but trial indicates that three coefficients should usually be adequate (for x^2, x^4, and x^6).

E. A. Farber.[8] In connection with heat-transfer-coefficient determinations from hot surfaces to boiling liquids, it was necessary to determine the surface temperature of a cylindrical wire heated electrically. To find the surface temperature, an expression representing the temperature field inside the wire had to be developed.

Using the relation

$$\text{Heat in} + \begin{bmatrix}\text{sensible heat generated}\\ \text{electrically within the}\\ \text{volume}\end{bmatrix} = \text{heat out} \qquad [39]$$

the differential equation

$$r\frac{\partial^2\theta}{\partial r^2} + \frac{\partial\theta}{\partial r} + \alpha\frac{E^2s^2}{k\rho L^2} r = 0 \qquad [40]$$

was obtained which is the same as Equation [15] of the paper, where

r,θ,s are defined in the paper
α = 3.413 Btu/watt
E = voltage drop across wire
k = thermal conductivity
ρ = resistivity
L = length of cylinder, ft

Both k and ρ were taken as linear functions of the temperature and the differential equation takes the following forms

$$r\frac{\partial^2\theta}{\partial r^2} + \frac{\partial\theta}{\partial r} + \alpha\frac{E^2s^2}{L^2} r(a + b\theta) = 0 \qquad [41]$$

This equation where a and b are constants can be solved as outlined by the author.

Experimental work shows that this relation, at least qualitatively, approximates the actual conditions over a rather wide range. Even using a small, 18-gage chromel wire (cylindrical) the temperature difference between the center of the wire and its surface exceeds 100 deg F for maximum heat transfer. From microstructure investigations of the wire after the experiment it was found that the grain structure of the center portion had changed, the extent of that portion depending upon the maximum temperature of the wire during the test. From these observations it is safe to say that the center part of the cylinder was in the molten or possibly in the vapor phase surrounded by solid material. At very high temperatures it could be seen from the change of the microstructure that the material was molten with only a thin solid crust remaining at the bottom and lower part of the sides acting as support for the molten material. The wire failed when this crust became too thin to carry the weight of the rest of the material.

Since the difference in grain structure and phase at higher temperatures lead to discontinuities in the assumed homogeneity of material, it was necessary to find some method of approximating the limiting factors of the equations. Equation [40] or [41] of this discussion certainly cannot represent the true conditions when those discontinuities appear, which means whenever the eutectic temperature of the material is exceeded at any point within the cylinder.

One possible method of approximating this critical limit or the end of the range is by the use of the mean field temperature which can be expressed by

$$\bar{\theta} = 2\int^s \theta r d\theta \qquad [42]$$

Equation [42] can be solved by means of infinite series, and 3 terms of the rapidly converging solution were found to be accurate enough for all practical purposes.

The mean temperature ($\bar{T}$) of the wire can be found from a resistivity (ρ) versus temperature graph (which can be obtained from many handbooks) of the material used since ρ is given by the physical dimensions of the wire and the voltage drop (E) across and the current (I) in the wire. Then the surface temperature (T_s) is given by

$$T_s = \bar{T} - \bar{\theta} \qquad [43]$$

as long as ($T_s + \theta_0$) is smaller than the eutectic temperature of the wire material.

For comparatively small values of E, it can be shown that

$$\bar{\theta} \cong \frac{1}{2}\theta_0 \qquad [44]$$

This method, approach, and analysis, although specifically applied to a cylindrical electrically heated wire can be extended to the other sections of the paper.

Author's Closure

Professor Dusinberre remarks that Equation [38] instead of Equation [3] should be used if k is not constant. The author has admitted this already in a previous discussion[9] of the same objection raised by T. J. Higgins. He has also mentioned in that discussion that he used the less exact form because k changes slightly only over the temperature range occurring in an electric coil and the change can be taken care of by a simple transforma-

[8] Research Fellow, University of Iowa, Iowa City, Iowa. Jun. ASME.

[9] M. Jakob, Transactions AIEE, vol. 64, 1945, p. 493.

tion, suggested as early as 1894 by W. Kirchhoff and dug out of oblivion by E. F. M. van der Held in 1936. Using this transformation the complications can be evaded which Dusinberre met in the attempt to solve Equation [38]. The procedure consists in introducing in this equation, in which t may be replaced by the temperature excess θ, an auxiliary variable Θ and a constant k_m, defined by

$$k(d\theta/dx) = k_m(d\Theta/dx) \qquad [45]$$

together with the boundary condition

$$\theta = \Theta \qquad [46]$$

which is to be satisfied for two values of x, for example, $x = 0$ and $x = s$. Herewith Equation [38] converts to

$$d^2\Theta/dx^2 = -q'''/k_m \qquad [47]$$

The constant k_m is obtained by integration of Equation [45] within the limits $x = 0$ and $x = s$, that is

$$\int_{\theta=\theta_0}^{\theta=\theta_s} k.d\theta = \int_{\Theta=\theta_0}^{\Theta=\theta_s} k_m.d\Theta = k_m(\theta_s - \theta_0) \qquad [48]$$

This holds for any given relationship of k to θ, independent of whether the first integral can be solved analytically or graphically only.

Since θ_0 is not known in the present case, the method would require a simple trial-and-error procedure, namely, estimating an average value of k, calculating herewith a first approximation of θ_0 from Equation [3], calculating herewith k_m from Equation [48], and using this as average of k for a second approximation if necessary. Since the solution of Equation [3] is given and Equation [48] is very simple, this calculation will not require much time. It may be used in such cases for which Dusinberre recommends to employ the last formula of his discussion. Introduction of $\xi = x/s$ as a new variable may somewhat simplify the use of this rather complex equation.

It should be remarked that Equations [15] and [24] are of course open to the same objection as Equation [3]. However, Dr. Farber, according to his discussion, has used Equation [15] for metal wires in the form of Equation [41]. Though structural changes and even melting occurred in the central parts of some wires, he obtained qualitatively satisfactory results. This is all that could be expected. A change of phase, in particular, is not included in the author's analysis. The theoretical result may be improved by replacing Equation [15] by

$$\frac{d^2\Theta}{dr^2} + \frac{1}{r}\frac{d\Theta}{dr} = -\frac{q'''}{k} \qquad [49]$$

using Kirchhoff's method with dr instead of dx in Equation [45]. This considers exactly the variability of k with θ as the author has proved by setting up the heat balance for a cylinder ring with radii r and $r + dr$, then substituting $k_m(d\Theta/dr)$ for $k(d\theta/dr)$ in the balance, and rearranging the resulting equation. The case of the sphere can be dealt with in the same way.

The author cannot understand why this procedure should not yield θ_0 up to the eutectic temperature, provided that the electric resistance can be expressed by a linear function of temperature between the temperatures t_s and t_0, and the variability of k with t is given in this range so that the first integral in Equation [48] can be determined up to the melting temperature, analytically or graphically. If these conditions are not satisfied, then, in the author's opinion, Equation [42] cannot be used either, since θ will not be known as a function of r.

Finally, the author wishes to express appreciation of the valuable and stimulating contributions of the discussers of his paper.

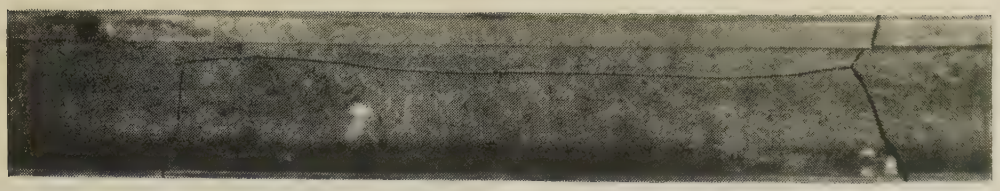

Fig. 1 Horizontally Split Web on 112-Lb Rail

Research Work on Rail Sections

By WALTER LEAF,[1] DENVER, COLO.

As a result of a failure in 112-lb rail on main-line track of the Denver and Rio Grande Western Railroad Company, early in 1940, studies of fatigue failure of rails were undertaken by the railroad. Faulty design of the rail in question was determined as the cause of failure and corrective measures were immediately put into effect. Out of this work and that of the American Railway Engineering Association, new rail designs have been evolved which avoid the difficulties experienced by this and other railroads.

Introduction

EARLY in 1940 a failure occurred in 112-lb rail on the Denver and Rio Grande Western Railroad Company's main-line track near Green River, Utah. It was unusual in nature, a fatigue crack having progressed horizontally about halfway through the upper portion of the web for a length of 2 ft, then sudden rupture took place through the remaining thickness of the web, a piece dropped out, and the rail broke in two, as shown in Fig. 1. Adjacent track was immediately investigated, and 29 rails were found which contained similar fatigue cracks of various lengths, but all horizontal, or nearly so, and predominantly in the upper portion of the web.

Immediate investigation of this failure was started in the research laboratory of the railroad, under the direction of Mr. Ray McBrian, engineer of Standards and Research. It was decided that the design of the web was such that operating stresses would at times be above the endurance limit of the steel, thus leading to fatigue failures.

Temporary corrective measures were taken by making slight design changes in the web, and recently the Rail Committee of the American Railway Engineering Association has approved several new rail sections which, supposedly, will eliminate this type of failure,[2] as well as correct several other weak points in design.

Faulty Design Probable Cause of Failure

There are four major causes of fatigue failure, i.e., design, fabrication, metallurgy, and mishandling in service. The rail failures were analyzed in each of these categories. Under mishandling in service, no spike-maul marks were noted on the webs, and engine driving tires were checked for excessive wear, none being found. The roadbed was in excellent condition with respect to line, grade, ballast, and ties. The metallurgy and fabrication of the rails met existing standards, there being no seams, slag inclusions, or the like, found at the fatigue cracks. Static strength and impact tests of the rail metal showed the expected values. This left design as the probable cause of failure. A program of photoelastic investigation of rail design was immediately started by the author.

The photoelastic method of design investigation was used because equipment was on hand, and the technique had been in use for several years on various projects. It is extremely simple and with proper precautions accurate predictions can be made. It has the disadvantage that all of the work must be done on models, loaded as best seen fit. If the model loading does not simulate loading in service, predictions are faulty. On the other hand, the entire stress distribution in the model is readily seen, and the effects of different types of model loading are easily noted. The final photoelastic analysis was checked very closely by later strain-gage readings in the field, consequently it must be concluded that the method was well adapted to the problem at hand.

Rail Details

The general shape of 112-lb rail is shown in Fig. 2. The minimum web thickness is $^{19}/_{32}$ in., at a height of $3^3/_4$ in. above the base; top fillet radius is $^3/_8$ in. and bottom fillet radius $^5/_8$ in.; rail is $6^5/_8$ in. high, $5^1/_2$ in. base width; head width is $2^{23}/_{32}$ in. An examination of general rail design of all weights from 60 lb per yd on up, showed that the 112-lb RE rail departed materially from previous practice. The usual rail had practically the same height as width, and as weight was increased, web thickness also increased. Extrapolating from lighter sections showed that the minimum web thickness should have been $^{23}/_{32}$ in. at 112-lb weight. This rail was much higher than its base width. A search through the records also showed that there had been practically no stress analysis applied to this 112-lb design when it was created.

A rail is very peculiar in shape. It is supported on the ties at irregular intervals and is loaded by the wheels of the locomotive and cars in quite variable fashion. The point of applied wheel load is confined to a small ellipse, which may vary in location from one side of the head to the other. The direction of applied load varies from possibly 45 deg from the vertical outwardly, to possibly 10 or 15 deg from the vertical inwardly. Wheel pressure is variable from a theoretical amount of 10,000 lb from an unloaded freight car to 37,000 lb from a driving wheel of a heavy locomotive. Under the influence of dynamic augment from the driving rods at high speed, lateral and vertical impact caused by track irregularities in line and surface, impact from nosing of the loco-

[1] Research Technician, The Denver & Rio Grande Western Railroad.

[2] Bulletin 465, American Railway Engineering Association February, 1947, pp. 657–673.

Contributed by the Metals Engineering Division and presented at the Fall Meeting, Salt Lake City, Utah, Sept. 1–4, 1947, of The American Society of Mechanical Engineers.

Note: Statements and opinions advanced in papers are to be understood as individual expressions of their authors and not those of the Society.

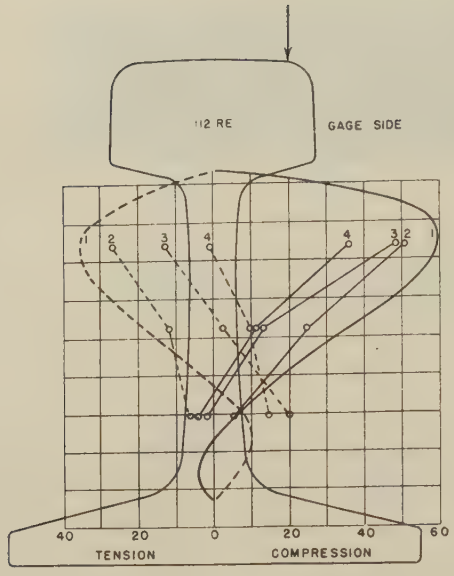

Fig. 2 Stress Distribution in 112-Lb Rail Section
(Stress in thousands of pounds per square inch. Gage side, solid lines. Field side, dotted lines. No. 1, predicted stress distribution with 40,000-lb load 1 in. off center, photoelastic analysis. No. 2, strain-gage reading tangent track. No. 3, strain-gage reading, high rail 1 deg 40 min curve. No. 4, strain-gage reading, low rail 1 deg 40 min curve.)

motive, and travel around curves at either greater or less than superelevation speed, the stress distribution in a rail is truly variable. In addition to the operating stresses, there are variable longitudinal stresses from temperature changes in a nonuniformly anchored rail, and possible residual circumferential stresses set up by differences in cooling rates between the head, web, and base. As a further point for consideration, the entire rail has a decarburized surface which has a very low endurance limit, heat numbers are stamped into the surface, and the branding letters are raised above the surrounding surface. Finally, the tie-plate design is somewhat variable, from a slightly dished shape across the base of the rail to a crowned shape. Some plates are crowned longitudinally to the rail length and some are flat; some are beveled and some not. All of these factors influence the stress distribution.

During the heating of the ingots and blooms at the mill, carbon is burned out of the outer layer of metal, and a decarburized surface results which is usually several hundredths of an inch in depth and is considerably weaker than the underlying core. As a result of this decarburized surface of the rail, fatigue tests on polished specimens are meaningless. Even fatigue tests of pieces with the original rolled surfaces are not too reliable in predicting rail performance, because the operating stress in most of the rail surface is two-dimensional, while the stress in the usual fatigue-test specimen is simple unidirectional in nature. It has been pointed out by several investigators that two-dimensional stress has a marked influence on the endurance limit of structures.

Photoelastic Investigation

These complications were not all apparent at the outset of the investigation but cropped up from time to time. The photoelastic investigation was started on a simple cross-sectional model of the 112-lb rail resting on a flat surface and loaded at various points across the head. The web stress in this model was simple compression with a centrally applied load, and simple bending plus direct stress with an eccentric load. The stress values could have been easily calculated from bending moments and section moduli. Next, a small three-dimensional model was made, and the frozen stress-pattern technique used. A section of this model cut from the location of the applied load showed an entirely different type of stress distribution than noted in the simple cross-sectional model.

The simple model under eccentric head loading showed merely compression on one side of the web and tension on the other side. The location of the neutral axis varied with the point of load application. The slice from the three-dimensional model showed compression near the top of the web on the loaded side, but tension in the bottom portion. Stress on the unloaded side was tension at the top and compression at the bottom.

Consideration of the deflections involved will readily explain this peculiar stress distribution. With the simple cross-sectional model loaded eccentrically on, say, the right side, the web bends slightly and the head moves a little to the right, assuming the rail base to be stationary. The head of a continuous rail has appreciable lateral stiffness which tends to resist this movement of the head sideways, so if the eccentrically loaded section is to be placed artificially back into a continuous rail, the head must be pushed to the left a little to get it in line. This action causes tension along the right-hand side of the web and compression on the left side. Now the bending moment on the section is merely the product of the applied load and the eccentricity, and is uniform from top to bottom of the web, assuming a strictly vertical load. The bending moment in the web caused by pushing the head to the left varies directly as the distance from the point of applied load and is of course greater near the bottom of the web. Thus a reversal of stress results from adding the two bending moments, and the amount and point of reversal depend upon the lateral stiffness of the head, the eccentricity of loading, and the general web shape.

In order to make a simple sectional model display the type of stress distribution experienced by a continuous rail, it is only necessary then to build a frame around the section with bearing against the side of the head to prevent lateral movement under an eccentric load.

Determination of the numerical value of the web stress required an added technique. A small three-dimensional model was made from bakelite and placed in a glass-sided tank full of liquid of the same index of refraction as the bakelite, so that no refraction of a light ray took place in passing through the odd-shaped section. The model was supported by tie models, and a wheel model was used to load the rail. Observation in polarized light of the length of rail model most highly compressed by the wheel load showed that about 4 in. of web length carried most of the load in the upper portion. Stress in the lower web depended upon whether the wheel was over a tie or between ties. Thus over a tie, about 8 in. of web was highly compressed, but between ties the compressed area bridged the gap between ties. With this information, the final stress diagram for the web under a 37,000-lb wheel load 1 in. off rail center could be calculated from the ratio of stress generated to load applied on the sectional model, and the ratio between the model thickness and length of web influenced as outlined.

Stress Conditons Found by Studies

The graph in Fig. 2 was thus constructed. It predicts a 60,000-psi compression in the web $4^1/_2$ in. above the base with 1-in. eccentric load and 38,000-psi tension on the opposite side, as shown by the heavy solid and dotted lines. These high values fall off quite rapidly on the way down the web, until a reversal of tension to compression takes place $2^1/_2$ in. above the base on the unloaded side, and reversal from compression to tension $1^1/_2$ in. above the base on the loaded side. This is the stress condition predicted over a tie. Between ties, approximately the same type would be experienced except the values would fall off to zero near the bottom of the web and no reversal would be noted.

The usual plain-carbon rail steel varies from 0.67 to 0.81 per cent carbon content, and has an ultimate strength ranging from about 117,000 psi to about 130,000 psi and yield-point range of about 68,000 psi to about 80,000 psi. Thus the polished-beam endurance limit would be about 60,000 psi, but with rolled surface, somewhat lower. Impact from rough track, dynamic augment, low temperature, and the like, would put the normal operating stress somewhat above the endurance limit of the actual rail, and failure in fatigue was to be expected. Of course not all of the wheels over any given point would cause the maximum stress at that point, since the eccentricity of bearing varies, yet high stresses were demonstrated as probable and fatigue failures had taken place. So the design must have been faulty.

Checking by Means of Strain Gages

Shortly after the photoelastic work was completed strain-gage equipment became available and was put to use. The equipment consisted of a six-element oscillograph, power supply, and amplifiers. Carbon-strip gages were used, this being shortly before the advent of the SR-4 wire gages. A thorough investigation of actual stress distribution in rail was made. The photoelastic investigation was quite closely confirmed. In Fig. 2 are shown some of the typical readings with gages at three different heights, on both sides of the web.

Train speeds up to 75 mph were investigated, with the conclusion that speed itself had little to do with web stress except as it might impose higher or lower pressure against the rail of a curve. Counterbalance position over the gage location was determined with motion pictures and also absolved. The entire problem was narrowed down to eccentricity of bearing.

With web design as the cause of failure, the question arose as to what could best be done. Any radical change in rail design would lead to many other changes, in joint bars, insulated joints, frog and switch castings, etc., so finally it was decided merely to thicken the web by running straight lines between the top and bottom fillets. This was done by turning down a set of rolls. Since then several hundred miles of this rail have been in service without a single web failure. Fillet cracks have been experienced, especially on curves, indicating that further design changes were necessary.

Corrective Measures Taken

Web stress is usually highest in the upper portion, since this location is nearest the point of applied load, and the web acts something like a brick wall in that a lesser length of web carries the load as the point of application is approached. Thus the lower portion need not be as thick as the upper portion. It was desired to create a rail design in which the maximum normal operating stress would not exceed 40,000 psi. By a consideration of actual strains measured and section moduli of the 112-lb rail web, a design was created which was predicted to give the desired maximum stress. In effect, the old web was turned upside down and thickened $^1/_{32}$ in. throughout. Fillet radii were increased to $^5/_8$ in.

The AREA research staff, over the next 3 or 4 years, made additional strain-gage readings under a great variety of service conditions, and finally arrived at what they considered an adequate design. It is shown in Fig. 3 and is close enough to the inverted-web design mentioned, seemingly to satisfy the requirements. As mentioned at the outset, this and two larger sections have now been adopted as standard design. As was fitting and proper, the Rio Grande bought and installed the first rolling of the new 114-lb section in 1946, and no trouble has been experienced. Of course the rail has not been in service very long.

Photoelastic Studies of Other Rail-Design Details

The original photoelastic study was confined to web design

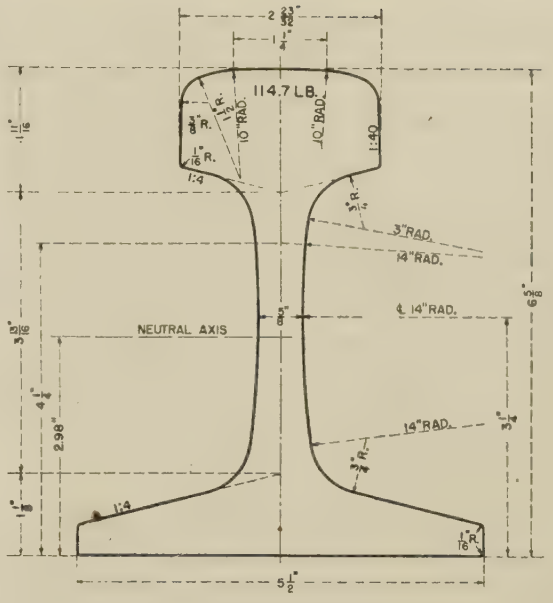

AREA :	HEAD	3.91	SQ. IN.	34.8 %	MOMENT OF INERTIA		65.6
	WEB	3.05	" "	27.1 %	SECTION MODULUS, HEAD		18.0
	BASE	4.29	" "	38.1 %	" "	BASE	22.0
	TOTAL	11.25	" "	100.0 %	RATIO M.I. TO AREA		5.8
					RATIO SEC. MOD. TO AREA		1.6
					RATIO HEIGHT TO BASE		1.20
					RATIO BASE TO HEIGHT		0.83

Fig. 3 Recently Adopted 114-Lb Rail Section

(Two other sections, 132.1 and 133.4 lb per yard have also been approved.)

but other features of general rail shape were questioned. No one seemed to know how wide the head of a rail should be. Worn rail with a narrow head was known to be bad from a standpoint of adhesion and wheel-tread wear on either curve of tangent track and too wide a head seemed objectionable from a standpoint of excessive metal where it did no good. The head width of $2^{21}/_{32}$ as used in the old 112-lb rail seemed good. However, the head contour was considered bad. The corner radius was $^3/_8$ in., while the standard wheel throat between flange and tread has a radius of $^5/_8$ in. It has been noted that the wheels wear toward a sharper radius in the throat, and the railhead metal flows over toward a larger radius. Obviously, the thing to do was to make the two radii the same so that an initial fit is obtained. This has been approached in the new design, in addition to making the running-surface radius a little sharper so that eccentric bearing is more difficult to obtain.

It is to be remembered that the actual track gage is somewhat variable, and that as wheels wear, their actual gage widens, so that a perfect fit is impossible even if all new rail and new wheels could be put in service.

It is to be emphasized at this point that the new rail designs are entirely the product of the research staff of the American Railway Engineering Association under Mr. Magee. However, the salient features and nearly the exact contours were indicated as desirable by the early photoelastic work. Likewise, the early program by the AREA staff was instituted at the request of officials of the Denver and Rio Grande Western Railroad Company.

Earlier Work on Web Failures

A search of the records showed that horizontal web failures had occurred on many other railroads, in not only the 112-lb section, but in practically all others used in main track, including the heavy 131-lb design. Some of these failures even dated back

almost to the turn of the century. True, they were not too numerous, but an inspection of the failed-rail report[3] for the period 1935 to 1944, shows 16.6 per cent of all rail failures in control-cooled rail to have taken place in the web, away from the joint, and 25.2 per cent in the joint. Thus 41.8 per cent of all rail failures were in the web, which is certainly enough to cause some concern. Fortunately, the condition has now been recognized and steps taken to correct it.

As far back as 1931, Timoshenko and Langer concluded that web design was faulty and urged rail designers to thicken the upper portion at the expense of the lower portion.[4] Their work did not come to light in the author's laboratory until after the investigation was completed, and apparently went unheeded in all quarters where rail was designed. They also showed a valuable diagram of safe operating stresses under various stress-reversal ranges, which also has gone unheeded. This diagram shows that the actual range of stress measured on the Denver and Rio Grande Western should have produced fatigue failure.

Experience With Strain Gages in the Field

Thousands of strain-gage readings have been made on our railroad. A large portion of them were of no significance. A few readings were really unique and will be discussed briefly.

In one type of distribution the six gages were placed in vertical directions on the web $3^3/_4$ in. above the rail base, 15 in. apart. One run showed that the first two gages were in tension under the first drive wheel of the locomotive, and the third gage showed compression. Thus in a space of 15 in. at about 40 mph one wheel had caused both compression and tension at similar locations in the web beneath the wheel.

In another setup three gages were placed at heights of 2 in., $3^1/_8$ in., and $4^1/_4$ in., respectively, above the base, on either side of the web in a vertical direction. Under a certain wheel the upper gage registered 40,000 psi compression, and the bottom one 24,000 psi tension, which is a truly remarkable reversal in only $2^1/_4$ in.

In order to determine the amount of lateral loading, gages were placed longitudinally on either edge of the rail base. With a vertical load on the head, each of these gages would be in tension, to the same value. Any difference in values would indicate a lateral component of loading. Under one wheel, the gage nearer the track center was in compression, indicating a very high lateral component. This reading was made on tangent track, and was evidently caused by nosing of the locomotive. This was the greatest lateral component measured in the investigation, and showed that curved track does not necessarily experience the greatest lateral force. Some readings were made wherein the inner gage registered higher tension than the outer one, indicating that wheel drag without flange pressure was sufficient to cause lateral loading.

Other Design Faults Discovered

It was realized at the time these web investigations were being made that there were other faults in general rail design. Fillet cracks at the juncture of head and web are of quite common occurrence, especially in the low rail of a sharp curve. This low rail carries somewhat more than one half the total load, with a train traveling at less than superelevation speed. It also loses considerable metal from the running surface by abrasion, and after the head is worn $^1/_4$ in. or so fillet cracks are always to be expected. With a worn head, the high vertical compression caused by the wheel load is transferred to the web by a shorter than normal head length, since stiffness has been lost. Thus unit stress is higher than with an unworn head. An increase in fillet radius is indicated as desirable to delay the appearance of these fillet cracks. However, an increase in fillet radius and thickening of the upper web leaves less area underneath the head for joint-bar contacts.

At the time of this investigation there was much argument about joint-bar design. It is to be remembered that rail is cut in 39-ft lengths, and joined by pairs of rolled bars bolted to the rail. There are two types of bars in use, the head-contact and the head-free designs. The head-contact bar is, in effect, a wedge, bearing on the so-called fishing surfaces of the head and base. These surfaces are sloped 1 in 4, so that the bars are wedged in place by bolt tension. If the bearing surface is restricted in area, high contact pressure leads to fatigue cracks forming in the bars. Some take-up space must be provided in the bar design, so that the bars can be tightened as the contact surface wears. Otherwise, bar life is short.

The head-free type of bar fits in the upper fillet of the rail, and wedges on the base. Thus very little fishing surface is required under the head. Although it was felt at the time that this bar gave poor support for the rail head at the joint, it has since been proved to be a good design, and is now widely used in new applications.

Bakelite models of a rail and joint bar with fillet radius of $^3/_4$ in. showed difficulty in keeping the bars in proper fit. The tendency was for the bar to climb upward, and slip around the large-radius curve. The trouble was particularly noticeable if the bars were slightly undersized. It must be remembered that rails and bars are rolled shapes, and as the roll wears, dimensions change slightly. Certain tolerances are allowed in dimensions to prevent excessive roll replacements.

Location of the bolt hole is somewhat restricted up and down by the necessary flanges of the bar and by the necessary size and clearance for the nut. It was found that a large-radius head-free bar required the bolt hole to be located relatively high in order to produce stability.

These points are mentioned to emphasize the fact that rail design must be co-ordinated with other designs, changes in one making necessary changes in others, and each requiring study to produce the optimum.

An attempt was made by the Rio Grande railroad in 1941, to have this inverted-web rail rolled, but it was unsuccessful owing to restrictions placed by the war production.

Improved Rails Now Being Produced

At the time of writing (September, 1947), most rail mills have made or are making rolls to produce the improved sections mentioned earlier. It is not known how many miles have been rolled, but the Rio Grande now has about 20 miles in track of the 114-lb section and about 50 miles have recently been rolled for the 1947 relay program. There are of course some roads which have had no trouble with the old rails, due to light traffic and axle loading, and they will probably continue to use the old sections. However, most rail laid in the future will be of the new shape. It is possible of course that trouble of some nature or other will appear from time to time, but these new rails were designed after a very thorough stress-analysis study, and are the best that could be designed with the information at hand. Of course a very heavy rail could be rolled, weighing, say, 200 lb per yd, and which could not possibly develop fatigue cracks, but the extra cost would not be warranted and also, rails wear out and must be replaced for other reasons. Flange wear on curves, shelling of the gage corner, flow of head metal, are some of these reasons. So even if a solid billet, say, 6 in. square, could be used for a rail, its life would be limited

[3] Reference 2, p. 684.

[4] "Stresses in Railroad Track," by S. Timoshenko and B. F. Langer, Trans. ASME, vol. 54, 1932, pp. 277–293; discussion, pp. 294–302.

Shelling of Rail

Shelling of rail is evidenced by plastic flow of the head metal especially at the gage corners where bearing pressures are highest. After considerable flow in one direction and another has taken place, the metal begins to separate from the parent body in thin leaves or slivers. Pieces break out, leaving sharp re-entrant angles which lead to transverse fatigue cracks, or possibly longitudinal split heads. It seems that a prolonged metallurgical study will be necessary to overcome this difficulty. Some work has already been done along this line, but much more is necessary. At least, the problem is recognized and a start made toward its solution.

On the Rio Grande Railroad, intermediate manganese rail with about 1.3 per cent manganese has been used quite successfully to prevent head checks, especially on the low rail of sharp curves. However, other difficulties were prevalent, the rail being prone to compound fracture, so that this type of alloy-steel rail has not proved satisfactory. High-silicon-content rail, 0.3 to 0.5 per cent has been in use on the Rio Grande road for many years and seems to resist shelling.

The American Railway Engineering Association has published an excellent report[5] on recent investigations of the cause and prevention of shelly spots. Briefly reviewed; a low-alloy heat-treated rail with 0.24 carbon, 1.28 manganese, 0.64 chromium, 0.57 nickel, 0.34 molybdenum, and 0.20 silicon, heat-treated to 157,600 psi ultimate strength, 145,400 yield strength, gave 7 times the life of plain-carbon-steel rail in a rolling-load test. So progress is being made.

In order to give a better concept of the actual loading on a rail several calculations have been made. If all of the weight of an L 105 class Rio Grande engine were concentrated in round billets of steel of the same diameter as the various wheels concerned, a fully loaded tender would be represented by six billets 36 inches diam and 9 ft 7 in. long. The driving wheels would be represented by six billets 70 in. diam and $34^1/_2$ in. long. Pilot and truck wheels are represented by somewhat smaller billets. The dimensions given are for billets to represent the wheel loading on one rail. For the entire locomotive, another set would be placed on the other rail.

The theoretical contact area between wheels and rail has also been calculated, assuming unworn wheels and rail. For a fully loaded tender wheel, this area is an elipse 0.63×0.50 in, and for a drive wheel, 0.93×0.50 in. The contact pressure varies from zero at the periphery of the elipse to a maximum at the center.

If we visualize steel bars, elliptical in cross section, of the given dimensions and with a flat end, resting on a flat steel surface, the bar representing the tender wheel would have to be 58,500 ft high, or 11.05 miles, in order to exert as much contact pressure as does the loaded tender wheel. For the driving wheel, a similar bar would be 42,000 ft, or 7.95 miles high. Worn wheels and rails would cause some variation in these figures; at times to lessen the contact pressure, at others to increase it.

[5] Reference 2, p. 750 et seq.

Recent Developments Concerning the Properties of Cast Steels

By C. W. Briggs,[1] Cleveland, Ohio

The properties of a number of low-alloy cast steels have been determined from production heats, hence the values obtained represent the values normally expected in the manufacture of steel castings. The cast low-alloy steels, in general, have slightly higher hardenability and strength and slightly lower ductility than wrought steels of similar composition, on heat-treatment. In this paper property ranges for strength and ductility are given for cast steels receiving different heat-treatments. The depth of section to which cast steel will harden can be estimated by the employment of the end-quench hardenability test. This test was used to study a number of carbon and alloy cast steels. It was found that the hardenability values of cast steels are similar to those of wrought steels of comparable analyses and grain sizes. Hardenability curves for typical carbon cast steels are given and hardenability bands for a number of low-alloy cast steels are illustrated. All degrees of hardenability, shallow- to deep-hardening, may be attained by the proper selection of cast steels. Studies on notched-bar impact specimens of cast steel revealed that by varying the structure of a single cast steel by heat-treatment, it is possible to change the low-temperature notched-bar impact values of the steel. Based upon the results of the investigation, it is concluded that no one alloy cast steel produces the best impact resistance, for all types of heat-treatments, at all testing temperatures. Alloy cast steels demonstrate excellent notched-bar impact properties at low-temperatures, which make them ideal for low-temperature-service applications.

Introduction

During the last two years considerable information has been developed on the properties of cast steels. The studies were formulated by the Steel Founders' Society, and the investigations were carried on at Carnegie Institute of Technology, Case School of Applied Science, and Michigan College of Mines and Technology, under the direction of the Metallurgical and Mechanical Engineering Department staffs of these schools.

The cast steels selected for study were compositions produced by commercial steel foundries for production steel castings. The steels for test were in most cases taken from a production heat. In some cases an entire heat was used to prepare the necessary coupons.

Research studies were made so as to obtain correlated information on the properties of cast steels so that engineers, designers, and the manufacturers of steel castings would be more familiar with the engineering properties of steel castings.

Purchasers of steel castings and their engineers are always interested in the mechanical properties of low-alloy cast steels, especially those properties which may be developed through the quench and temper heat-treatments. This is understandable, since the steel-casting industry during the war quenched and tempered castings of various sizes and degrees of complexity. Interest in notched-bar impact properties is continuing, especially at low temperatures, not only because of equipment operating under these conditions but low-temperature impact testing gives an indication of what may be expected when parts operate at high speeds under impact.

Purchasers' metallurgists are likewise interested in hardenability of cast steel, time-temperature-transformation curves for cast steel, and austenite grain size of cast steel, especially in knowing how these properties of cast steels compare with those of wrought steels. Also, since engineers are invariably placing requirements on heat-treating operations in purchase specifications, certain information on the heat-treatment of cast steels is valuable, especially if it can alter certain misconceptions. Information on all these matters will be presented.

Individual test data are omitted, but summarizing curves are illustrated. Substantiating data are available at the universities conducting the tests. Also, procedures conform to standard methods promulgated by the American Society for Testing Materials.

Properties of Low-Alloy Cast Steels

Cast steels can be produced in all the chemical ranges available to wrought steels, as well as several others which do not lend themselves to rolling or forging techniques; in fact, prior to the war, more than 60 alloy-cast-steel types were produced by the steel-casting industry in the production of alloy-steel castings to meet the requirements of purchasers. However, in recent years, the trend in the industry has been toward producing cast steels to meet certain minimum mechanical properties rather than to produce steels to chemical ranges such as the SAE or AISI tables of steels. This trend started before the war and has continued today.

The ASTM specifications for property requirements as shown in Table 1, are becoming much more universally used. Most of these property values can be obtained by alloy cast steel containing but small percentages of alloying elements.

Most property values for cast steels reported in publications

TABLE 1 AMERICAN SOCIETY FOR TESTING MATERIALS SPECIFICATIONS FOR STEEL CASTINGS

	Mechanical properties—minimum			
Class	Tensile strength, psi	Yield point, psi	Elongation in 2 in., per cent	Reduction of area, per cent
A27-46T				
60-30	60000	30000	24	35
65-30	65000	30000	20	30
65-35	65000	35000	24	35
70-36	70000	36000	22	30
A148-46T				
80-40	80000	40000	18	30
80-50	80000	50000	22	35
90-60	90000	60000	20	40
105-85	105000	85000	17	35
120-100	120000	100000	14	30
150-125	150000	125000	9	22
175-145	175000	145000	6	12

[1] Technical and Research Director, Steel Founders' Society of America. Member ASME.

Contributed by the Metals Engineering Division and presented at the Semi-Annual Meeting, Chicago, Ill., June 16–19, 1947, of The American Society of Mechanical Engineers.

Note: Statements and opinions advanced in papers are to be understood as individual expressions of their authors and not those of the Society.

show the use of cast steels with one or two alloying elements in quantities of 1.50 to 3.50 per cent each. It is the thought of purchasers that relatively large amounts of alloy are needed to produce alloy cast steels of greater than average mechanical properties.

In order to illustrate the advantage of the use of alloy steels with small percentages of alloying content, a co-operative study was undertaken by 30 steel foundries, under the auspices of Steel Founders' Society, working in collaboration with Carnegie Institute of Technology. These lean alloy steels were produced by adding from one to four alloying elements, representing combined additions of only 0.70 to 2.00 per cent. The NE number series was prefixed to these steels, although all the manganese and manganese-molybdenum series was produced regularly in substantial quantities by the steel-casting industry long before the NE series was devised.

The properties listed represent the mode of distribution curve or values that would normally be expected in the production of low-alloy cast steels. These values act as reference points to help the designer and purchaser of steel castings to select the proper steel for the required application.

In order to be able to report property values that would be absolutely representative of commercial steel for castings, some open-hearth foundries produced heats upward of 35 tons from which the necessary coupons were obtained for the test studies.

This study was conducted on a regular manufacturing basis in order that the production and heat-treatment of the steels should reflect commercial conditions rather than those obtained by precise laboratory control. Thus while the mechanical testing procedures were precise, there was some spread in the data, as would be normally expected from commercial operations. The results obtained, regardless of the methods used to make the steels, were combined, and mean property values were computed.

Chemical Ranges. The chemical ranges of the low-alloy cast steels are listed in Table 2. The steels were produced by standard melting practices normally used by the foundries which produced them. The austenite grain size of all the steels produced to the compositions shown in Table 2 was from 5 to 8.

TABLE 2 CHEMICAL COMPOSITION OF THE LOW-ALLOY CAST STEELS

Grade of steel	Composition specified, per cent				
	C	Mn	Cr	Ni	Mo
NE 1330...	0.27–0.33	1.35–1.70	...	...	...
NE 8030...	0.27–0.33	1.00–1.30	...	...	0.10–0.20
NE 8430...	0.27–0.33	1.30–1.60	...	..	0.30–0.40
NE 8620...	0.17–0.23	0.70–0.90	0.40–0.60	0.40–0.70	0.10–0.20
NE 8630...	0.27–0.33	0.70–0.90	0.40–0.60	0.40–0.70	0.10–0.20
NE 8640...	0.37–0.43	0.70–0.90	0.40–0.60	0.40–0.70	0.10–0.20
NE 8730...	0.27–0.33	0.70–0.90	0.40–0.60	0.40–0.70	0.25–0.35
NE 9430...	0.27–0.33	1.00–1.30	0.20–0.40	0.40–0.70	0.08–0.15
NE 9530...	0.27–0.33	1.30–1.60	0.40–0.60	0.40–0.70	0.30–0.40

NOTE: Silicon 0.40 to 0.60 per cent; phosphorus 0.05 per cent maximum; sulphur 0.06 per cent maximum.

Heat-Treatment. The popular heat-treatments of (1) normalizing, followed by tempering, and (2) water-quenching, followed by tempering, were employed to enhance the mechanical properties of the low-alloy cast steels.

Strength Values. The great amount of tensile property data collected on all heats of the various classes of steel is presented in block-diagram form for rapid visual examination and comparison. All test studies were made at Carnegie Institute of Technology. It was reported by the staff of the Institute: "The consistency of results indicates that two tests are almost always sufficient" to establish the mechanical properties of each heat of steel for any particular section thickness.

The tensile strengths of the steels studied are shown in Fig. 1. It will be noted that there is a gradual increase in properties with changing of composition from a medium manganese steel to the

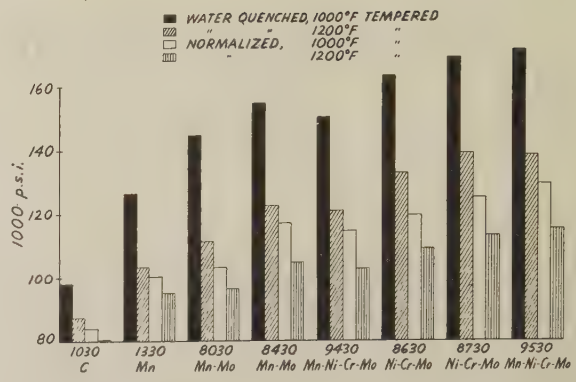

FIG. 1 TENSILE STRENGTHS OF TYPICAL LOW-ALLOY CAST STEELS OF SIMILAR CARBON CONTENTS WITH VARIOUS HEAT TREATMENTS

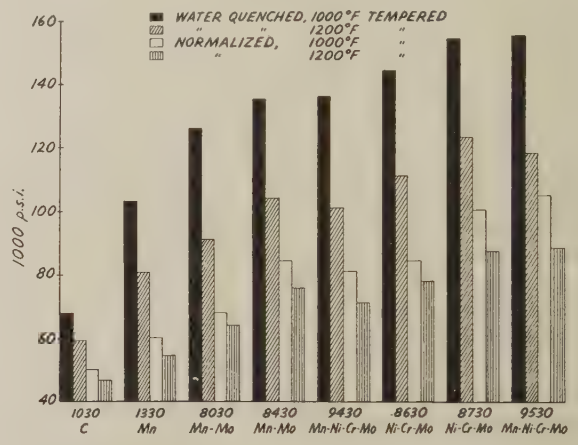

FIG. 2 YIELD POINTS OF TYPICAL LOW-ALLOY CAST STEELS OF APPROXIMATELY 0.30 PER CENT CARBON CONTENT

manganese-nickel-chromium-molybdenum steel, with tensile properties varying from about 100,000 psi to 160,000 psi, depending upon the heat-treatment. Low-alloy steels having a 0.30 per cent carbon content were selected as the basis of comparison, since cast steels of about this carbon content are most commonly produced in the industry. Normal tensile strengths for a plain (unalloyed) carbon steel are also included for comparative purposes since its properties are already well known to engineers and designers.

It is noteworthy that there is a relatively small spread in the properties of the various low-alloy cast steels when normalized, followed by a temper heat-treatment at 1200 F.

Fig. 2 shows graphically the yield-point values which may be obtained from the low-alloy cast steels in response to various heat-treatments. These values are found to correlate closely with the tensile properties, as would normally be expected. In Table 3 are given the ratios between the yield and tensile strengths of the various low-alloy cast steels. The general average for the low-alloy steels is compared with the ratio normally obtained for carbon cast steel of similar carbon content. The yield-tensile ratio of 0.84 to 0.88 for quenched and tempered steels is considered excellent.

Ductility Values. Ductility, as measured in terms of percentage elongation in a 2-in. gage length of the low-alloy cast steels is shown graphically in Fig. 3. The results are fairly uniform for all these steels, and the elongation values of 10 to 15 per cent for quenched and tempered steels having tensile strengths of 155,000 to 165,000 psi are considered excellent.

Reduction-of-area values are shown graphically in Fig. 4

TABLE 3 YIELD-TENSILE STRENGTH RATIOS FOR LOW-ALLOY CAST STEELS

	Yield-tensile ratio			
	Water quench		Normalize	
Steel	1000 F Temper	1200 F Temper	1000 F Temper	1200 F Temper
1330	0.82	0.78	0.60	0.60
8030	0.87	0.82	0.66	0.67
8430	0.88	0.85	0.72	0.73
9430	0.90	0.84	0.71	0.70
8630	0.89	0.84	0.71	0.72
8730	0.91	0.89	0.80	0.77
9530	0.91	0.86	0.82	0.77
Avg.	0.88	0.84	0.72	0.71
1030[a]	0.69	0.68	0.60	0.59

[a] 0.30 per cent plain-carbon cast steel.

Values of about 50 per cent or over can be expected for quenched low-alloy cast steels when followed by a tempering treatment at 1200 F.

Factors affecting toughness are shown graphically in Fig. 5, by plotting the elongation values in relation to the tensile strengths.

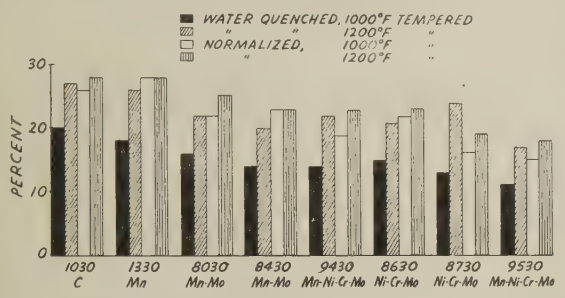

FIG. 3 EFFECT OF HEAT-TREATMENT ON PER CENT ELONGATION OF LOW-ALLOY CAST STEELS OF SIMILAR CARBON CONTENTS

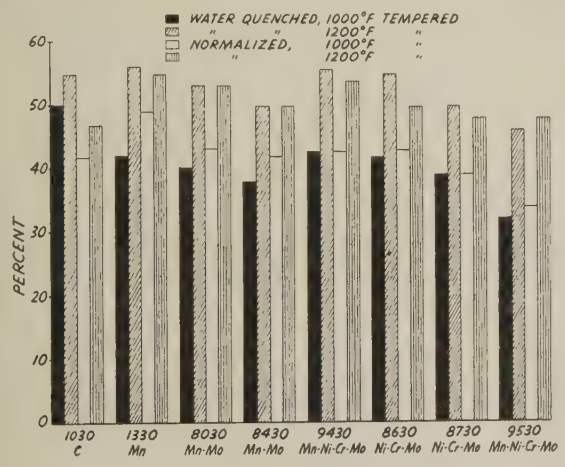

FIG. 4 REDUCTION OF AREA OF CERTAIN LOW-ALLOY CAST STEELS OF SIMILAR CARBON CONTENTS WITH VARIOUS HEAT-TREATMENTS

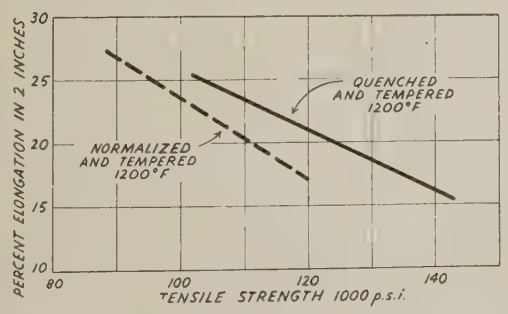

FIG. 5 EFFECT OF HEAT-TREATMENT ON DUCTILITY OF 0.30 PER CENT CARBON LOW-ALLOY CAST STEELS

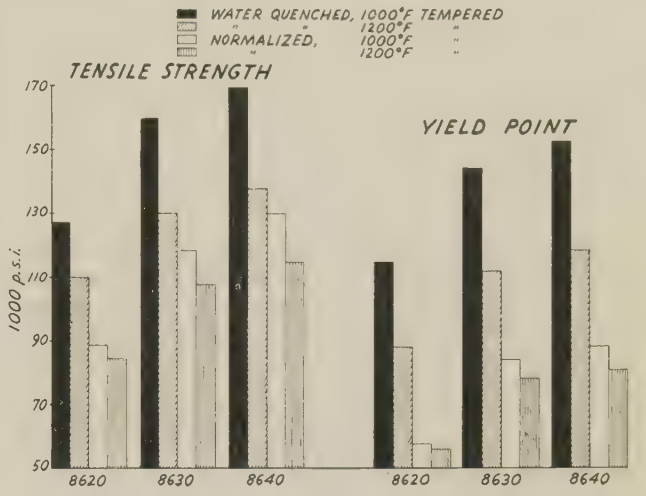

FIG. 6 EFFECT OF CARBON CONTENT ON STRENGTHS OF A NI-CR-MO CAST STEEL OF 8600 TYPE AFTER VARIOUS HEAT-TREATMENTS

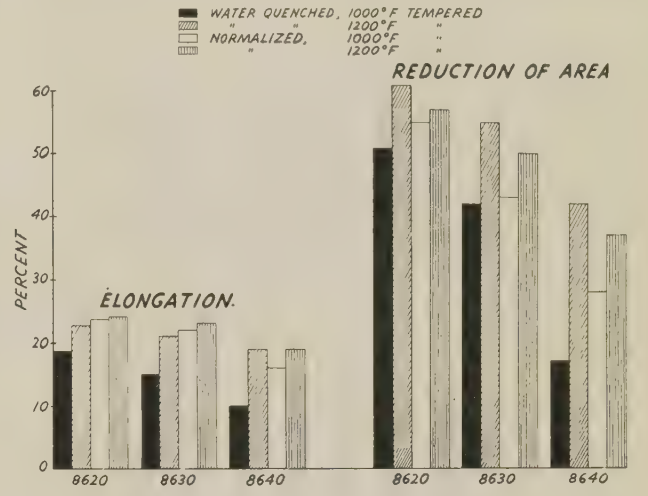

FIG. 7 DUCTILITY OF NI-CR-MO CAST STEEL OF VARYING CARBON CONTENTS AND HEAT-TREATMENTS

Quenching produces better ductility in a steel having a given tensile strength than does normalizing.

Effect of Varying Carbon Content. It is well known that the carbon content of a steel affects its mechanical properties. This is also true of the low-alloy cast steels, as shown graphically in Figs. 6 and 7. Normally, steels for the production of castings have carbon contents ranging from 0.20 to 0.45 per cent. Figs. 6 and 7 illustrate the range of properties that can be obtained for one low-alloy steel (Ni-Cr-Mo). Similar ranges can be obtained for the other low-alloy cast steels.

COMPARISON WITH WROUGHT STEELS

Figs. 1 to 7 can be used to compare with similar data which the engineer has acquired for wrought steels. In general, the tensile strengths of cast steels are slightly higher than for corresponding wrought steels. The differences are slight, however (see typical examples of data on wrought steels given in Table 4), and can be accounted for by the higher contents of manganese and silicon normally present in cast steels.

Based on the data in Table 4, the cast steels have lower ductility values than the corresponding wrought steels. However, the wrought-steel values reported are for specimens taken parallel to the direction of rolling; specimens perpendicular to the direc-

TABLE 4 SOME DATA ON WROUGHT ALLOY NE STEELS FOR COMPARISON WITH FIGS. 1 TO 8

	Tensile strength, psi	Reduction of area, per cent
Wrought NE 8630: Normalized, 1000 F, temp....	96–102000	58 to 63
Wrought NE 8630: Normalized, 1200 F, temp....	88– 94000	62 to 66
Wrought NE 8630: Quenched, 1200 F, temp.....	118–122000	64 to 68
Wrought NE 9430: Quenched, 1200 F, temp.....	109–120000	63 to 66

tion of rolling give considerably lower ductility values. For example, a wrought steel having values of 60 to 65 per cent reduction of area in the direction of rolling would have only 33 to 38 per cent reduction of area transverse to the direction of rolling. Averages of these values are only slightly different from those of cast steels in which properties do not vary according to the manner in which specimens are taken. The fact that cast steel does not have directional properties—greater in one direction, less in another—is a matter of great significance and importance to designers of products in which uniform properties are desirable.

The notched-bar impact values for low-alloy cast steels are shown graphically in Figs. 8 and 9. In general, the variation from

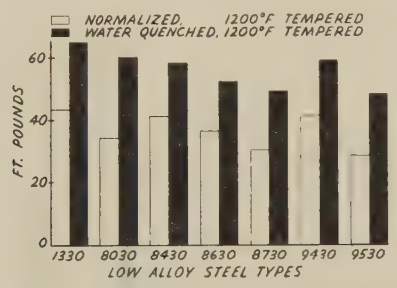

Fig. 8 Izod Impact Strength of Typical Low-Alloy Cast Steels With Two Types of Treatment

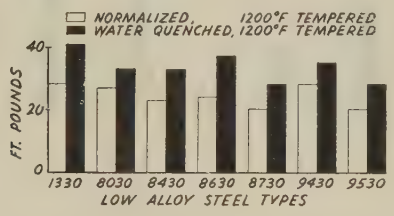

Fig. 9 Charpy Impact Strength of Typical Low-Alloy Cast Steels

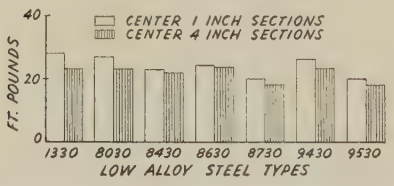

Fig. 10 Charpy Impact Strength of Normalized and Tempered Low-Alloy Cast Steels for 1- and 4-in. Sections

grade to grade is not great, but does show a tendency for impact strength to be high when ductility is high.

Fig. 10 shows graphically the Charpy keyhole notched-bar impact strengths of low-alloy cast steels which were normalized, followed by a temper of 1200 F, bars having been machined from the center of 1- and 4-in. cast-steel sections. It is of considerable interest to the designer that little variation exists between the two values, which means that steel castings of heavy section have notched-bar impact properties similar to castings of light wall section.

The low-alloy cast steels have excellent notched-bar impact properties at low temperatures, as shown graphically in Fig. 11. In this figure the impact data for all the low-alloy steels were averaged to indicate a high and low range of values. The values normally expected for the low-alloy steels are indicated by the band labeled "Average Range." Fig. 12 shows that the impact

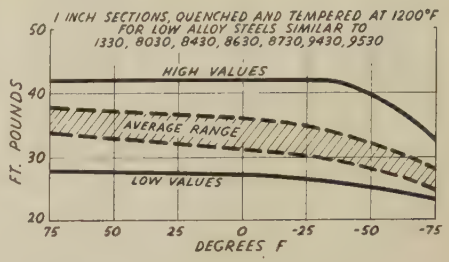

Fig. 11 Charpy Impact Strength of Low-Alloy Cast Steels at Low Temperatures

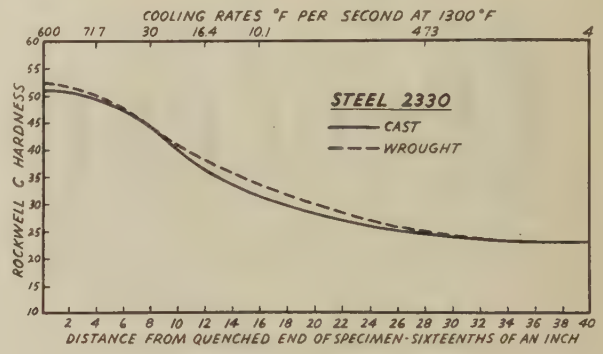

Fig. 12 Comparative Hardenability Curve for Cast and Wrought Steel Similar to 2330

Characteristics of Steels

	C	Mn	Ni	Grain size
Cast.....	0.28	0.69	3.30	7–8
Wrought.....	0.29	0.61	3.41	7

values, as measured at room temperature, do not fall off materially at temperatures as low as —75 F, practically no change taking place until a temperature of —25 F is reached.

Figs. 8, 9, and 11 show another advantage of quenching. It produces better impact-strength values than normalizing. Increasing the tempering temperature from 1000 F to 1200 F usually gives an appreciable improvement in notched-bar impact strength. Additional tests indicate higher impact strengths for the quenched steels over the normalized steels at both tempering temperatures.

Fig. 11 also shows that the low-alloy cast steels retain most of their resistance to impact at temperatures as low as —75 F. This is usual in the case of cast alloy steels, as contrasted with plain-carbon cast steels.

Because of the many variables involved and the lack of agreement in application of results, it is hazardous to attempt quantitative comparisons of notched-bar impact properties. However, the general statement may be made that although low-alloy cast steels tend to have slightly lower indicated impact strength than their wrought-steel counterparts, this slight difference is not indicative of their probable relative performance in actual industrial application. This is particularly true since impact values which have been reported for specimens taken transverse to the direction of rolling or to the direction of forging flow lines, may be as little as one half the value of those reported for specimens taken parallel therewith.

Hardenability of Cast Steels

The ability of steel to harden upon quenching has long been recognized as one of its most valuable properties. It is known that when steel is heated to the proper temperature and quenched, the hardness of the steel depends upon the speed of the quenching process; the more rapid the quench, the higher the hardness. Thus a study of the manner in which a steel hardens when applying different cooling rates indicates the degree of hardenability obtainable.

The term "hardenability" as applied to any particular steel embraces two basic principles: (1) quenching develops a maximum hardness; and (2) there is a limit to the section size which will be completely hardened upon quenching. The degree of hardness attainable increases with the carbon content of the steel. The maximum hardness obtainable is not significantly affected by the presence of alloy contents up to approximately 5 per cent.

It has long been recognized that plain-carbon steels are shallow hardening, and that alloy additions to steel increase the depth of hardening; but such generalizations are not sufficient for modern-day engineering needs. Recordable hardenability values for various steels are required. Such values are obtained by applying the "end-quench" or "Jominy" hardenability test.

The end-quench hardenability test has made it possible to predict the depth to which a particular steel can be hardened by applying a specific quenching rate. The test is simple, easy to perform, and remarkably consistent and accurate in its results. Approved procedures for conducting the tests have been published.

Quenching Treatment of Castings. Steel castings that have received a quench-temper heat-treatment are daily gaining greater favor among engineers. During the second war, large quantities of steel castings, ranging from simple to complex shapes, were given routine quench and temper heat-treatments. Although quenching and tempering should not be applied to some steel castings, because of large variations in sectional thickness or too complicated design, nearly all steel castings can be successfully heat-treated in this manner.

A point worthy of special emphasis is the fact that complete hardening of a cast-steel section, after tempering, produces a higher ratio of ductility to tensile strength than full annealing, or normalizing and tempering, of the same steel section of the same tensile strength. The cast steel of course must have the capacity to be hardened completely by the quench which is used. A section may be considered hardened throughout for most commercial purposes when it has a microstructure of 50 per cent martensite at the center. The best combination of strength, ductility, and toughness, as measured by resistance to impact, is produced in cast steels by quenching and tempering treatments.

It should be remembered that the maximum mechanical properties attainable from quenching and tempering cannot be secured in a partially hardened section. For example, if a cast steel is of such a composition that, upon quenching, it will just harden throughout a 1-in. section, any section larger than 1 in., when similarly quenched, will have an unhardened center. The thicker the section, the greater will be that portion of the section not completely hardened, with the result that the average mechanical properties will be lower than the maximum potential properties of the steel.

The factors which limit the depth to which a steel will harden are: (1) the severity of the quench; (2) the sectional thickness of the casting; and (3) the influence of chemical composition and grain size. The third factor, which determines the inherent response to hardening, is the characteristic of steel known as hardenability. The severity of quench is expressed in terms of the diameter of a round section of steel which will just harden through under the most severe quenching conditions.

Hardenability Values. The hardenability values of cast steels are similar to those of wrought steels if compositions and grain sizes are similar. Fig. 12 indicates good correlation between cast and wrought 2330 steel. Additional comparative data further substantiate the fact that the hardenability factors established for wrought steels can be applied also to corresponding cast steels. Furthermore, the methods and factors applicable to the calculation of hardenability for wrought steels can be used for cast steels. It should be pointed out, however, that cast steels may have slightly higher hardenability values than corresponding wrought steels because of their normally higher silicon content and possibly higher manganese content. This is illustrated in Table 5, where cast-steel data are compared with American Iron and Steel Institute data on wrought steels.

TABLE 5 COMPARISON OF END-QUENCH HARDENABILITY OF CAST AND WROUGHT STEELS

Grade	Distance from quenched end to 50 per cent martensite in sixteenths of an inch: Cast steel	Wrought steel
NE 8620	3½–7	2 – 6
NE 8630	7–13	4 – 9
NE 8640	11–19	5–13

The hardenability values for carbon cast steels of austenitic grain size 5 to 9 are presented in Fig. 13. For typical compositions of these steels see Table 6. The curves are representative of values normally expected in the production of the various carbon-steel grades. The great majority of carbon-steel castings are produced to carbon contents below 0.50 per cent. Hardenability curves for cast steels having carbon contents of 0.50 per cent and over are similar to those of wrought steels. Few hardenability studies have been made on carbon steels of 0.40 per cent carbon and under, hence the curves in Fig. 13 are of exceptional interest.

The hardenability bands illustrated in Figs. 14 to 22, inclusive,

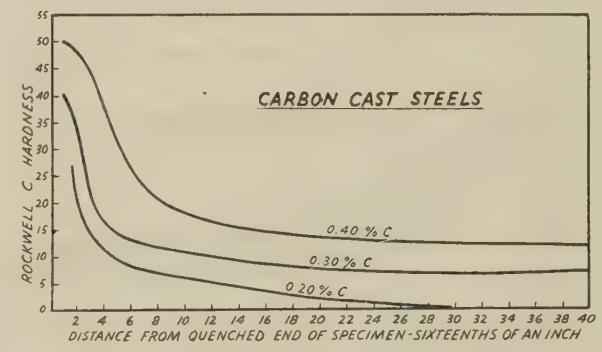

Fig. 13 Hardenability Curves for Typical Carbon Cast Steels; Grain Size 5 to 9

TABLE 6 CHEMICAL COMPOSITION OF CAST STEELS USED FOR HARDENABILITY STUDIES

Grade of cast steel	Composition specified, per cent: C	Mn	Cr	Ni	Mo
1020	0.17–0.23	0.55–0.80	...	...	...
1030	0.27–0.33	0.55–0.80	...	...	...
1040	0.37–0.43	0.55–0.80	...	...	...
1330	0.27–0.33	1.35–1.70	...	...	...
8030	0.27–0.33	1.00–1.30	...	...	0.10–0.20
8430	0.27–0.33	1.30–1.60	...	...	0.30–0.40
8620	0.17–0.23	0.70–0.90	0.40–0.60	0.40–0.70	0.10–0.20
8630	0.27–0.33	0.70–0.90	0.40–0.60	0.40–0.70	0.10–0.20
8640	0.37–0.43	0.70–0.90	0.40–0.60	0.40–0.70	0.10–0.20
8730	0.27–0.33	0.70–0.90	0.40–0.60	0.40–0.70	0.25–0.35
9430	0.27–0.33	1.00–1.30	0.20–0.40	0.40–0.70	0.08–0.15
9530	0.27–0.33	1.30–1.60	0.40–0.60	0.40–0.70	0.30–0.40
2330	0.27–0.33	0.55–0.90	...	3.25–3.75	...
4130	0.27–0.33	0.55–0.90	0.50–0.80	...	0.20–0.30
4330	0.27–0.33	0.55–0.90	0.50–0.80	1.40–2.00	0.25–0.35

Note: Silicon 0.40 to 0.60 per cent, phosphorus 0.50 per cent maximum, sulphur 0.60 per cent maximum.

were obtained from tests made on cast steels produced by 33 steel foundries. These bands represent values that would normally be expected in the production of low-alloy cast steels of from 5 to 9 austenitic grain size, and therefore should not be used to establish specification rejection limits. The bands prepared by the American Iron and Steel Institute would be more appropriate for use in establishing such limits.

The principal reason for studying 0.30 per cent carbon steel, having a wide variety of alloy contents, was to demonstrate the extensive range of hardenability values obtainable. Higher alloy contents provide higher hardenability values, which means that thicker sections can be hardened throughout or that higher hardness and strength can be imparted to sections which cannot be hardened throughout.

Additions of various percentages of alloying elements do enhance the strength of steels in the quenched and tempered condition, but their greatest value lies in the fact that they increase the depths to which such steels can be hardened. These points can be checked by comparing the mechanical properties of low-alloy cast steels, as set forth in the preceding section, with the hardenability values of the same steels as shown in the charts.

The effect of carbon content on the hardenability of a single alloy-steel composition is shown in Fig. 17, which sets forth values for a nickel-chromium-molybdenum cast steel (8600 class) produced with various carbon contents.

The degree of hardenability required for specific steel castings depends largely upon the type of stresses to which the castings will be subjected in service. These requirements may vary from a deep-hardening steel to a shallow-hardening steel. It will be noted from the illustrations in this paper that any degree of hardenability can be attained by selecting the proper cast steel.

Low-Temperature Properties

Steel castings are being used as parts of industrial units which, in service, operate all the way from atmospheric temperatures to as low as —300 F. Applications of steel castings in the low-temperature processing fields will be extended manyfold when engineers acquire a better understanding of the properties of cast steels at low temperatures. The comprehensive test results on the low-temperature properties of cast steels presented here should give engineers and purchasers a handy reference to aid

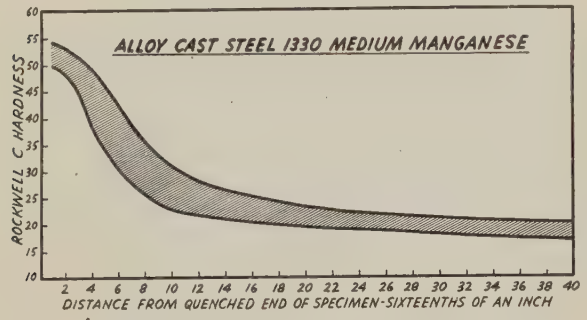

Fig. 14 Hardenability Band for Alloy Cast Steel 1330 of Medium Manganese; Grain Size 5 to 9

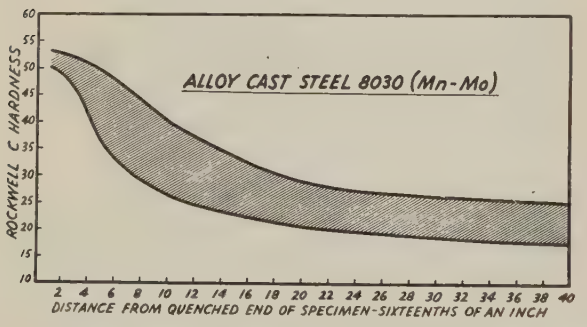

Fig. 15 Hardenability Band for Mn-Mo Alloy Cast Steel 8030; Grain Size 5 to 9

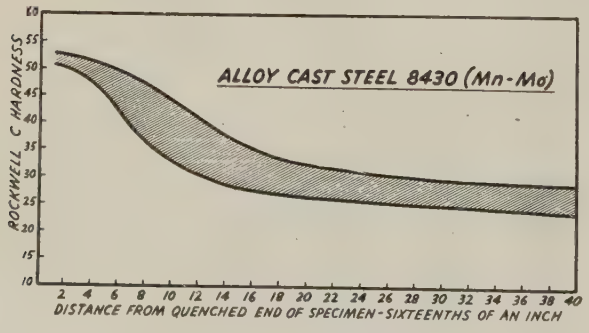

Fig. 16 Hardenability Band for Mn-Mo Alloy Cast Steel 8430; Grain Size 5 to 9

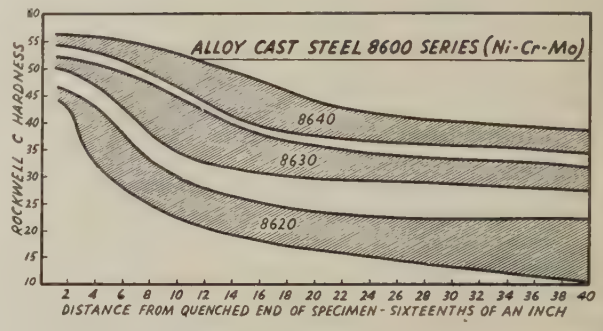

Fig. 17 Hardenability Band for Ni-Cr-Mo Alloy Cast Steels 8620, 8630, and 8640; Grain Size 5 to 9

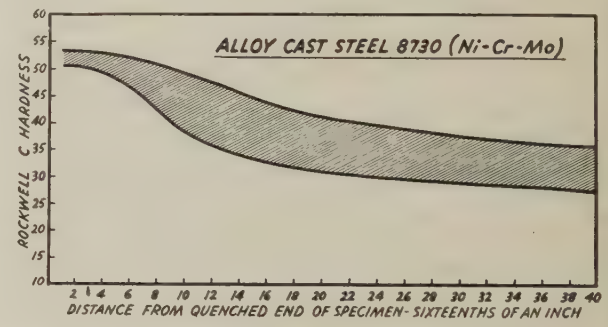

Fig. 18 Hardenability Band for Ni-Cr-Mo Alloy Cast Steel 8730; Grain Size 5 to 9

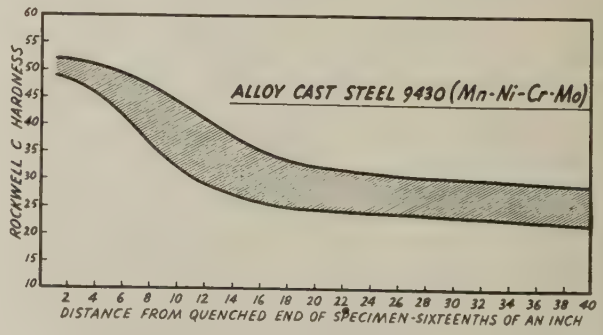

Fig. 19 Hardenability Band for Mn-Ni-Cr-Mo Alloy Cast Steel 9430; Grain Size 5 to 9

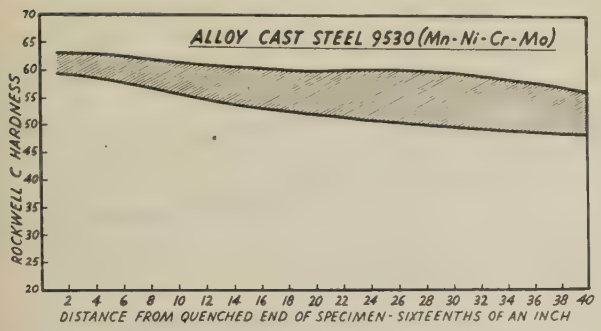

Fig. 20 Hardenability Band for Mn-Ni-Cr-Mo Alloy Cast Steel 9530; Grain Size 5 to 9

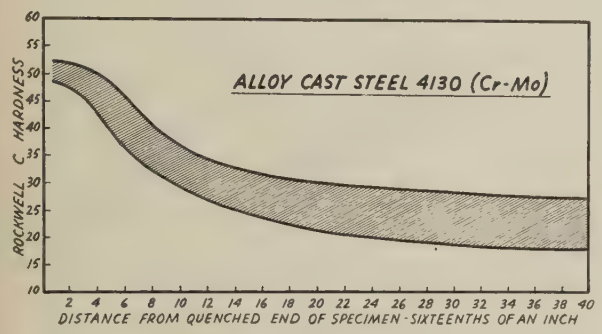

Fig. 21 Hardenability Band for Cr-Mo Alloy Cast Steel 4130; Grain Size 5 to 9

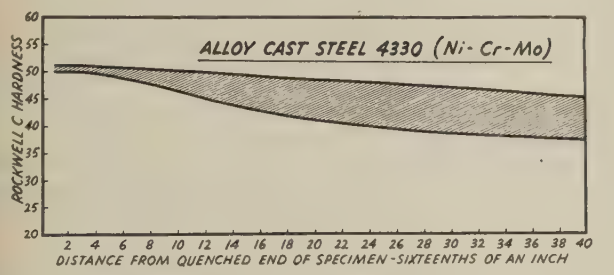

Fig. 22 Hardenability Band for Ni-Cr-Mo Alloy Cast Steel 4330; Grain Size 5 to 9

them in the selection of materials for low-temperature applications.

Static Tests. The results of the study of cast steels, as well as similar studies of wrought steels, show that there is little change in the strength and hardness properties of steels as the temperature of testing is lowered. Steels become harder and stronger as the temperature drops. This increase in strength is accompanied by a small decrease in ductility; however, the decrease is less than that resulting from variations of composition or heat-treatment measured at room temperatures.

The block diagram in Fig. 23 illustrates increases in tensile strengths which may be expected when cast steels are tested at room and low temperatures. The values, illustrated in Fig. 23, are typical of results recorded for other grades of cast steel. The elongation values will drop approximately 2 per cent and the Rockwell C hardness will increase about 4 points when testing temperature is lowered from 75 to —150 F.

It is evident that the change in static properties is very slight at service temperatures down to —150 F, and that engineers need have little or no concern regarding changes in static properties of cast steels when used in low-temperature services.

Notched-Bar Impact Tests. The failure of static tests to serve

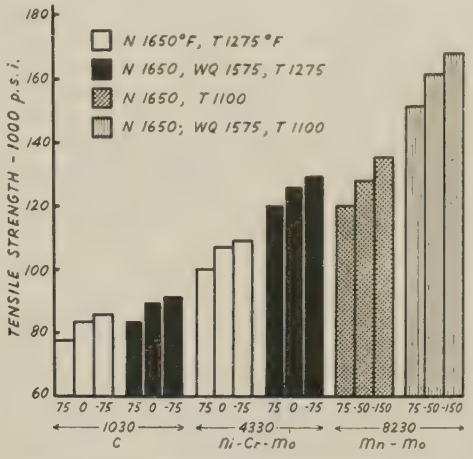

Fig. 23 Static Tensile-Strength Properties of Cast Steels at Normal and Low Temperatures

as accurate criteria of the fitness of metals and alloys for low-temperature service applications prompted users to devise a test which would differentiate more clearly between ductile and brittle fracture conditions. It was observed that the single-blow notched-bar test, known as the "impact test," may disclose a brittle fracture in a steel tested at low temperatures even though tension-impact tests on unnotched bars and static tests indicate a steel having satisfactory ductility. Accordingly, the notched-bar impact test has become quite widely accepted as a means of determining the brittle or ductile behavior of steels at temperatures below 70 F. The acceptability of steels for low-temperature applications is based almost entirely on their reaction to notched-bar impact tests at service temperatures.

The two types of test specimens most frequently used for low-temperature impact testing are the keyhole Charpy bar, and the V-notch Charpy bar. The test specimens have the same-size cross section (10 × 10 mm). The keyhole notched bar has a round hole at the base of the notch. The V-notch is a much sharper notch, and subjects the specimen to a severe stress concentration. The V-notch is cut to a depth of 2 mm, leaving a breaking section of 10 × 8 mm, instead of the 10 × 5-mm breaking section of the keyhole notch type.

At temperatures approaching normal atmospheric conditions, the V-notch bar is more sensitive to small changes than the keyhole notch bar. Values, recorded for the V-notch bar may be more than twice those recorded for the keyhole notch bar on the same steel at temperatures in the neighborhood of 70 F. However, at low temperatures, the V-notch bar values may be equal to, or even less than, the keyhole notch-bar values for the same steel. This greater spread in V-notch bar values magnifies the transition range from ductile to brittle fracture conditions and provides more exact differentiation.

Both the keyhole notch bar and the V-notch bar were used in reporting test values for the study of cast steels.

Certain carbon and low-alloy steels show a rather pronounced transition range. The change from a tough ductile fracture to a brittle fracture occurs over a range of temperatures, and, if testing is carried on in this temperature range, the resulting fractures may be mixed, with brittle patches appearing along with tough ductile areas. Since the fracture characteristics do not change abruptly from a ductile to a brittle fracture at any specific low temperature, there are bound to be certain variations in the individual test-bar results in the transition range. In some cases these variations may be quite wide.

The position of the transition range cannot be predicted from

mechanical testing other than notched-bar impact tests, nor from the composition, microstructure, or heat-treatment of the steel. One might conclude that steel heats are individualistic from the standpoint of notched-bar impact values at low temperatures. This is not true, however, if the steels are produced as dead-killed fine-grained steels without deleterious types of nonmetallic inclusions. Such steels, if they have comparable hardenabilities, may be presumed to have somewhat similar low-temperature impact properties.

Carbon Cast Steels

Information as to the normally expected impact properties of carbon cast steels is included in this paper, not because carbon-steel castings are commonly used in low-temperature applications, but because they provide a set of reference points by which to gage the effect of the carbon content of steels on their low-temperature notched-bar impact properties. A knowledge of the effect of carbon content on notched-bar impact properties simplifies the study of a number of alloy steels, since impact values for such steels, all having a single selected carbon content, can be compared.

The analyses of the carbon cast steels for which impact values are given are set forth in Table 7.

TABLE 7 CARBON CAST-STEEL ANALYSES, PER CENT

	1015	1030	1040
Carbon	0.17	0.30	0.38
Manganese	0.74	0.60	0.72
Silicon	0.49	0.36	0.41
Phosphorus	0.032	0.035	0.030
Sulphur	0.033	0.034	0.037
Nickel	0.09	0.07	0.09
Chromium	0.04	Trace	0.03
Molybdenum	0.02	0.02	0.03

Fig. 24 shows the impact values that were obtained after subjecting the three carbon steels to two different heat-treatments. The curves show that the carbon content of a steel affects the notched-bar values at both normal and subnormal temperatures. In general, the lower the carbon content of the steel, the higher are the impact properties. This principle also applies to alloy steels. A study of Fig. 24 reveals the fact that the carbon cast steels lost about one third of their impact strength between 70 and 0 F; however, the fractures were not of the characteristic brittle type. The impact strength decreased fairly uniformly from 0 to —75 F, with still no pronounced transition range. Normally, if the Charpy impact value is greater than 10 ft-lb, there is little brittle constituent in the fracture. Carbon steels were not tested below —75 F, since carbon-steel castings are not normally used for such low-temperature service.

The type of heat-treatment given to carbon steels has a marked effect on their impact values. At all testing temperatures down to —75 F, the annealing treatment produces the lowest values, whereas a water quench and high-temperature temper give the highest value. However, the effect of different heat-treatments diminishes at the lower testing temperature. It should be stressed that while fine-grained fully hardenable carbon steels in the quenched and tempered state exhibit fairly high impact values at low temperatures, casting sections must be rather thin in order that the characteristic quenched structure be produced throughout the cross section. Since the addition of alloys to steel permits greater opportunity for the casting section to be hardened completely throughout by liquid quenching, it is usual to add alloys to steel in order to secure improved notched-bar impact values.

Alloy Cast Steels

A number of representative alloy cast steels were tested at low

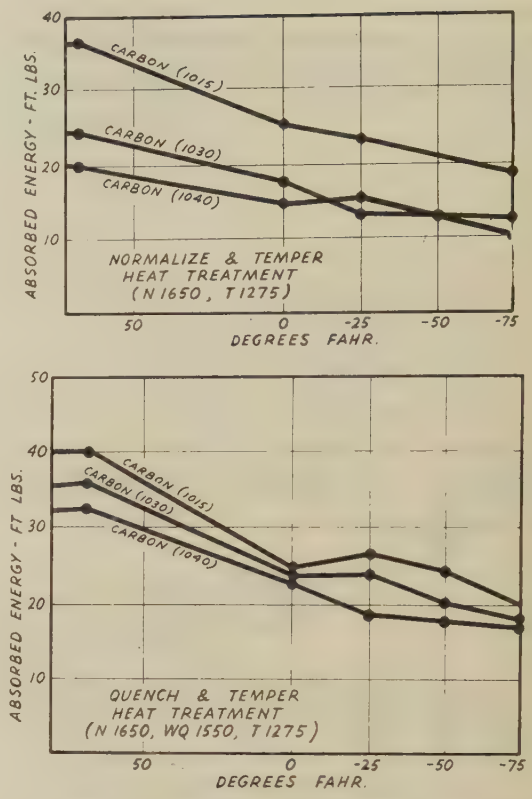

Fig. 24 Effect of Temperature on Impact Strength-Charpy Keyhole Notch Properties of Carbon Cast Steels (N = normalized; WQ = water-quenched, T = tempered.)

temperatures to indicate their possible application and comparative merits for low-temperature service.

The analyses of the alloy cast steels for which notched-bar impact properties at low temperatures were determined are given in Table 8.

TABLE 8 ALLOY CAST-STEEL ANALYSES, PER CENT

	X4130	2330	3130	4630	4330	8230
Carbon	0.30	0.26	0.26	0.30	0.26	0.33
Manganese	0.71	0.62	0.73	0.68	0.59	1.38
Silicon	0.29	0.31	0.43	0.39	0.44	0.58
Phosphorus	0.022	0.029	0.030	0.025	0.032	0.023
Sulphur	0.019	0.026	0.042	0.042	0.023	0.031
Nickel	0.03	3.36	1.10	1.66	1.82	...
Chromium	0.82	0.10	0.69	0.20	0.62	...
Molybdenum	0.22	...	...	0.28	0.20	0.28

Three alloy cast steels were tested by using both keyhole notch and V-notch specimens after various heat-treatments had been given the steels. The results of the tests are presented in graphic form in Figs. 26, 27, and 28.

In Fig. 25 it will be noted that by using X4130 steel it was possible to triple the Charpy keyhole notch value at atmospheric temperature by the employment of a tempering treatment following the normalizing treatment. When a quench-and-temper treatment was used, the impact value was over 4 times that obtained when the steel was given only a normalizing treatment. The keyhole notch impact values for the steel in the normalized and tempered condition decreased almost in direct proportion to the drop in testing temperature, with a value at —150 F almost equal to that recorded for the same steel at 70 F, with only a normalize heat-treatment.

If a water-quench-and-temper heat-treatment is applied, the keyhole impact values remain high until the testing temperature has dropped below —50 F. An impact value of 17 ft-lb at —185

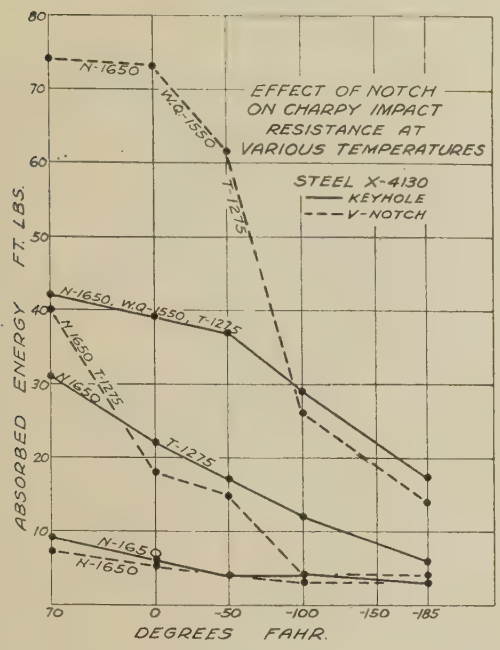

Fig. 25 Effect of Notch on Charpy Impact Resistance at Various Temperatures for Cr-Mo Cast Steel X4130

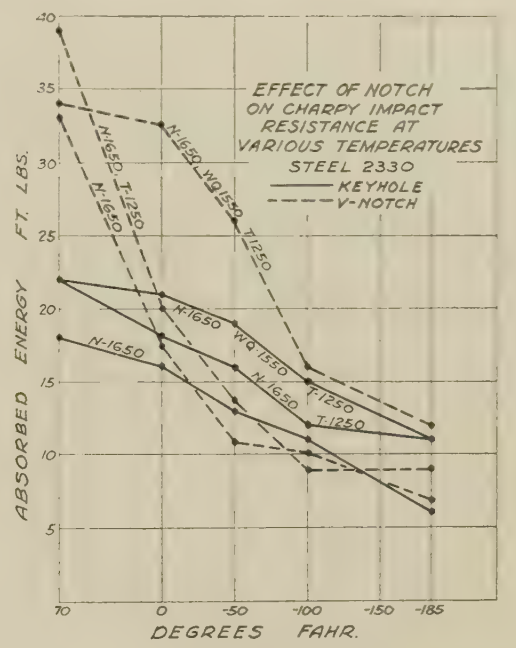

Fig. 26 Effect of Notch on Charpy Impact Resistance at Various Temperatures for Nickel Cast Steel 2330

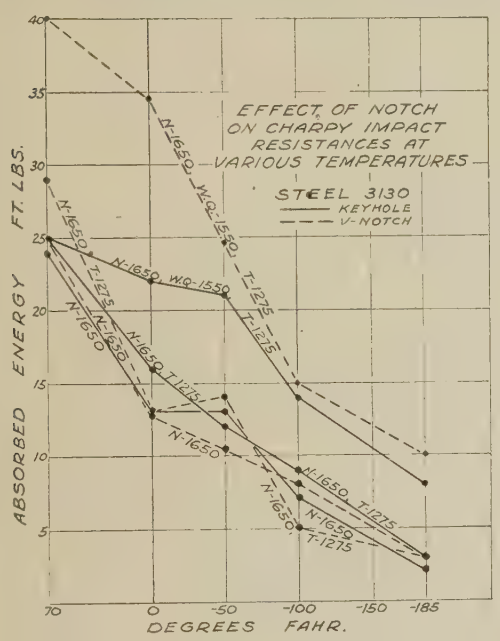

Fig. 27 Effect of Notch on Charpy Impact Resistance at Various Temperatures for Ni-Cr Cast Steel 3130

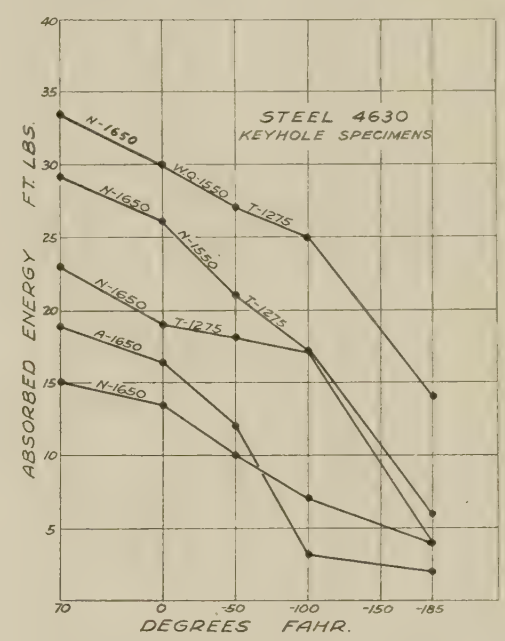

Fig. 28 Charpy Keyhole Impact Values for Ni-Mo Cast Steel 4630

F, with the broken bars all showing ductile fractures is excellent.

The various types of heat-treatment applied to X4130 cast steel had a pronounced effect upon the V-notch impact values, especially at temperatures above —100 F. Values greater than 70 ft-lb at 70 F, and more than 60 ft-lb at —50 F, are certainly impressive. The room-temperature impact values obtained from the quenched and tempered steel were nearly double those of the normalized and tempered steel. The X4130 normalized steel had low impact values at all testing temperatures.

Fig. 26 shows that changes in heat-treatment are not so influential in the case of a nickel (2330) steel at various low temperatures. Impact values of the normalized steel are good, in fact, much superior to those of X4130 for the same heat-treatment. The keyhole notch test indicates that there is little to be gained by using the quench-and-temper heat-treatment rather than the normalize-and-temper treatment; however, the V-notch bar shows that there is considerable advantage to be gained by using a quenched and tempered steel for low-temperature applications. The V-notch tests indicate that while there is no great difference in values at 70 F, regardless of heat-treatment, at testing temperatures of 0 to —100 F, there is considerable difference between the quench-and-temper curve and the two curves for the normalized steel.

The Ni-Cr steel 3130 in Fig. 27 exhibits little difference be-

tween the keyhole notch impact values and two of the three V-notch values at 70 F. There is a wider spread between the quenched and tempered values and those from the two normalize treatments than was found in the case of 2330 steel.

There is a noticeable break in the quenched and tempered curves at —50 F; nevertheless, at —185 F the fracture surfaces had a predominantly ductile appearance.

An interesting observation regarding Figs. 25, 26, and 27, is the fact that higher values are obtained when using the V-notch specimen at 70 F for normalized and tempered, and quenched and tempered steels. The V-notch specimen values remain high as compared to the keyhole notch specimen values for the water-quenched and tempered steels to testing temperatures as low as —50 F. At temperatures of —100 F, and below, there is little difference between the values, regardless of the type of notch used. If anything, the keyhole notch specimen values were higher than those obtained from the V-notch specimens. There appeared to be little difference whether the V-notch or the keyhole specimen was used, in the case of steel subjected to a simple normalizing heat-treatment.

The comparative V-notch and keyhole notch impact values for the three alloy steels (X4130, 2330, and 3130) are indicative of what would be found for other alloy cast steels.

Effect of Heat-Treatments

The type of heat-treatment is usually very important in determining the values obtained in notched-bar impact testing. Fig. 28 graphically illustrates the effect of heat-treatment on a Ni-Mo (4630) cast steel. An annealing treatment gives higher values than a normalizing heat-treatment for temperatures of from 70 to —50 F. The curve for the annealed steel then falls off rapidly. At 70 F, a double normalizing treatment produced double the keyhole Charpy value of specimens given only a single normalize heat-treatment. However, as the testing temperature was dropped, the values converged until at —185 F they were only a few foot-pounds apart. The values obtained from testing the quenched and tempered steel were highest, regardless of temperature.

Figs. 25 to 28, inclusive, definitely establish the fact that

Fig. 29 Comparison Charpy Keyhole Impact Resistance at Various Temperatures for Alloy Cast Steels Given a Normalize Heat-Treatment

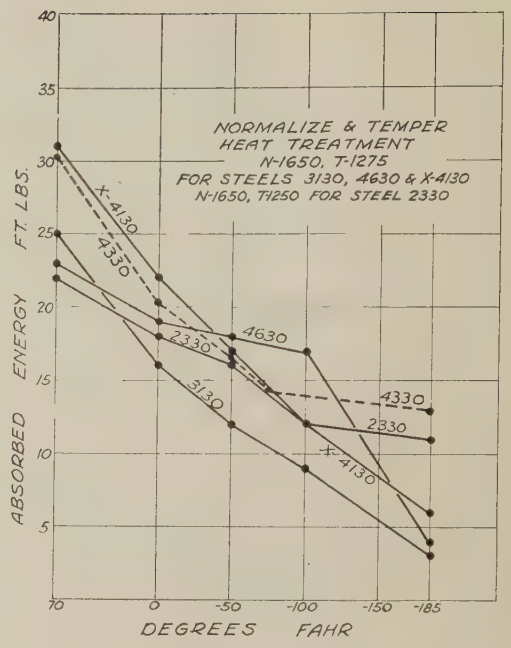

Fig. 30 Comparison Charpy Keyhole Impact Resistance at Various Temperatures for Alloy Cast Steels Given a Normalize and Temper Heat-Treatment

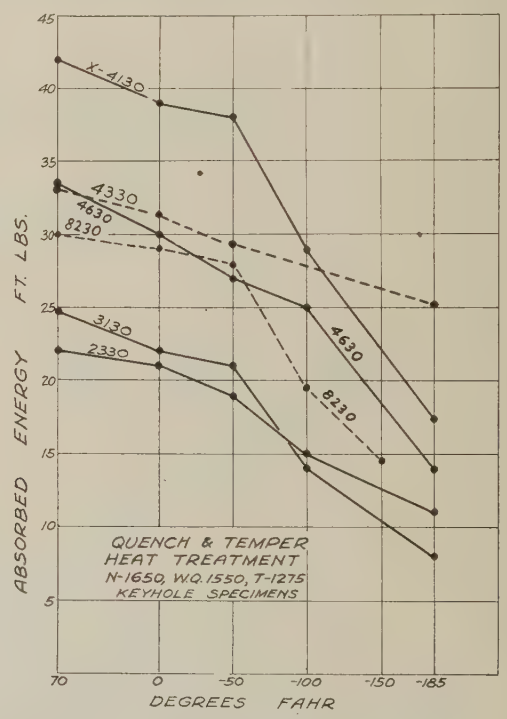

Fig. 31 Comparison Charpy Keyhole Impact Resistance at Various Temperatures for Alloy Cast Steels Given a Water Quench and Temper Heat-Treatment

neither an annealing nor a normalizing heat-treatment develop the best low-temperature impact properties at temperatures o —100 F and below. If a normalizing heat-treatment is advisable the best impact values at low temperatures can be obtained from the nickel-steel (2330), as is clearly shown in Fig. 29.

The effect of the same heat-treatment on various cast steels i shown graphically in Figs. 29, 30, and 31. These curves speak largely for themselves. The steel-casting industry has lon

known that a nickel cast steel with only a normalizing heat-treatment gave good results in low-temperature service. However, service requirements in the past did not often go to temperatures below —50 F. In the case of steels for service below —50 F, it is evident that a normalize-and-temper or a quench-and-temper heat-treatment should be used.

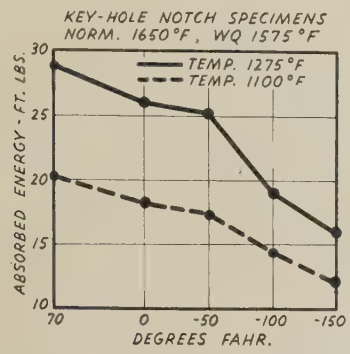

Fig. 32 Effect of Tempering Treatment on the Keyhole Notch Impact Resistance of a Water-Quenched and Tempered Mn-Mo Cast Steel 8230 at Various Temperatures

It will be noted from Fig. 30 that the results for five alloy cast steels which received a normalize-and-temper heat-treatment are very close together in keyhole notch values over the entire testing range, the values for no one steel being outstanding.

Fig. 31 shows that X4130 cast steel is superior to the others for low-temperature service when a quench-and-tempering treatment is used. This is especially true for service requirements at temperatures down to —100 F. Even though the alloy steels do show a change in direction of the curves at —50 F, they nevertheless exhibit ductile fractures and high impact values at —100 and —185 F.

The tempering temperature that should be employed, regardless of the heat-treatment specified, to obtain the best notched-bar impact values for cast steels is very high; close to the lower critical temperature of the steel. This fact is illustrated in Fig. 32. A Mn-Mo (8320) cast steel was tested after two different tempering treatments following a water-quenching operation. It was found that the higher tempering temperature (1275 F) was responsible for the highest impact values at all testing temperatures down to —150 F.

The use of the impact test for determining the acceptability of material does not necessarily insure that such material will be acceptable for the service intended. In other words, the notched-bar impact test does not simulate service conditions. If anything, it is more exacting, as a casting is usually not so severely notched or of as small a section as the notched impact-test bar. If a casting could be tested in impact at low temperatures, it might give a tough fracture when the notched impact-test bar of the steel from the casting showed a brittle fracture. Also, castings are usually subjected to repeated stresses in actual service, and the single-blow notched-bar test gives no indication of the notch sensitivity or lack of notch sensitivity. Passing or failing to pass an arbitrary foot-pound specification carries no certainty of endurance or failure of a casting in actual service. However, a uniform test, even though it be an artificial one, is necessary to give an indication of the character of the steel.

The notched-bar impact test is valuable in that it aids the manufacturer in selecting a steel, composition and heat-treatment, and in controlling the steelmaking conditions that will give high impact values at the particular temperature of testing desired. In view of these statements, it is suggested to the purchaser of steel castings for low-temperature application that his specification carry only a requirement of a minimum notched-bar impact value at a definite temperature, and that the steel foundry be permitted to select the steel and prescribe the steelmaking and the heat-treatment which will meet this requirement.

Impact Values of Cast Steels Versus Impact Values of Wrought Steels

Studies of wrought steels by various investigators tend to show that there are considerable differences between impact values obtained from test specimens taken in the direction of rolling, as compared with those obtained when the specimens are taken transverse to the direction of rolling. The latter values are usually much lower than the former. The differences are accentuated by steels of high inclusion content and banded structures. Also, it cannot be assumed from notched-bar data on longitudinal specimens of wrought steel that a given piece of wrought steel will behave in the same fashion when the notch and the applied stress come in another direction.

Generally speaking, wrought steels, when tested in the direction of rolling, show higher impact values than cast steels of similar composition. However, cast steels do not show directional properties; hence the notched-bar impact values are greater than those of wrought steels when tested transverse to the direction of rolling. If the two wrought-steel values are averaged, they are comparable to the values obtained for cast steels of similar composition. Hence what seem to be low impact values for a cast steel, as compared with the most favorable values for a wrought steel, may, in fact, reflect an ability to withstand notches in any direction much better than a wrought steel having large directional differences.

Practically all cast steels used for low-temperature service are deoxidized with aluminum and are fine-grained. These steels have ductile fractures at testing temperatures as low as —150 and —185 F. The trend of the curves of many of the alloy cast steels indicates that ductile fractures would be found at testing temperatures below —185 F.

Temporary Installation of Shasta Turbines at Grand Coulee

By H. H. SLOANE,[1] DENVER, COLO.

Two hydraulic turbines of 103,000 hp at rated head of 330 ft, designed for the Shasta power plant were transferred to Grand Coulee early in 1942, to supply power for war industries. The engineering problems encountered in installing the units in the completed Coulee turbine pits and methods of solving them were unique. The installation, as measured by the efficient performance of the units and large amount of power made available at a critical time, proved a very valuable asset to the war effort.

At the start of World War II, it became vitally important to put into the war effort every available source of power. The shortage of power in the Pacific Northwest for operation of rapidly expanding shipyards and other war industries was critical. A proposal by Reclamation Bureau engineers to install temporarily in available spaces at Grand Coulee power plant on the Columbia River the first two of the 75,000-kw units just completed for the Shasta power plant was promptly approved by the War Production Board. These units could not be placed in immediate service at Shasta since construction of the dam and power plant was not sufficiently advanced. Also the three remaining generating units on which work was in progress in the shops would provide for the initial power requirements at Shasta.

The hydraulic turbines and governors of the Shasta units were designed and built by the Allis-Chalmers Manufacturing Company. In a paper by J. F. Roberts,[2] the turbines, their characteristics, and special features are described. At the rated head of 330 ft, the discharge of the Shasta turbine equals 3200 cfs at full gate, and, for the units of the Coulee power plant, the corresponding design discharge is 4500 cfs. From this comparison it is seen that the Coulee draft tube is about 40 per cent larger than the Shasta tube. A cross section of a Shasta unit installed in the Grand Coulee power plant is shown in Fig. 1.

Installation Problems and Procedure

Since the Shasta units and the Coulee units in the left powerhouse have opposite hand rotation, it was necessary to make some alterations in the unit bays already constructed at Coulee and also in the connections to penstocks and draft tubes, in order to install the Shasta units in their temporary location. New turbine-inlet pipes were designed so that the Shasta counterclockwise units could be placed in the Coulee pits and connected to the existing penstocks. Three bays of the Coulee left powerhouse were required to accommodate the two units. Unit A was located in bay L-7 and supplied from the penstock in bay L-8. Unit B was located in bay L-8 and connected to the penstock in bay L-9. The penstock leading to bay L-7 was temporarily closed off. Fig. 2 shows this arrangement.

The work of preparing the turbine pits for the temporary units required cutting openings approximately 20 ft high and 30 ft long in double walls each of 4 ft in thickness between bays L-7 and L-8, and also between L-8 and L-9. Excavation of concrete work was begun on May 1, 1942, and was completed in the following month. The completed excavated opening between bays L-7 and L-8 is shown in Fig. 3.

The first carload of parts of the Shasta turbines arrived at the Coulee project in the latter part of May, 1942. The foundation for support of the discharge-ring, speed-ring, and scroll-case sections was constructed so that the leveling jacks, hold-down bolts, and H-column supports which had been furnished for erecting the turbine at Shasta could be used with very few minor changes. Assembly of scroll-case supports and anchors is shown in Fig. 4. The draft-tube liner, forming the transition from the top section of the Shasta liner to the formed concrete elbow of the Coulee draft tube, had to be specially fabricated for this installation. Since delivery of the plate-steel liners could not be obtained until much later in the year, block-outs were left in the concrete, and work proceeded in assembling the sections of speed-ring castings and plate-steel casings.

When completely erected in proper alignment with the double-butt-strap-riveted joints closely fitted and bolted, the rivet holes were field-reamed to $^1/_{16}$ in. over the rivet diameter, and the joints riveted and calked, Fig. 5. The discharge ring and draft-tube top were raised and bolted to the speed ring after all shrink links connecting the speed-ring sections had been installed. A test-ring bulkhead to close off the wicket-gate openings was secured in place by bolting the top cover plate temporarily to the speed ring. A test bulkhead was then bolted to the inlet of the scroll and the casing tested under a hydrostatic pressure of 175 psi. Reports of the test indicated that the amount of leakage was practically negligible.

Just prior to embedding the turbine parts, the concrete saddles, which are indicated in Fig. 4, were constructed and dry-packed against the scroll case. These saddles are provided for the purpose of holding the casing against lateral movement while the concrete is being placed around it. The usual Bureau procedure of maintaining hydrostatic pressure within the casing equal to the normal operating head without water-hammer pressure was followed in embedding the temporary units. This method reduces the stresses in the surrounding concrete to a minimum by assuring that the casing has its normal shape when embedded. The normal pressure for the Coulee installations, which was maintained until after the initial set of the concrete, equaled 145 psi. The turbine casing erected in bay L-7 was tested and embedded during August, 1942. Thirty to forty days later installation was completed of the similar parts of unit L-8. Two sets of test bulkheads were transferred to Coulee so that this phase of the work could proceed on both units at the same time.

The seats for the upper and lower stationary seal rings were bored with a portable rig set in the wheel pit with the test bulkheads in place and with the casing under pressure. Performing this final machine operation in the field after the casing was embedded and with the cover plates in place assured obtaining the

[1] Mechanical Engineer, Department of Design and Construction, Bureau of Reclamation, Denver, Colo.

[2] "The 103,000-Hp Turbines at Shasta Dam," by J. F. Roberts, presented at the Fall Meeting, Salt Lake City, Utah, Sept. 1–4, 1947, of The American Society of Mechanical Engineers.

Contributed by the Hydraulic Division and presented at the Fall Meeting, Salt Lake City, Utah, Sept. 1–4, 1947, of The American Society of Mechanical Engineers.

Note: Statements and opinions advanced in papers are to be understood as individual expressions of their authors and not those of the Society.

design clearance between the stationary and rotating turbine parts. The remaining parts of the turbine, consisting of runner and shaft, wicket gates, top cover plate, shifting ring, stuffing box, etc., were then installed. All the piping in the wheel pit was used as transferred from Shasta with only a few minor changes.

Unit L-7 turbine had been virtually assembled before the new plate-steel draft-tube liner was received at the project. It was then necessary to cut the liner plates so that they could be taken into the draft-tube blockout through the elevation 921 gallery. The strut portion of a concrete collar which had been built at elevation 930.25 to permit placing concrete above this elevation, prior to receipt of draft-tube liner, was chipped out. The liner sections were then assembled in place with fitting-up bolts and the seams welded. It was not necessary to follow this erection procedure for the L-8 unit, since the draft-tube liner arrived in time to permit lowering the plates through the central opening of the scroll case before the runner and cover plate were installed.

The installation of the turbine-inlet pipe of the L-7 unit also followed after complete erection of the turbine proper. The inlets designed for this temporary installation were fabricated by the Western Pipe and Steel Company. They are 15 ft ID at the connection to the Coulee penstocks and reduce to 12 ft 8 in. ID at the turbine-casing inlet. Expansion joints are provided at the upstream wall of the powerhouse and also where they cross the building expansion joint between adjacent bays.

Concreting and other work on the L-8 unit could not be completed until the inlet pipe to unit L-7 was installed, since the clearance between inlet pipe and casing was not sufficient to permit separate placing of the surrounding concrete.

Assembling the Generators

While the turbines were being installed work was in progress in assembling the rotors and stators of the 75,000-kva generators furnished by the General Electric Company for the Shasta units. On completion of the generator foundations, these assemblies were moved from the temporary erection foundations to bays L-7 and L-8, Fig. 6. Piping was installed to the turbine governors which had been set in position in the gallery at elevation 951.00 and the operating mechanism of the actuators removed, cleaned, reassembled, and adjusted. Except for the substitution of a cable restoring mechanism in lieu of the pull rod furnished for the Shasta installation, the governors were used in the temporary Coulee location without change. On February 14, 1943, unit L-7 was started for the first time. Dry-out of the unit was completed in the following few days and on February 25 the unit was put on the line. It was May 4 when unit L-8 was first synchronized to the bus.

The predicated performance of these units in the turbine setting and water passages constructed for the Coulee turbines was determined from model tests conducted in the laboratories of the Allis-Chalmers Manufacturing Company at the time the temporary transfer of the units to Coulee was proposed. Comparative tests of power efficiencies with models of the Shasta and Coulee draft tubes were made, and the tests were conducted with booster fins installed in the draft tubes and also without the fins. Booster fins in the Shasta draft tube were found to improve operation. In the Coulee-draft-tube model, however, the turbine showed efficiencies practically the same as the original Shasta-model tests, with smoother operation obtained without the fins. Therefore booster fins were not installed in the L-7 and L-8 units at Coulee.

Efficiency Test and Performance Record

After unit L-7 had been in operation in the Coulee plant about 6 months, an efficiency test was made by the Gibson time-pressure method of water measurement. The Gibson apparatus was connected to the straight section of the penstock at two piezometer sections 99.96 ft apart. The turbine-gate leakage, which was added to each Gibson-diagram quantity, was found to be 7 cfs, as computed from observing the rate of fall of the water surface in the penstock. The headgate leakage of 0.11 cfs was determined by observing the flow over a circular weir at the entrance to the scroll-case drain line. During the test, the servomotor piston was held in position for each run by means of blocks specially prepared for this purpose. The generator was used as a brake to determine the horsepower output of the turbine. The generator output was measured by electrical meters, and the generator losses were added in determining the turbine output.

Correct head readings could not be obtained by using the net head piezometers since they were located downstream from the inlet elbow and at a section containing a slight taper. Manometer readings taken from the piezometers located in this converging section actually showed a gain in energy due to impact on the piezometers. Therefore it was necessary to determine the loss of head from manometer readings taken with the instrument connected to the forebay static line and the lower Gibson taps and compute the remaining loss consisting of pipe friction and bend losses. The headwater elevation was measured by a float gage installed in a stilling well in the dam. The readings of the tail-water level were taken by means of a water manometer connected to a pipe line to the tailrace. To insure uniform tail-water levels, two units with a combined gate opening of 100 per cent were used throughout the tests.

The maximum efficiency of the turbine under a net head of 330 ft was found to be 92.1 per cent, with an output of 95,000 hp and 2760 cfs discharge. From the results of this Gibson test and the model tests, the turbine manufacturer calculated the performance curves shown in Fig. 7. The turbine efficiencies in per cent, and discharge in cubic feet per second are plotted against the horsepower output for operating heads of 263, 290, 310, 330, and 355 ft.

Records show that the two Shasta generating units performed well in their temporary location. Together they supplied over 3,000,000,000 kwhr of energy to the war industries of the Northwest. Although the units were rated at 75,000 kw, they were able to produce 84,000 kw continuously, and, when extra power was needed, it was possible for each unit to produce up to 92,500 kw until the peak demand was over.

This performance was obtained throughout the length of their temporary service without any major repairs being needed to either machine.

Units Returned to Shasta

In the latter part of 1945, arrangements were made to return the units to Shasta and on December 3 unit L-8 was taken out of service and dismantling was started immediately. The unit in bay L-7 was not removed from service until January 16, 1946. The biggest job was the removal of the temporary concrete supporting the generator and embedding the turbine casings. The concrete to be removed amounted to about 6500 cu yd. Most of it was broken out in large blocks, some of which weighed as much as 87 tons. The concrete around the turbine casing and draft-tube liner, however, had to be removed by hand-operated chipping guns, which was a slow and difficult job.

By September, 1947, the reassembly of these units in their final location in the Shasta power plant was nearing completion. The scroll-case sections fitted together so accurately that reaming of rivet holes, and the use of larger-size rivets in the field joints between sections was not necessary.

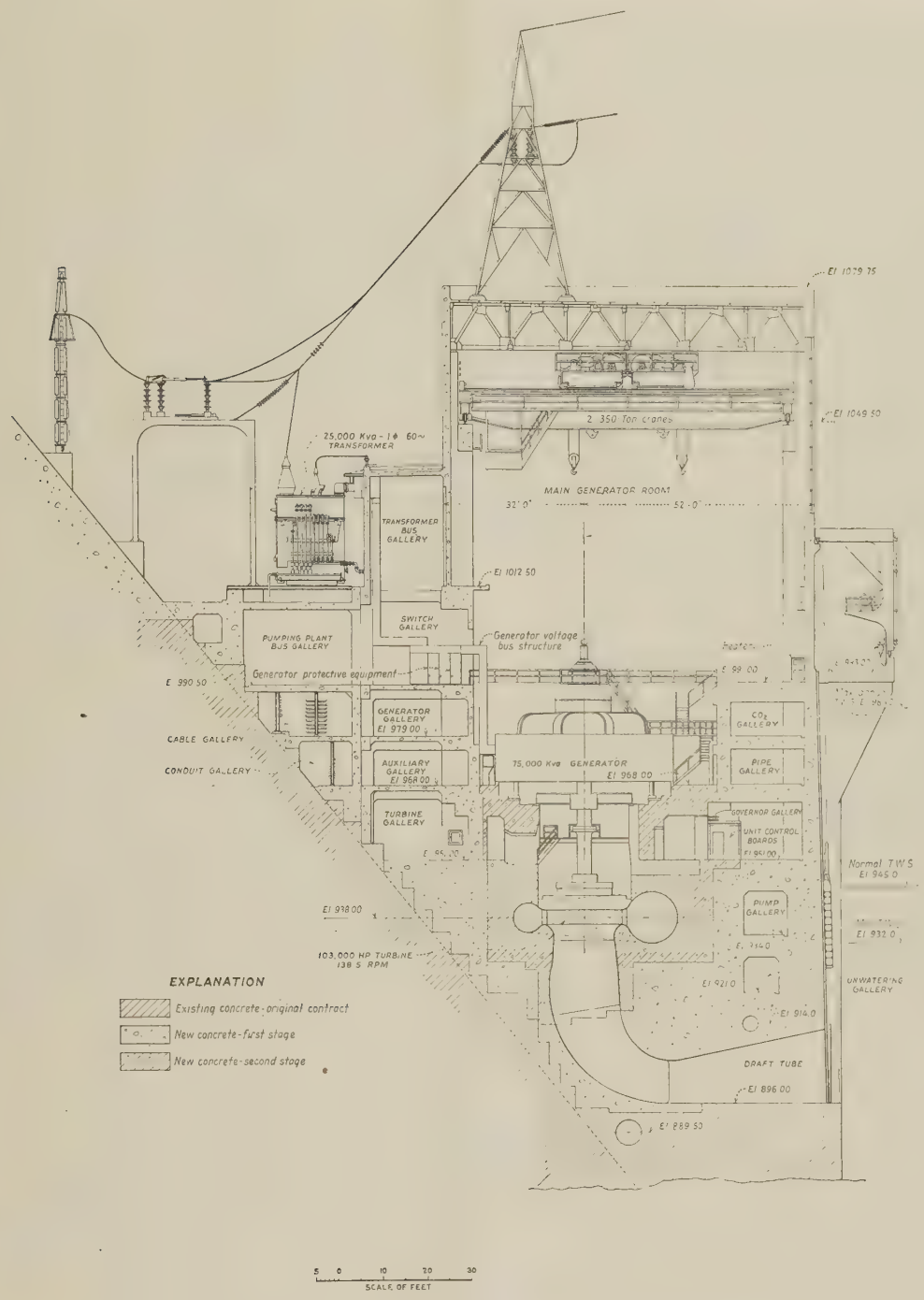

Fig. 1 Cross Section of Shasta Unit in Grand Coulee Power Plant

U OF I

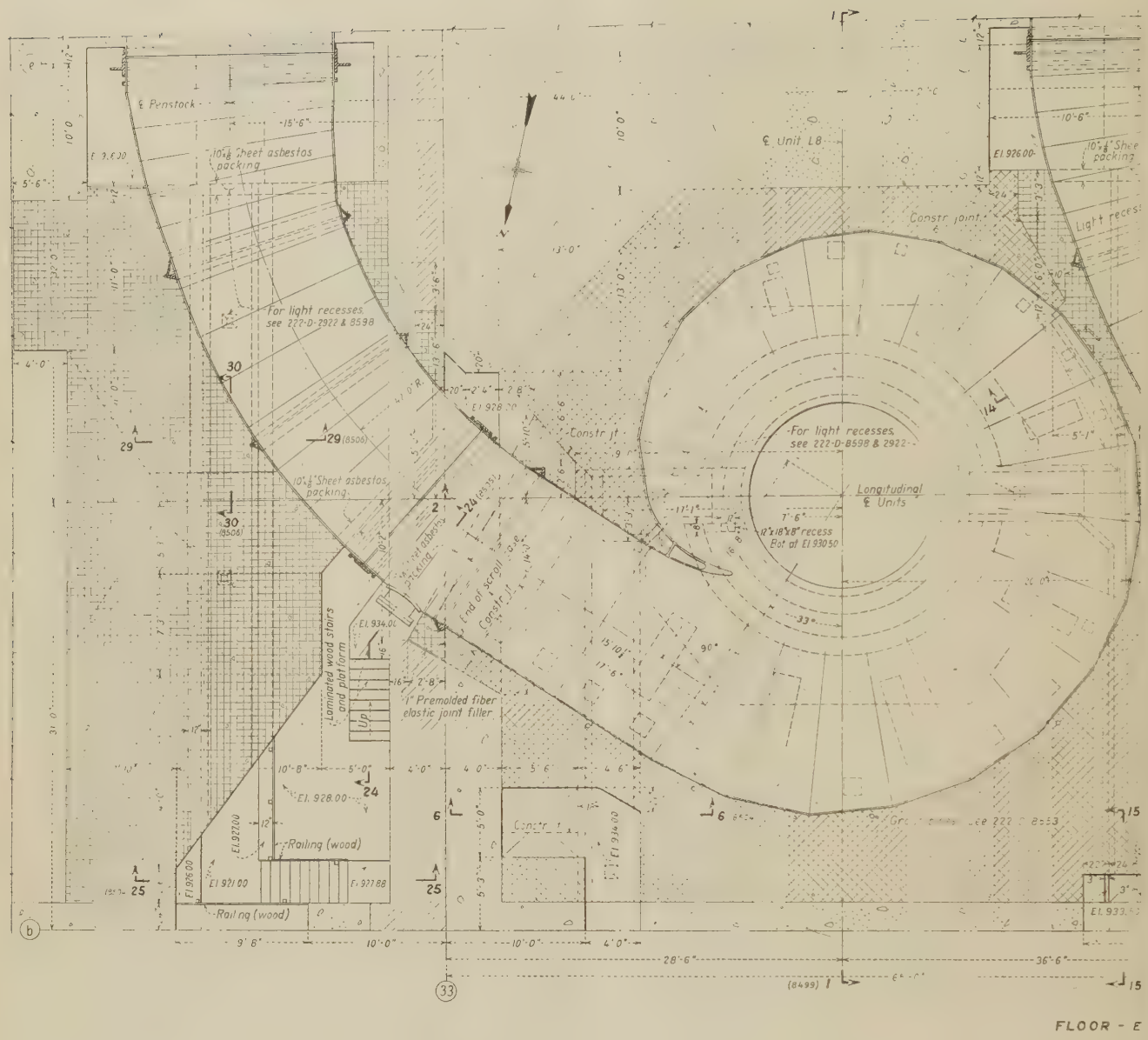

Fig. 2 Arrangement of Inlet Con-

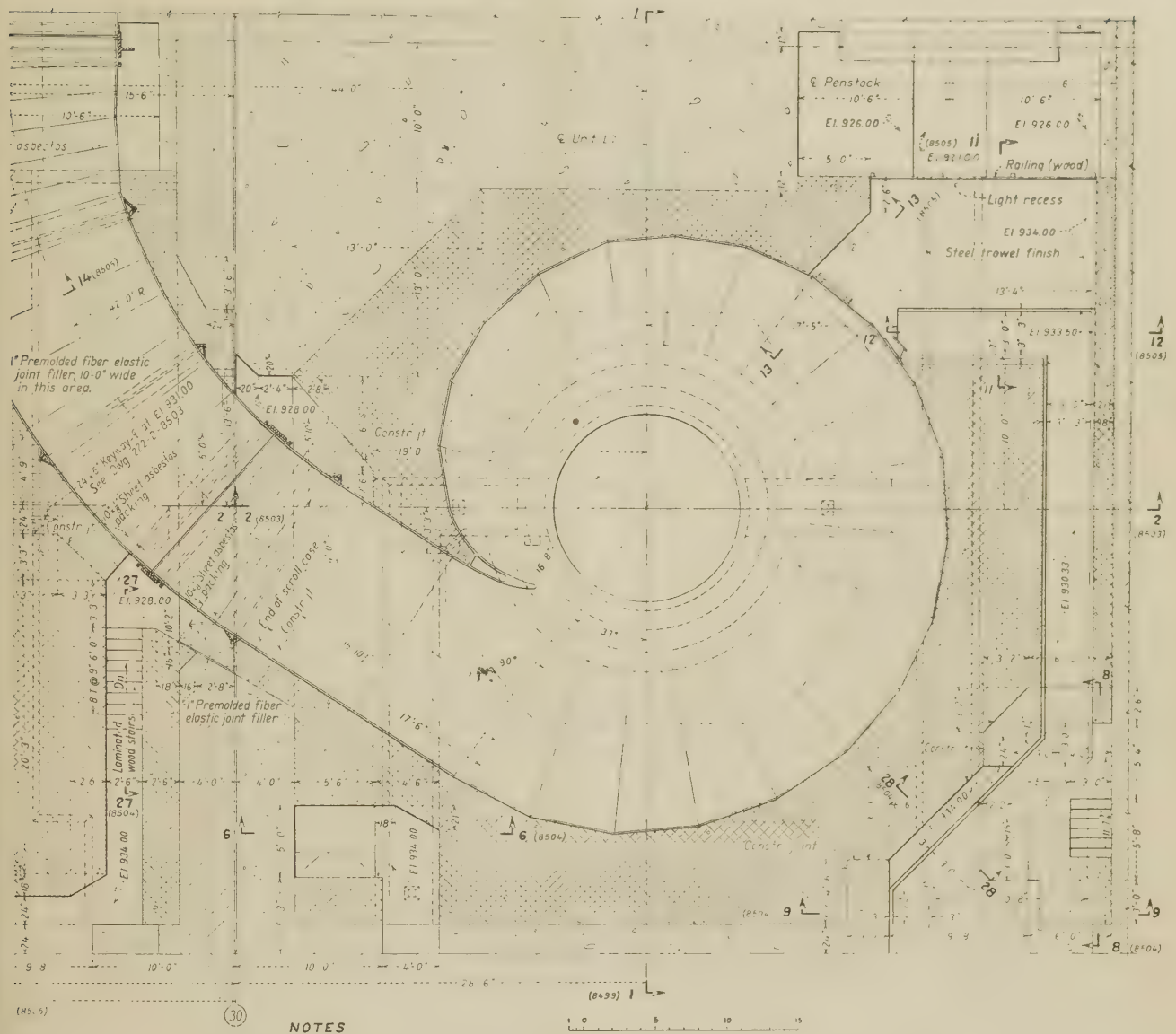

L. 934.00

NOTES

All passageways and floors to be steel trowel finished
For general arrangement, notes, concrete symbols and reference drawings see 222-D-8437 & 8498.
Saddles for erection of turbine inlet pipes to be located in the middle of pipe sections, for details, see 222-D-8646
Saddles and jack plates under scroll case and grout pipes shown for L8 same for L7.
Do not remove forms over El. 931.00 tunnel until concrete has been poured to El. 935.00.

SCALE OF FEET

Provide 1" radius semicircular or 1" high triangular shaped formed drains around all circumferential and along all horizontal joints of turbine inlet pipes; these drains to be interconnected and taken to a header at the bottom of the pipe and discharging to both expansion joint chambers.

NECTIONS TO TURBINES L-7 AND L-8

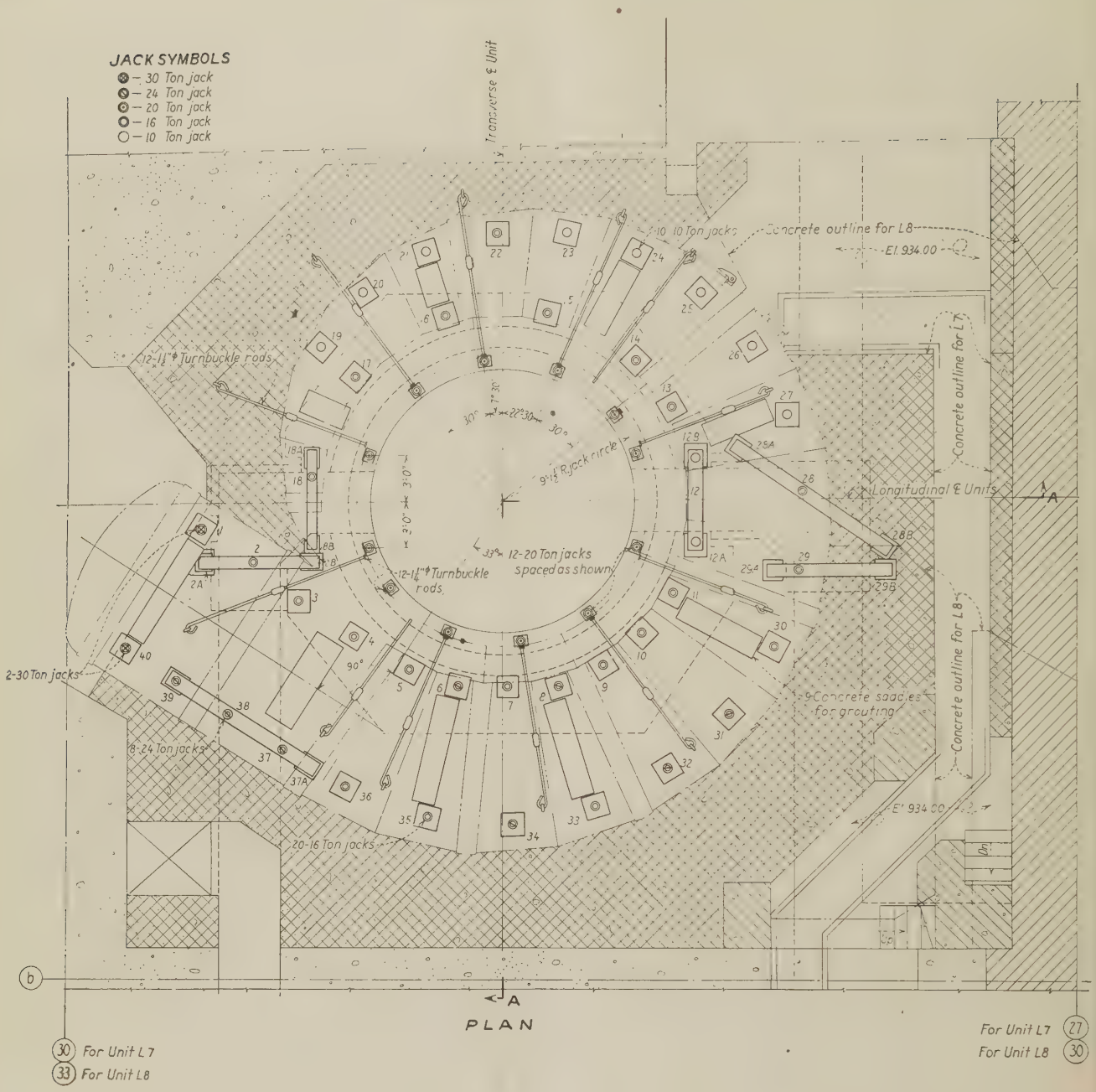

Fig. 4 Arrangement of Scroll-

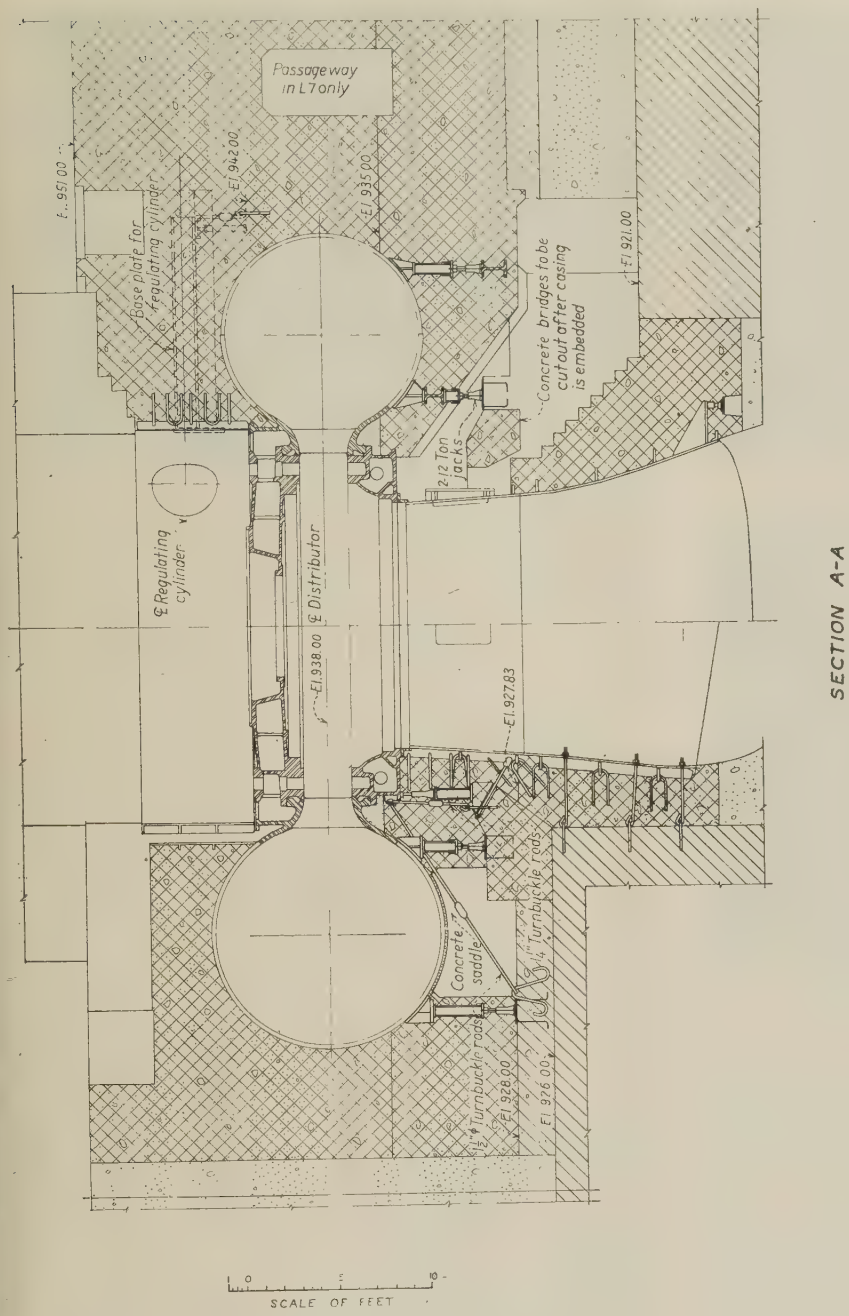

Case Supports and Anchors

Fig. 3 Opening Excavated for L-7 Inlet Pipe

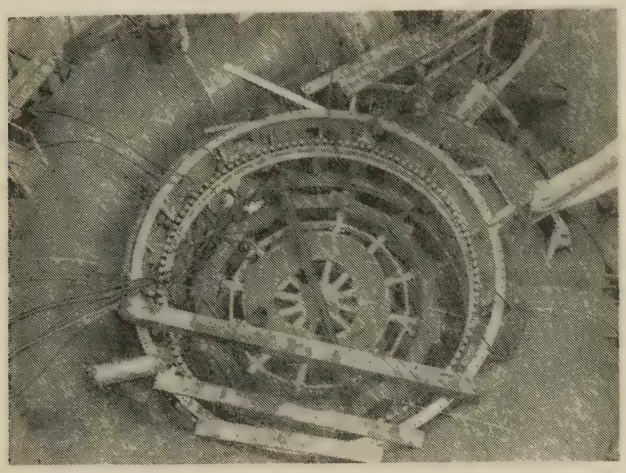

Fig. 5 Assembled View of Scroll Case

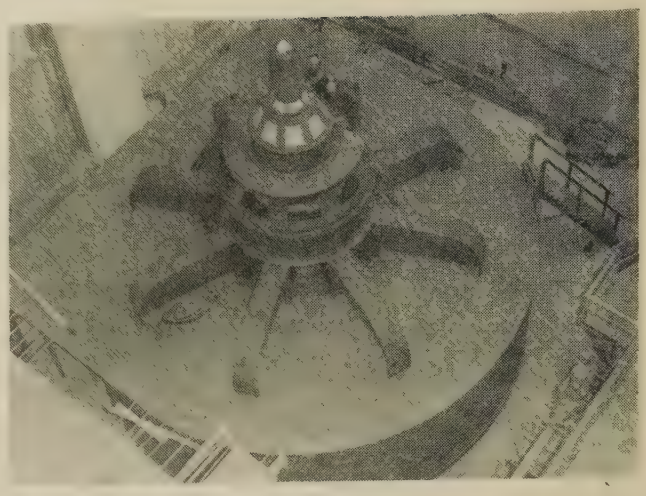

Fig. 6 Unit L-7 Generator Immediately Before Starting Its First Test Run

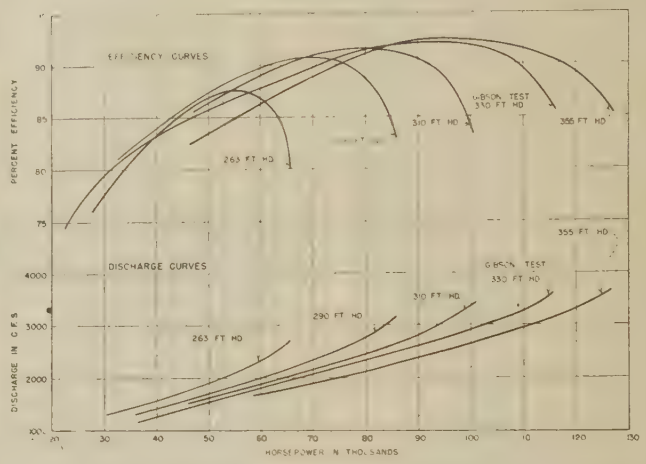

Fig. 7 Performance Curves of the 103,000-Hp Shasta Turbine Installed in Grand Coulee Power Plant

Discussion

J. F. Roberts.[3] The author has presented a very interesting paper on a rather unusual subject. To the writer's knowledge, we have never had a previous case where turbines designed for one set of conditions were installed and operated in a plant under different conditions.

The author mentions the design of draft tube which was necessary in order to accommodate the Shasta turbines in the Grand Coulee powerhouse, where the draft tubes had already been built. Actually, the difference in the discharge diameter of the runners was 16 in., the Grand Coulee runner having a discharge diameter of 172 in., as compared with 156 in. for the Shasta turbine runners. This 16-in. difference in diameter had to be taken care of in a new upper draft-tube liner designed with considerably more flare than ordinarily would be used in a draft-tube liner or in a good Venturi section.

The Gibson tests, however, showing a maximum efficiency of 92.1 per cent for the Shasta turbines installed in the modified Grand Coulee draft tube is a relatively good performance and compares with the 93.3 per cent obtained on similar turbines when tested on their own draft tubes in the Shasta plant. This difference of 1.2 per cent cannot all be attributed to the difference in the draft tubes, however, as the tests at Coulee were made under 330-ft head, whereas the tests at Shasta were made under 380 ft-head. The runners were actually designed to give their best efficiency at heads between 380 and 400 ft, and the models show that under the 380-ft head, the runner is considerably more efficient than at the 330-ft conditions; therefore only part of the 1.2 per cent difference should be attributed to the draft-tube conditions.

[3] Manager, Hydraulic Department, Allis-Chalmers Manufacturing Company, Milwaukee, Wis. Mem. ASME.

Author's Closure

Mr. Roberts' discussion adds valuable data on the subject regarding the difference in size and shape of the draft tubes designed for the Shasta turbines and the modified tube used in the temporary Coulee installation. The slightly lower turbine efficiency as measured by the Gibson tests is attributed mainly to the difference between the 380-ft design head, or best efficiency head of the runner, and the design head of the Coulee turbines of 330 ft at which unit L-7 of the temporary installation was tested and compared. The unusual elbow bend immediately upstream of the turbine casing, shown in Fig. 2, required to connect the counterclockwise units to the existing penstocks, probably accounted for some of the difference in turbine performance in addition to the bend losses, which were computed and allowed for in determining the turbine efficiency.

The author agrees with the points brought out in the discussion showing that the larger Coulee draft tube, and necessary changes in the flared top, affected performance very little.

Applications of Mechanical Cascade Control Systems

By J. N. SWARR,[1] ARGO, ILL.

The development of the concept of the cascade controller placed a very powerful tool in the hands of the process-control engineer. The continued refinement of the continuous process has required an extension of the original concept so that cascade systems of increasing complexity are becoming more and more commonplace. Six distinct types of cascade systems are herein classified. A discussion of each type covers the method by which the cascade system is built up from component instruments, the operating characteristics of each system, the field of application for each system with actual illustrations, and benefits to be derived. It is suggested that the classification herein initiated be reviewed officially and perhaps extended to cover some of the more complex installations made within the past several years.

THE term "cascade controller" became a part of the control engineer's vocabulary when it was introduced by C. E. Mason to describe a combination of control devices wherein the output pressure from a pneumatic controller was used, not to position a control valve, but to select and adjust the set point of a rate-of-flow controller. The output pressure from the flow controller then adjusted the position of the valve.

The progressive refinement of the continuous process has made it necessary to bring more and more variables under automatic control, a condition which has made it desirable, and in many cases essential, to provide control devices which could be combined in other and more complex ways. In this paper the term cascade controller is used to designate any control system in which the set point of one or more controllers is adjusted automatically by any one of several means.

In order to simplify the presentation, the author has assigned type numbers to the several classes of cascade combinations discussed. This is a purely arbitrary classification and obviously has no official sanction.

Type I Control System

The need for the cascade control system which is classified here as Type I can be illustrated by studying the unit process illustrated diagrammatically in Fig. 1. This unit process is in widespread use in the pulp and paper industry.

Wood chips are converted to pulp in digesters on a batch basis. When the conversion is complete, the contents of the digester are blown into the blow tank. One blow tank is common to a number of digesters, the operations of which are staggered so that the contents of successive digesters are received at regular intervals. The pulp is withdrawn from the blow tank at a uniform rate by means of a pump. Therefore the level in the tank rises rapidly when a digester is being blown and then falls very slowly as the pulp is withdrawn between blows.

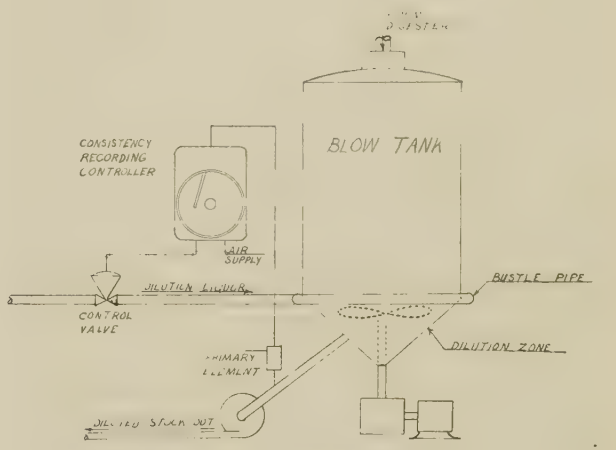

Fig. 1

The portion of the blow tank which extends upward from the base of the cone is nothing more than a surge tank. The portion within the cone is operated as a continuous dilution station in which the pulp, which comes from the digesters at approximately 12 per cent consistency, is diluted with black liquor to an accurately controlled consistency of approximately 2 per cent. The dilution liquor reaches the dilution zone through a number of radial pipes which are fed from a bustle surrounding the cone. The rate of flow is controlled by means of a valve on the basis of the consistency of the outgoing stock, as measured by the consistency controller. Thorough mixing in the dilution zone is assured by a large motor-driven agitator.

The following three load changes affect the controllability of this dilution process:

1 There will be a demand-side load change in the form of variations in consistency of the incoming pulp between successive discharges from digesters. In this particular process both the magnitude and the rate of change of this load change are small so that the resultant deviations in controlled consistency, using the simple controller illustrated, are insignificant.

2 The downstream pressure on the control valve is the head due to the level in the blow tank, and this varies at a high rate and by a large amount whenever a digester is discharged. With the valve in a given position, the flow, following a discharge, may be reduced to as little as 40 per cent of that existing before the discharge occurred. An appreciable dead-time lag and a relatively small capacity in the dilution zone result in a large deviation from the set point before the controller senses the need for a change in the valve position.

3 In many cases, the upstream pressure on the control valve is also subject to large pressure changes which occur at a high rate, and these likewise will cause large deviations in the controlled consistency.

These upstream and downstream pressure variations on the valve are supply-side load changes.

Using the simple reset consistency controller and valve, as shown in Fig. 1, the deviation which will occur before the con-

[1] Corn Products Refining Company. Mem. ASME.

Presented at the National Conference of the Industrial Instruments and Regulators Division, Chicago, Ill., Sept. 8–9, 1947, of The American Society of Mechanical Engineers.

Note: Statements and opinions advanced in papers are to be understood as individual expressions of their authors and not those of the Society.

troller senses the need for a change in the position of the valve is given by[2]

$$\Delta C = \left[\frac{0.12}{1 + 5\sqrt{\dfrac{P_1' - P_2'}{P_1 - P_2}}} - 0.02 \right] \left(1 - \epsilon^{\frac{-FT}{v}} \right) \ldots [1]$$

where ΔC is change in consistency; P_1 and P_2 are upstream and downstream pressures, respectively, on valve before supply-side load changes occurred; P_1' and P_2' are the same pressures after the load change occurred; 0.02 is the consistency to which the stock was being diluted before the load change occurred; 0.12 is the consistency of the stock entering the blow tank from the digesters; F is the rate of flow of dilute stock out of the blow tank; T is the dead-time lag in the measuring system; v is the effective volume of stock in the dilution zone.

By substituting representative constants we find that in a typical case the consistency might increase to 0.026 before the controller initiates any corrective action. This is a 30 per cent variation in the controlled variable, a variation which obviously cannot be tolerated by any modern standards. It must be concluded, therefore, and this conclusion is well substantiated by experience, that the simple controller is unsatisfactory for this application.

In order to hold the deviations, due to supply-side load changes, within required limits, it is necessary that a cascade control system be installed as shown in Fig. 2. Here a rate-of-flow con-

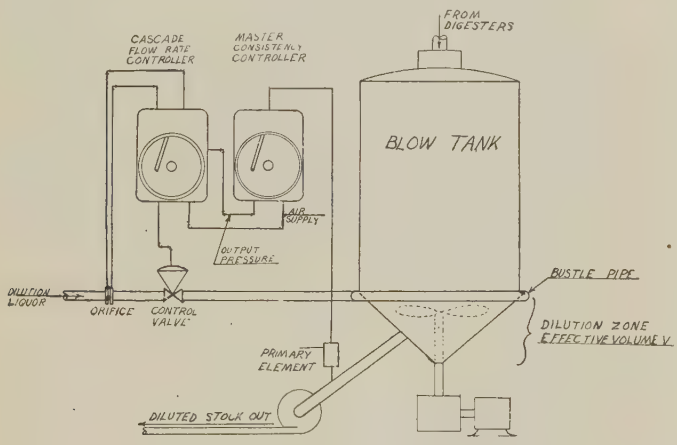

Fig. 2

troller and its associated valve maintain a rate of flow of dilution liquor which is determined only by the set point on the controller. The consistency controller, instead of positioning the valve, automatically selects and adjusts the set point on the flow controller at whatever value is required to hold the consistency at the desired value.

With this system, a variation in either the upstream or downstream pressure on the control valve will not produce a change in the rate of flow but merely a change in the valve position, the result being that supply-side load changes are eliminated so that the consistency controller is required to compensate only for demand-side load changes. Since all continuous processes are subjected to supply- as well as demand-side load changes, the development of the simple cascade control system placed a very effective and powerful tool in the hands of the control engineer.

In addition to the usual adjustments for sensitivity and reset rate, it is desirable that the Type I cascade controller be equipped with two extra adjustments which are associated only with its cascade mechanism.

The first of these determines the position of the set point when the output pressure of the master controller is zero. This is a low-limit setting in that it determines the point below which the set point cannot be moved by the master controller. It assures a safe measured minimum flow into the process in case of failure of the master controller.

The second adjustment determines the ratio between a given change in air pressure from the master controller and the resultant change in the set-point position. This can be used to advantage in several different ways. For example, it can be used to establish the set point which will exist when the output pressure from the master controller is at maximum, thereby establishing a measured maximum flow rate which the control system will permit to the process.

It can also be used as a sensitivity adjustment for the control system in that it has exactly the same effect on the system as changes in the throttling-range adjustment in the master controller.

Type II Control System

The combination which is classified as Type II in this paper

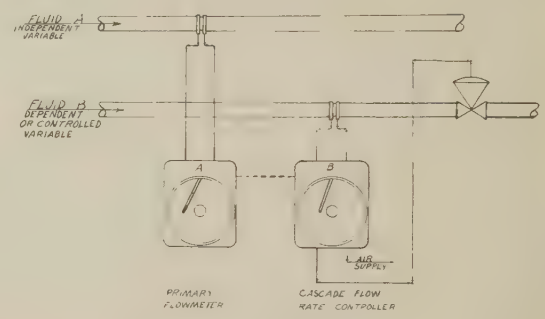

Fig. 3

is illustrated in Fig. 3, and is perhaps the most widely used cascade control system. It will be recognized as the "flow ratio controller." In the diagram the rate of flow of fluid A varies at will. The problem is to control the rate of flow of fluid B, which is usually referred to as the dependent or controlled variable, so that it bears a fixed predetermined ratio to the flow rate of fluid A, which is the independent variable. This is accomplished by interconnecting the two instruments so that the position of the set point of controller B, at all times, bears a definite predetermined relation to the instantaneous flow rate as measured by instrument A. In other words, the set point of controller B is continuously adjusted by the measuring element of instrument A. This differs from the Type I system in which the set point of the cascade controller was adjusted by the output pressure from the master controller. In many cases a simple mechanical linkage connects the measuring element of A to the set point of B which often makes it possible to record both flows on a single chart by combining both instruments in a single case. The ratio between the pen movement of A and the set-point movement of B is determined by an adjustment provided for the purpose. Since the indicating pointer or recording pen of controller B should coincide with its set point, this adjustment will determine the ratio between the deflections of the two pens; thus

[2] This expression assumes an instantaneous change from P_1 to P_1' or from P_2 to P_2'. Actually of course the change in pressure is at a constant rate so that the precise expression is somewhat more complex. Since this is a descriptive rather than a theoretical paper, the author feels the simplification here made is justified on the basis of keeping the mathematics as simple as possible.

$$\frac{D_d}{D_i} = K \qquad [2]$$

where D_i is the linear deflection of the pen which records the independent variable; D_d is the corresponding linear deflection of the pen which records the dependent variable when it is on its set point.

In order to express the ratio K in terms of flow units, let

D_l = linear length of scale in inches
S_d = full scale range of dependent variable meter
S_i = full scale range of independent variable meter
F_d = indicated scale reading of dependent variable corresponding to pen deflection D_d
F_i = indicated scale reading of independent variable corresponding to pen deflection D_i

Then if the flow scales are linear

$$F_i = S_i \frac{D_i}{D_l} \qquad [3]$$

from which

$$D_i = \frac{F_i D_l}{S_i} \qquad [4]$$

and

$$F_d = S_d \frac{D_d}{D_l} \qquad [5]$$

from which

$$D_d = \frac{F_d D_l}{S_d} \qquad [6]$$

Substituting Equations [4] and [6] into [2], we obtain

$$\frac{F_d}{F_i} \frac{S_i}{S_d} = K \qquad [7]$$

Most modern flow-ratio controllers are equipped with ratio-adjusting scales which are graduated to read K values, as defined by Equation [2]. The range of adjustment normally supplied extends from about 3:1 to 1:3.

Equation [7] shows that in order to determine the K scale setting which is required to provide the desired flow ratio F_d/F_i, it is necessary to multiply the desired flow ratio by the reciprocal of the scale ratio S_d/S_i.

If the pens are recording on a square-root chart, then

$$F_d = S_d \sqrt{\frac{D_d}{D_l}} \qquad [8]$$

$$F_i = S_i \sqrt{\frac{D_i}{D_l}} \qquad [9]$$

from which

$$\frac{F_d}{F_i} \times \frac{S_i}{S_d} = \sqrt{\frac{D_d}{D_i}} = \sqrt{K} \qquad [10]$$

Most manufacturers of square-root-scale instruments now graduate the ratio-adjusting scale to read $\sqrt{K}$ directly. As in the case of the linear-scale instrument, the setting on the ratio-adjusting scale, which is required to produce the desired flow ratio F_d/F_i, is obtained by multiplying the desired flow ratio by the reciprocal of the scale ratio S_d/S_i. If the two flow rates are read on identical scales, the scale ratio is unity, and the flow ratio is obviously exactly equal to $\sqrt{K}$.

With K adjustable from 3:1 to 1:3, the maximum ratio setting on an instrument with a square-root scale is 1.7:1, while the minimum is 0.57:1. There are, however, several commercially available instruments whose adjustability covers a much wider range.

Occasionally a condition arises wherein a greater range of ratio adjustability is required. One way of meeting this requirement is shown in Fig. 4 in which the ratio of F_d/F_i is controlled in-

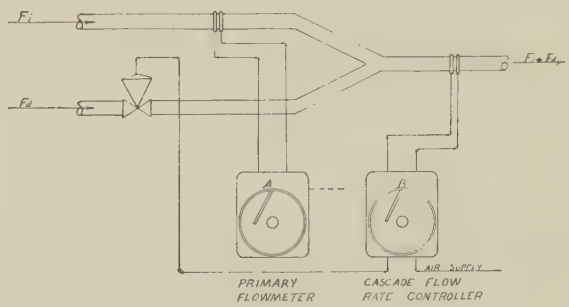

FIG. 4

directly by maintaining a predetermined ratio between $(F_i + F_d)$ and F_i.

The ratio of the flow rate as measured by instrument B to that measured by instrument A is given by

$$\frac{F_i + F_d}{F_i} = \frac{S_{i+d}}{S_i} \sqrt{K} \qquad [11]$$

where S_{i+d} is the full scale range of instrument B. From Equation [11]

$$F_i + F_d = F_i \frac{S_{i+d}}{S_i} \sqrt{K} \qquad [12]$$

$$F_i \left(\frac{S_{i+d}}{S_i}\right) \sqrt{K} - F_i = F_d \qquad [13]$$

from which

$$\frac{F_d}{F_i} = \frac{S_{i+d}}{S_i} \sqrt{K} - 1 \qquad [14]$$

Equation [14] gives the ratio which will be maintained between F_d and F_i for any setting of $\sqrt{K}$.

In order to obtain a direct comparison of the range of adjustability of the two methods of installation, assume that F_d and F_i are of the same order of magnitude so that the scale ranges S_d and S_i would be equal if installed as in Fig. 3. If installed as in Fig. 4, then S_{i+d} would be 2 S_i. Substituting this value in Equation [14] and setting $\sqrt{K}$ = 1.7, which is its maximum value, we find F_d/F_i = 2.46. With $\sqrt{K}$ = 0.57, which is its minimum value, F_d/F_i = 0.14. In this instance, therefore, this method of installation provides a range of adjustment in flow ratio of 17.5:1 whereas the installation illustrated in Fig. 3 provides a range of only 3:1.

As an alternative to the use of a direct mechanical linkage for connecting the measuring element of A with the set point of B, the pneumatic connection provides a somewhat more flexible system with only a slight sacrifice in simplicity. With this method the primary flowmeter is equipped with a pneumatic pilot device which produces an output pressure proportional to the instantaneous flow rate measured by its measuring element.

This pressure is applied to the flow controller to position its set point proportional to pressure. The desired ratio between

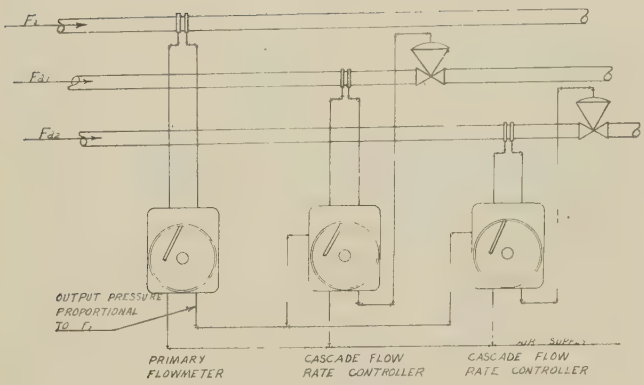

Fig. 5

the two flow rates is determined by the K value set on the ratio scale of the flow controller if the instruments have linear scales, or to the $\sqrt{K}$ value if they have square-root scales.

The pneumatic connection is generally considered a necessity where a ratio must be maintained between more than two flow rates, as is illustrated in Fig. 5. Here there are two dependent variables indicated as F_{d1} and F_{d2}. Each of the flow controllers is equipped with a ratio-adjusting device by which the ratio between any dependent flow and the independent flow may be selected. Thus (assuming square-root scales)

$$\frac{F_{d1}}{F_i} = \frac{S_{d1}}{S_i}\sqrt{K_1} \qquad [15]$$

and

$$\frac{F_{d2}}{F_i} = \frac{S_{d2}}{S_i}\sqrt{K_2} \qquad [16]$$

Obviously, this method can be extended to control any desired number of dependent flows by merely connecting additional cascade controllers to the output pressure line of the primary instrument. The author knows of one installation where constant ratios are maintained between fourteen different flow rates with this system.

Type III Control System

The rate-of-flow scale is somewhat unique in that scale zero is also absolute zero. This is generally not true of other physical quantities commonly measured in the process industries so that the lowest graduation on a commercial instrument scale is usually some arbitrarily selected value which is either higher or lower than absolute zero. For example, liquid levels are rarely, if ever, measured from exactly the bottom or top of a vessel; pressures are more often measured up or down from atmosphere than from absolute zero; temperatures are apt to be measured from any point which happens to be convenient; and zero on the pH or specific-gravity scales is practically meaningless.

If an instrument scale does not go to absolute zero it follows that a control mechanism which maintains a predetermined ratio between pen deflections will not maintain a fixed ratio between absolute values but between increments of absolute values. This action can be illustrated by the expression

$$\frac{S_i(P_d - R_d)}{S_d(P_i - R_i)} = K \qquad [17]$$

where

R_i = value, on scale of instrument which is measuring independent variable, from which the increments are measured

P_i = instantaneous value of independent variable or in other words, the pen reading

S_i = number of scale units on independent variable scale

R_d, P_d, S_d = corresponding values on dependent variable scale

K = ratio between linear movement of adjusting pen and that of dependent variable pen, or in other words, it is the ratio between linear distances on scale represented by increments $(P_i - R_i)$ and $(P_d - R_d)$

The ratio between the increments, in scale units, is given by

$$\frac{P_d - R_d}{P_i - R_i} = \frac{S_d}{S_i}K \qquad [18]$$

Where it is desirable to control the ratios of increments of physical quantities other than flow, it is obvious that the values of R_i and R_d, from which the increments are to be measured, will depend entirely upon the particular control problem on hand and will vary with each application. Also, for a given application it may be, and usually is, desirable to be able to change these values at will to meet varying operating requirements and conditions. For these reasons the cascade controller, classified here as Type III, has three manual adjustments. Two of these permit setting R_i and R_d to any desired points on the instrument scale. The third adjusts the ratio K.

As a purely hypothetical illustration of an application for this type of controller, it can be assumed that a given process requires that for every 1 F variation of P_i above the boiling point of ethyl alcohol at atmospheric pressure (173 F), P_d must vary 0.5 F above the boiling point of water at 40 psia (267 F). The ethyl-alcohol temperature is to be measured on a scale graduated 0 to 200 F and the water temperature on a scale graduated 200 to 400 F. In this case R_d is set at 267 F, and R_i at 173 F. The ratio between the increments in scale units is 0.5/1 so that $(S_d/S_i)K = 0.5$. S_i in this case is 200, while S_d is 400—200 = 200 also. Thus

$$K = 0.5\,\frac{200}{400 - 200} = 0.5$$

With these settings the relationship between the two variables can be illustrated in Fig. 6. Here the dotted horizontal line through 267 represents the R_d setting, while the dotted vertical line through 173 represents the R_i setting. The solid sloping line represents the relationship maintained between the two variables, the slope being determined by the ratio setting. A change in the R_i setting moves the curve horizontally along the P_i scale, while a change in the R_d setting moves it vertically along the P_d scale. A change in the K setting rotates the curve around the point of intersection of R_i and R_d.

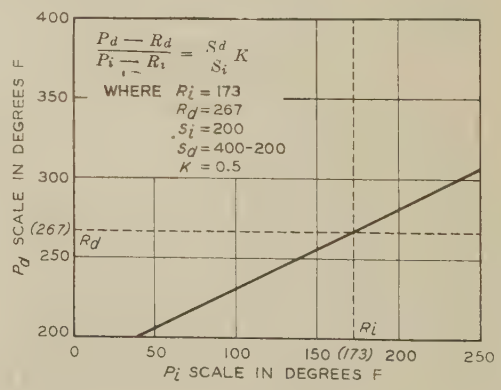

Fig. 6

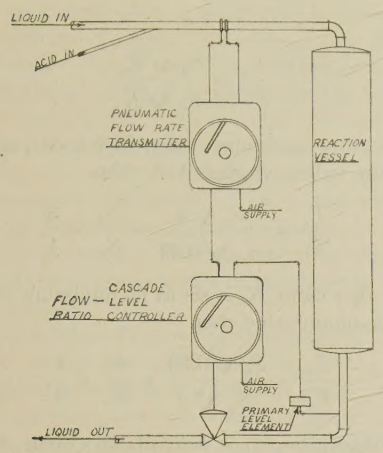

Fig. 7

An actual example of the application of this type of cascade controller is illustrated in Fig. 7. Briefly, the process involves the continuous acidification of a fluid, which then flows into a large tank through which it moves at a very low velocity. The fluid is neutralized immediately upon leaving the vessel, the only function of which is to hold the acid in contact with the fluid for a predetermined time. The contact time must be controlled automatically, and provision must be made for varying the contact time as required. The relation between the several variables is given by

$$T = \frac{\pi D^2}{4} \times \frac{L}{F} \qquad [19]$$

where

T = contact time, min
L = level maintained in vessel, ft
F = rate of flow of fluid through system cu ft per min
D = diameter of vessel, ft

Thus for any given flow rate through the system, the contact time is a function only of the L/F ratio, the time being constant so long as the ratio is maintained.

The control problem was solved as indicated. The flow rate is measured and converted to a pneumatic pressure which is directly proportional to flow. This pressure is applied to one element of the level-flow ratio controller and becomes P_i. The level in the reaction vessel is measured by means of a diaphragm bulb and becomes P_d. R_i is zero, as is usually the case with rate of flow. In this particular installation it was impractical to locate the primary element of the level instrument on a level with the bottom of the reaction vessel, so it was actually mounted 5 ft below this point. Therefore R_d was set at 5 ft on the level scale. The holding time can be set to any desired value within the range of adjustment of the instrument by merely changing the setting on the ratio or K scale.

There are some applications which require that an increase in P_i produce a decrease in P_d. This relationship is called an inverse ratio and the characteristic expression is given by

$$\frac{P_d - R_d}{P_i - R_i} = -\frac{S_d}{S_i} K \qquad [20]$$

The modern Type III cascade controller provides for both direct and inverse ratios, the ratio scale extending generally from 3:1 to 1:3 direct and from 1:3 to 3:1 inverse. Actually, the scale goes through 0:1 in going from direct to inverse, but because of the limitations inherent in mechanical linkages, the ratios between approximately 1:3 and 0:1 are not constant, and manufacturers generally do not recommend the use of these low-ratio settings.

Type IV Control System

The system classified here as Type IV is a combination of Types I and II. A typical application is illustrated in Fig. 8. Here a finely divided but insoluble carbohydrate is carried into the process in the form of a water suspension. It is required that sulphuric acid be added to this slurry at a rate which will produce a constant pH at the outlet of the mixer.

If there are appreciable pressure variations in either the slurry line or the acid-supply line, a Type I cascade controller is required. Hence the control system must consist fundamentally of a pH controller, the output pressure from which continuously selects and adjusts the set point of the acid-flow controller which in turn operates the valve in the acid line.

The acid will be received and stored at the plant in concentrated form. However, if it is added directly to the slurry in concentrated form, localized destruction of the carbohydrate will occur due to dehydration. It is therefore necessary to dilute the acid before admitting it to the process. If dilution is done on a batch basis a large storage tank will be required for the dilute acid. In addition, a small bulge tank will be required to supply the process demands while a new batch is being diluted.

On the other hand, if the acid can be diluted on a continuous basis under automatically controlled conditions while it is being used, the dilute-acid storage tank and the bulge tank can be eliminated, and the time required for an operator to make up the dilute acid can be saved.

Controlled dilution can be obtained by the use of a Type II, or flow-ratio, controller which will maintain any predetermined ratio between concentrated acid flow and water flow. The illustration shows the acid flow as the independent variable or P_i while the water flow, which is controlled by the valve, is P_d.

The complete Type IV system therefore consists of a reset type of controller, the output pressure of which selects and adjusts the set point of a flow controller at whatever value is required to hold the measured variable on its set point. The measuring element of this flow controller in turn adjusts the set point of a second flow controller to maintain a predetermined ratio between the two flow rates.

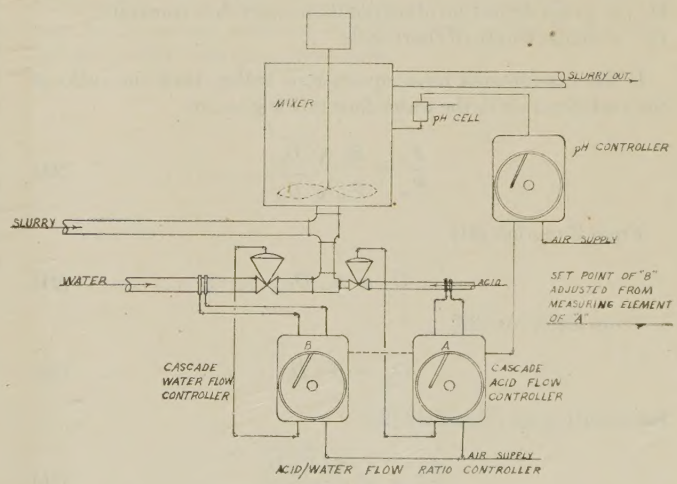

Fig. 8

Type V Control System

It was pointed out previously that the range of adjustability of the $\sqrt{K}$ factor on most commercially available flow-ratio controllers extends from about 1:0.57 to 1:1.7, which gives a total adjustability of approximately 3:1. On applications such as the one just discussed, the Type V system can be utilized to obtain a much wider range of adjustability.

With this system, which is illustrated in Fig. 9, the set point on

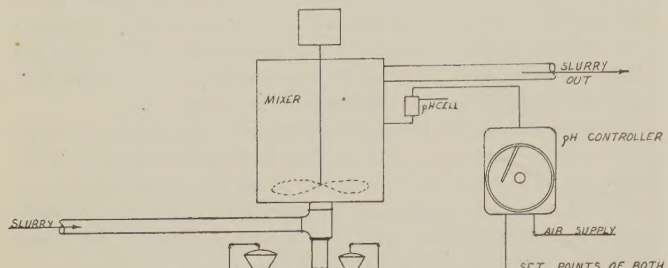

Fig. 9

the water-rate-of-flow controller, instead of being adjusted by the measuring element of the acid-flow controller, as in the previous case, is also adjusted from the output pressure from the pH controller. Each flow controller has a ratio adjustment which determines the ratio between the set-point deflection and output pressure, that is

$$K_a = \frac{D_a}{D_l} \qquad [21]$$

and

$$K_w = \frac{D_w}{D_l} \qquad [22]$$

where

K_a = ratio setting on acid-flow controller
K_w = ratio setting on water-flow controller
D_a = linear deflection of set point on acid-flow controller
D_w = linear deflection of set point on water-flow controller
D_l = linear length of chart scale

If the instruments have square-root scales, then the ratio of the acid-flow rate to the water-flow rate is given by

$$\frac{F_a}{F_w} = \frac{S_a\sqrt{D_a}}{S_w\sqrt{D_w}} \qquad [23]$$

From Equation [21]

$$D_a = K_a D_l \qquad [24]$$

From Equation [22]

$$D_w = K_w D_l \qquad [25]$$

Substituting into Equation [23]

$$\frac{F_a}{F_w} = \frac{S_a\sqrt{K_a D_l}}{S_w\sqrt{K_w D_l}} \qquad [26]$$

from which

$$\frac{F_a}{F_w} = \frac{S_a\sqrt{K_a}}{S_w\sqrt{K_w}} \qquad [27]$$

If K_a is set at its maximum value which is 3:1, and if K_w is set at its minimum value, which is 1:3, then

$$\frac{F_a}{F_w} = \frac{S_a\sqrt{3}}{S_w\sqrt{0.33}} = \frac{S_a}{S_w} \times \frac{3}{1} \qquad [28]$$

If, on the other hand, K_a is set at its minimum value while K_w is set at its maximum value, then

$$\frac{F_a}{F_w} = \frac{S_a\sqrt{0.33}}{S_w\sqrt{3}} = \frac{S_a}{S_w} \times \frac{1}{3} \qquad [29]$$

Thus with this system there is available a range of adjustability extending from 3:1 to 1:3.

Type VI Control System

The field of application of the Type VI system can best be appreciated by studying the typical process-control problem illustrated in Fig. 10. Here two different fluids flow in a pipe or conduit to a common point. The point of combination is the process, and the processed material is carried away in a third or effluent line. In the general case, the two fluids may be either liquid or gaseous, or even solid. The problem is to mix these two fluids in proportions which will produce a constant

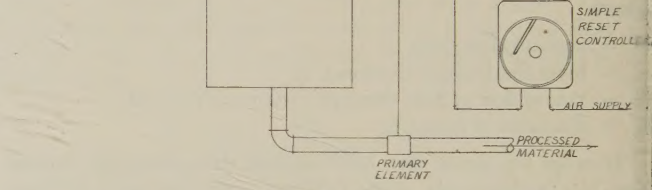

Fig. 10

predetermined result or value at the outlet point. One of the lines will carry the fluid with which the independent variable is associated. That is, some physical factor associated with the fluid such as temperature, pH, density, rate of flow, or combinations of these and other factors, will vary at will. The controlled variable is the rate of flow of fluid in the second line and the function of the control mechanism is continuously to adjust the rate of flow so that the desired result is maintained in the processed material despite variations in the independent variables.

The simple control system illustrated depends upon, and therefore requires, a deviation of the controlled variable, in order to produce the corrective impulse which is necessary to counteract any load change. The theoretical minimum value of the deviation resulting from a given load change, on the simple single capacity process illustrated, is given by

$$\theta = \Delta L\left(1 - \epsilon^{\frac{-FT}{v}}\right) \qquad [30]$$

where

ΔL = magnitude of load change
F = rate of flow through process
v = capacity of process
T = dead-time lag in system

In the usual case the maximum permissible value of θ is spe

fied when the control problem is submitted to the control engineer. The maximum possible load change ΔL can, in most cases, be predicted. Since F and T are always known, or can be determined, Equation [29] can be solved for the minimum permissible volume or capacity of the process. Then, if the process is designed with a capacity equal to or greater than this calculated minimum value, it can be controlled satisfactorily with the simple control system illustrated. This is the solution which has been used for this problem since the advent of the continuous process, and it was not until very recently that plant designers and control engineers became aware of an alternate and, in most cases, a better solution.

The alternate solution is shown diagrammatically in Fig. 11. For purposes of illustration a pH control problem is assumed in which the fluid in the independent variable line is to be acidified to a constant predetermined pH value by controlling the rate of acid flow through the control valve. The dominant load change is assumed to be a large and sudden change in the flow rate of the fluid to be acidified. If this were the only variable, the pH could be accurately controlled by means of a simple flow-ratio controller. The relation between the variables in this case would be simply

$$\text{pH} = a\frac{F_d}{F_i} = a\frac{S_d}{S_i} \quad [31]$$

Here the K factor would be set manually at whatever value would be required to produce the desired pH. However, there will be other variables such as the pH and buffering capacity of the incoming fluid, the pressure in the acid line, the acid concentration, etc. Each of these individually is assumed, in this case, to be of much smaller magnitude. If K remained fixed, any of these minor variables would cause a change in the outgoing pH, and conversely, in order that the pH remain constant, it would be necessary for the value of K to change whenever any of these minor load changes occurred. In other words, the K value required to produce a constant pH is a function of all variables other than F_i. Equation [31] therefore can be written as

$$\text{pH} = f(x), f(y), f(z), \frac{F_d}{F_i} = f(x), f(y), f(z)\frac{S_d}{S_i}K \quad [32]$$

where x, y, and z represent all variables other than F_i.

Equation [32] indicates that the basic requirement is for a flow-ratio controller which will maintain a constant pH despite wide variations in F_i. A further requirement is that the K value must be automatically selected and adjusted depending upon the instantaneous values of x, y, and z. In the system as illustrated, any change in the measured pH is an indication of a change in one of the minor variables. The pH controller re-

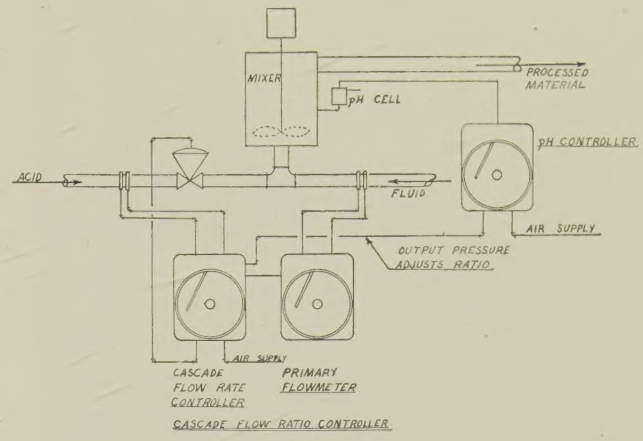

Fig. 11

sponds by sending an impulse to the cascade controller which in this Type VI system is applied to the mechanism which adjusts the ratio or K setting.

The effectiveness of this type of control system in reducing both capital investment and operating costs, can be illustrated by citing an actual example. Using a simple density controller on a dilution station, the unit process would have consisted of a 5000-gal tank equipped with a turboagitator capable of providing a turnover of 20,000 gpm. The agitator required a large drive motor and expensive speed reducer on which the daily operating costs would have been high. Using the Type VI cascade control system instead of the simple controller, the process was reduced to a 300-gal line-type mixer, the initial cost and the power consumption of which were but a small fraction of the alternate system. There was also a considerable saving in floor space, foundations, and similar items.

Conclusion

While six types of cascade controllers have been described as complete systems in themselves, there have been installations made within the past few years wherein several of these types have been combined to form more complex integrated control systems. Possibly some of these combinations would yield to classification, and some useful purpose might be served if this point were to be investigated.

As the continuous process becomes more complex, and as more variables are brought under control, we can expect to see further development in the art of designing and applying cascade control systems in the process industries. It is the author's opinion that the important advances in control engineering for the next few years will follow along these lines.